

AD A070273

DDC FILE COPY

REPORT DOCUMENTATION PAGE		READ INSTRUCTIONS RECIPIENT'S CATALOGUE NUMBER	
1. REPORT NUMBER AFOSR TR- 79-0702	2. GOVT ACCESSION NO.	2. PERIOD COVERED INTERIM Report	
3. TITLE (and Subtitle) Quantitative Synthesis of Multiple Loop Feedback Systems with Large Uncertainty		4. PERFORMING ORG. REPORT NUMBER 143	
5. AUTHOR(s) Isaac Horowitz & Te-Shing Wang		6. CONTRACT OR GRANT NUMBER AFOSR-76-2946	
7. PERFORMING ORGANIZATION NAME AND ADDRESS University of Colorado Department of Electrical Engineering Boulder, Colorado 80309		8. PROGRAM ELEMENT, PROJECT, TASK AREA & WORK UNIT NUMBERS 61102F 2304/A1	
9. CONTROLLING OFFICE NAME AND ADDRESS Air Force Office of Scientific Research/NM Bolling Air Force Base, D.C. 20332		10. REPORT DATE May 1979	
11. MONITORING AGENCY NAME & ADDRESS (if different from Controlling Office) LEVEL		12. NUMBER OF PAGES 75	
13. SECURITY CLASS. (of this report) Unclassified		14. DECLASSIFICATION/DOWNGRADING SCHEDULE	
15. DISTRIBUTION STATEMENT (or abstract entered in Block 20) Approved for public release; distribution unlimited.			
16. DISTRIBUTION STATEMENT (or abstract entered in Block 20, if different from Report)			
17. SUPPLEMENTARY TES			
18. KEY WORDS (Continue on reverse side if necessary and identify by block number) multiple loop feedback systems uncertain feedback systems			
19. ABSTRACT (Continue on reverse side if necessary and identify by block number) This work extends single input-output linear time-invariant minimum-phase "quantitative feedback synthesis" to two new complex plant structures with internal sensing points. One is the triangular structure. The second consists of parallel branches, each with cascaded sections. Due to uncertainty the plant parameters are elements of given sets. The system responses satisfy specified time or frequency domain tolerances. The basic problem is how to divide the feedback burden among the available loops so as			

20. ABSTRACT (continued)

minimize the net rms effect at the plant input, of the various sensor noise sources.

Frequency-response formulations are presented which provide a deep understanding of the tradeoff among the feedback loops. One vital feature is "free uncertainty", wherein a loop optimized to cope with uncertainty U_1 , may in fact for some frequency ranges handle uncertainty U_1 . A second is "bandwidth propagation", wherein the loops take turns in dominating the design over the frequency range. Together, they locate the frequency regions in which the respective loops dominate, and the key tradeoff parameters among them. "Design Perspective" then enables the designer to very rapidly find a close approximation to the precise design, based on any choice of these parameters. Numerous design examples with very large uncertainty illustrate the design procedures and the advantages of multiple-loop design.

Accession For	
NTIS GRA&I	<input checked="" type="checkbox"/>
DDC TAB	<input type="checkbox"/>
Unannounced	<input type="checkbox"/>
Justification _____	
By _____	
Distribution/ _____	
Availability Codes _____	
Dist.	Avail and/or special
A	

UNCLASSIFIED

SECURITY CLASSIFICATION OF THIS PAGE (When Data Entered)

QUANTITATIVE SYNTHESIS OF MULTIPLE LOOP FEEDBACK SYSTEMS
WITH LARGE UNCERTAINTY

ISAAC HOROWITZ* and TE-SHING WANG†

Abstract

This work extends single input-output linear time invariant minimum-phase "quantitative feedback synthesis" to two new complex plant structures with internal sensing points. One is the triangular structure. The second consists of parallel branches, each with cascaded sections. Due to uncertainty, the plant parameters are elements of given sets. The system response must satisfy specified time or frequency domain tolerances. The basic problem is how to divide the feedback burden among the available loops so as to minimize the net rms effect at the plant input, of the various sensor noise sources.

Frequency-response formulations are presented which provide a deep understanding of the trade-off among the feedback loops. One vital feature is "free uncertainty", wherein a loop optimized to cope with uncertainty U_1 , may in fact for some frequency ranges, handle uncertainty $U \gg U_1$. A second is "bandwidth propagation", wherein the loops take turns in dominating the design over the frequency range. Together, they locate the frequency regions in which the respective loops dominate, and the key trade-off parameters among them. "Design Perspective" then enables the designer to very rapidly find a close approximation to the precise design based on any choice of these parameters. Numerous design examples with very large uncertainty, illustrate the design procedures and the advantages of multiple-loop design. A -

* Cohen Professor of Applied Mathematics, Weizmann Institute of Science, Rehovot, Israel, and Dept. of Electrical Engineering, University of Colorado, Boulder.

† Dept. of Applied Mathematics, Weizmann Institute of Science, on leave from Chung-Shan Institute of Science and Technology, Taiwan, Republic of China.

This research was supported in part by the United States Air Force Office of Scientific Research, under Grant AFOSR 76-2946B at the University of Colorado.

**AIR FORCE OFFICE OF SCIENTIFIC RESEARCH (AFSC)
NOTICE OF TRANSMITTAL TO DDC**

This technical report has been reviewed and is
approved for public release IAW AFR 190-12 (7b).
Distribution is unlimited.

**A. D. BLOSE
Technical Information Officer**

Symbols

a_{ij} , b_{ij}	lower and upper bounds of k_{ij} , (5)
$B_{ij}(\omega)$	bounds on $L_{ijo}(j\omega)$, (4)
B_{hij}	UHF bounds on L_{ijo} (2.1, Figs. 3,5)
e_{ij}	excess of poles over zeros of P_{ij} (5)
g_{ij}	$= G_{ij}/s^{e_{ij}}$ (28)
hf	high frequencies
k_{ij}	hf gain factor of P_{ij} (5)
k_{ijx}	max. k_{ij} (28)
lf	low frequencies
$\ell(B_{hij})$	length in db of B_{hij} (8)
L_{ij}	ij loop transmission function
L_{ijo}	nominal L_{ij}
L_{ij}^A	approximate L_{ijo} by Design Perspective, Section 2.4
$L_{io}(HF,IF)$	Section 2.4, Fig. 8
M_{ik}	$= L_{ijo}(j\omega_{mik}) $, Section 2.4
\circ	as sub indicates nominal values
P_{ijx}	P_{ij} at k_{ijx} (34)
P_{ij}	set $\{P_{ij}\}$ due to uncertainty
s	as sub indicates a single-loop design
T	closed loop transfer function (1a)
T_{Nij}	$= X/N_{ij}$ (6)
T'	$= L/(1+L)$, 2.
T_d	C/D' (1b, Fig. 1)
$T(\cdot)_{ij}$	template of effective uncertainty L_{ij} must cope with, Sec. 2
UHF	universal high-frequency, Section 2.1

$U(P_{ij})$	uncertainty due to $\{P_{ij}\}$
α_i	trade-off factor between L_i and L_{i+1} (8)
γ_i	bound on $ T_d(j\omega) $, (1b)
Δ_i	Section 2.4
θ_{mij}	phase margin assigned to L_{ij} (5)
Φ_1	(8)
λ_{ij}	(11,12,15)
ω_{mij}	at which $ L_{ij}(j\omega) $ is a maximum, $i > 1$, Section 2.1
ω_{xij}	at which L_{ijo} turns corner of B_{hij} , Section 2.1.

1. INTRODUCTION

This paper presents quantitative synthesis techniques for the linear time invariant multiple-loop feedback structures of Figs. 1,2. The constrained part ("Plant" - darker lines) has internal variables which may be sensed and used in independent feedback loops. With each sensor there is associated a noise source with power spectrum $N_i(s)N_i(-s)$. Due to uncertainty it is only known that each $P_{ij} \in$ a given set P_{ij} . "Quantitative" denotes "design to specifications" - to satisfy given closed-loop tolerances $\forall P_{ij} \in P_{ij}$. The problem is how to best divide this "feedback burden" among the loops. Since the principal "cost of feedback" is in the bandwidth of the feedback loops and resulting large sensitivity to sensor noise, this design freedom is used to decrease the loop bandwidths and sensor noise effects.

The above is a very complex nonlinear optimization problem, obviously not amenable to the theorem-proving approach of "modern" control theory. The approach taken here is to attain a deep understanding of the important conflicting factors and trade-offs, permitting great simplification. Based on this, simple transparent design techniques are developed which rapidly give the designer excellent overall design perspective. Plants with large uncertainty are emphasized because the advantage of multiple over single loop design is then very great.

Minimum-phase systems are assumed in this paper, but open-loop unstable plants are permitted (Horowitz and Sidi 1972, 1978). The tolerances on the system response to command inputs R , are then completely specified by the requirement (Figs. 1,2)

$$\left| \frac{C}{R}(j\omega) \right| \triangleq |T(j\omega)| \in [A(\omega), B(\omega)] , \quad \forall P_{ij} \in P_{ij} \quad (1a)$$

with $A(\omega)$, $B(\omega)$ the given upper and lower bounds on $|T(j\omega)|$. This paper concentrates on (1a) with disturbance attenuation considered by the requirement (Figs. 1,2)

$$|T_d| \triangleq \left| \frac{C}{D_T(j\omega)} \right| \leq \gamma_1, \quad \forall P_{ij} \in P_{ij}. \quad (1b)$$

Plant modification. In Figs. 1,2 all the feedback loops are returned to the plant input X . This is denoted as "no plant modification", for the following reason. It is assumed that the "plant specialist" has designed the plant with the capacity to deliver $C = TR$ in (1a) for a given set $\{R\}$. Feedback is needed because of the uncertainty, but the "feedback specialist" is not allowed to tamper with the plant. In Figs. 1,2 all internal plant variables are completely determined by C and the P_{ij} , so have safe values, if (1a) is satisfied. If feedback H_1 from C to C_1^* in the insert in Fig. 1a is used, then $C_2 = \frac{C(1+P_1H_1)}{P_1}$ a function of the feedback design and which may be unsafe (instead of C/P_1), constituting "plant modification", which is forbidden. Some work has been done on the plant modification case for the cascade plant (Wang and Horowitz, 1978).

In this paper, synthesis is in the frequency domain, because of the simplicity and transparency thereby achievable. But it is emphasized that by means of tolerances of the (1a) type one can guarantee (Horowitz 1976, Krishnan and Cruickshanks 1977) that time-domain tolerances on the output of the form

$$a_i \leq \frac{d^{(i)} c}{dt^i} \leq b_i \quad (2)$$

can be satisfied for $i = 0, 1, \dots, n$ any finite number.

Previous work. Quantitative design in the above sense has been presented (Horowitz and Sidi 1972, 1973; Horowitz and Wang 1977) for Fig. 1a, and for a special case of Fig. 2a with $m=2$, $n_1=n$, $n_2=1$. This paper considerably sharpens the results and extends them to the much more general structures in Figs. 1b,2a.

2. BASIC FEATURES OF MULTIPLE-LOOP DESIGN

Some key features of multiple-loop design for plants with large uncertainty, are next explained. Consider first a single-loop design (with sub-S designations below) of the n -loop plant of Fig. 1a, $P = P_1 P_2 \dots P_n$, i.e. $G_2 = G_3 = \dots = G_n = 0$, $G_1 = G_S$ (Fig. 3).

$$T = \frac{F_S L_S}{1 + L_S} , \quad L_S = G_S P , \quad L_{S0} = G_S P_0 \quad (3a-c)$$

where the sub-oh always indicates a fixed "nominal" L or P . Due to uncertainty when $P \neq P_0$,

$$\Delta \ln |T| = \Delta \ln \left| \frac{L_S}{1 + L_S} \right| , \quad \Delta \ln L_S = \Delta \ln P = \ln \frac{P}{P_0} . \quad (4a,b)$$

The complex number set $\{P(j\omega)\}$ gives a region in the complex plane, denoted as the plant template $T(P)$. The bounds (ia,b) impose bounds $B_S(\omega)$ on $L_{S0}(j\omega)$ - see Fig. 3. Manipulation of $T(P)$ on the logarithmic complex plane, Nichols chart, with its loci of constant $T' \triangleq |L/(1+L)|$ is very convenient for understanding the relations between $T(P)$, (1a,b) and $B(\omega)$.

2.1 Design Example 1 (Fig. 3)

The above is illustrated by the following design problem with deliberately chosen great uncertainty, to emphasize the advantage of multiple-loop design. Parameter uncertainties are assumed independent in all the examples.

Plant and Tolerances:

$$P = P_1 P_2 P_3 , \quad P_1 = k_1 / (s^2 + 2\zeta\omega_n s + \omega_n^2) ,$$

$$P_2 = K_2 / (\tau_2 s + 1) , \quad P_3 = K_3 / (\tau_3 s + 1) ,$$

$$\zeta\omega_n \in [-3, 5] , \quad \omega_n \sqrt{1 - \zeta^2} \in [2, 10] , \quad k_1 \in [4, 1250] ,$$

$$\tau_2 \in [1/3, 1] , \quad K_2 \in [10, 33.3] , \quad \tau_3 \in [.05, .1] ,$$

$$K_3 \in [100, 158] .$$

The tolerances (1a) on $|T(j\omega)|$ are shown in Fig. 19b, derived from original time-domain tolerances of Fig. 19a; $\gamma_1 = 3$ db.

Bounds $B_S(\omega)$ on $L_{S0}(j\omega)$. The manipulation mentioned after (4), gives the bounds $B_S(\omega)$ in Fig. 3. At low frequencies (1f), (1a) dominates but sooner or later as ω increases, (1b) dominates because of Bode's "equality of positive and negative feedback areas" (Bode 1945, Horowitz 1963). The latter dictates that in realistic specifications, at "large" ω , it is essential that $[\Delta \ln |T|]_{\max}$ (permitted by the specifications) $> [\Delta \ln |P|]_{\max}$. Also, at high frequencies (hf)

$$P_{ij} \rightarrow \frac{k_{ij}}{s^{e_{ij}}} , \quad e_{ij} > 0 , \quad k_{ij} \in [a_{ij}, b_{ij}] . \quad (5)$$

These two factors lead to the $B(\omega)$ merging into a single "universal hf boundary" (UHFB) B_{hs} effective for $\omega >$ some ω_H value whose width $2\theta_{ms}$ is determined by γ_1 of (1b) — see Fig. 3.

Practical optimum design. In minimum-phase systems any L_{io} problem with bounds $B_i(\omega)$ and UHFB B_{hi} as in Fig. 3, is solvable (Horowitz 1975) by an infinitude of satisfactory L_{io} , permitting optimization. As $\omega \rightarrow \infty$, $L_{io}(s) \rightarrow k_{io}/s^{e_i}$. The optimum has been defined as that, which for a fixed e_i , minimizes k_{io} . It has been proven (Horowitz 1973, Horowitz and Sidi 1978) that a unique optimum L_{io} exists in the limit, and which lies on its

$B_i(\omega)$ for each $\omega \in [0, \infty)$. However, $L_{io} \neq L_{io,opt}$ may require a very high order transfer function, so there is trade-off between order of L_{io} and the optimization.

Most important, is that in significant uncertainty problems (wherein there is great advantage in multiple-loop design), a sensibly optimum L_{io} closely follows its uHFB B_{hi} along its right boundary, e.g. $U_S V_S$ in Figs. 3,4 for L_{so} , up to its "corner" frequency ω_{xi} , at which L_{io} turns the "corner" of its B_{hi} . Along the right vertical side ($U_i V_i$) of B_{hi} , the average slope of $|L_{io}(j\omega)|$ is approximately $-\frac{(180 - \theta_m)}{180} 40$ db per decade, where θ_m , the "phase margin", is defined in Figs. 3,5. For some interval $(\omega_{xi}, \omega_{m,i+1})$, $|L_{ic}(j\omega)|$ is fairly constant but $\text{Arg } L_{io}(j\omega)$ decreases rapidly towards its final value of $-e_i 90^\circ$, and $|L_{io}|$ to its final slope of $-20e_i$ db per decade.

In significant hf uncertainty problems, all the sensibly optimum L_{io} have the above properties in the hf region — see Figs. 3-5, 11a,b, 12, 15, etc. The great advantage of multi-loop design is in this hf region. Therefore, several standard universal hf patterns have been prepared in Fig. 8 for various θ_m values, based upon the experience of the authors. These enable fast estimates of L_{io} , as explained in 2.4.

2.1.1 The Sensor Noise Problem

It is well known that feedback is ineffective for uncertainty and noise in the return path. The noise problem is especially crucial in highly uncertain systems, in its effect at the plant input X . In the single-loop design

$$T_{N_1} \triangleq \frac{-X}{N_1} = \frac{G_S}{1 + G_S P} = \frac{1/P}{1 + L_S} = \frac{L_S}{P} = \frac{L_{so}}{P_o} \quad (6)$$

in the hf range where $|L_S(j\omega)| \ll 1$. The difference between $|L_{S0}|$ and $|P_0|$ in Fig. 4 reveals at once the great amplification of N_1 over an enormous band - see Fig. 6. Even if N_1 rms is very small, such amplification may make $|X_N|$ so large as to saturate elements near X , most of the time. This is a serious limitation which a multiple-loop design may greatly alleviate. Such fantastic sensor noise amplification likely makes a single-loop design impractical, but this is the price paid for coping with the extremely large uncertainty in this example. Note that in "modern state-variable" designs, sensor noise amplification is infinite, even in problems with no uncertainty. No wonder this serious practical problem is ignored in "modern control theory" (Horowitz and Shaked 1975).

2.2 Outer Loop Design in Multiple-Loop System

Multiple-loop design can help in the T_{N1} problem by having the inner loops handle the uncertainty in P_2 , P_3 . Replace the dashed portion in Figs. 1a,3 by P_{2e} etc., giving

$$\frac{C}{R} = T = \frac{FG_1 P_1 P_{2e}}{1 + G_1 P_1 P_{2e}} \triangleq F \frac{L_1}{1 + L_1}, \quad P_{2e} = \frac{P_2 P_{3e}}{1 + G_2 P_2 P_{3e}} \triangleq \frac{L_2}{G_2 (1 + L_2)}$$

$$P_{3e} = \frac{P_3}{1 + G_3 P_3} \triangleq \frac{L_3}{G_3 (1 + L_3)} \quad (n=3 \text{ here})$$

$$T_{N_1} = \frac{-X}{N_1} = \frac{L_1 / P_1 P_2 P_3}{1 + L_1} \triangleq \frac{L_1}{P_1 P_2 P_3} = \frac{L_{10}}{P_0} \quad \text{in hf} \quad (7a-f)$$

$$T_{N_2} = \frac{-X}{N_2} = \frac{L_2 / P_2 P_3}{(1 + L_1)(1 + L_2)} \triangleq \frac{L_2}{P_2 P_3} = \frac{L_{20}}{P_{20} P_{30}} \quad \text{in hf}$$

$$T_{N_3} = \frac{-X}{N_3} = \frac{L_3 / P_3}{(1 + L_1)(1 + L_2)(1 + L_3)} \triangleq \frac{L_3}{P_3} = \frac{L_{30}}{P_{30}} \quad \text{in hf}.$$

The best that can be done for the outer loop L_1 is to let L_2 handle $T(P_{se})$, so L_1 need cope only with $T(P_1)$. The savings in hf are quickly seen. From (5), $T(P_1) \rightarrow b_1/a_1 = 312.5 \ll T(P_1P_2P_3) \rightarrow b_1b_2b_3/a_1a_2a_3 \approx 10^4$ in Ex. 1, a saving ϕ_1 of 30 db. The length of the UHFB $B_{h1}(\omega)$ of L_{10} , $\ell(B_{h1}) = (\ell(B_{hs}) - 30)$ db. It is useful to allow a trade-off factor α_1 between L_{10} and L_{20} , making

$$\ell_{\text{eff}}(B_{h1}) = \ell(B_{hs}) - (\phi_1 - \alpha_1) . \quad (8)$$

The assumption $L_{10}(j\omega) \approx L_{S0}(j\omega)$ in lf is later justified. If so, an excellent approximation of L_{10} (denoted by L_{10}^A , hardly distinguishable from the exact L_{10}), is achieved by shifting in Figs. 3,4 the hf $V_S W_S X_S$ part of L_{S0} , upwards by $(\phi_1 - \alpha_1)$ db and in Fig. 4 also to the left until it merges with the upper part of L_{S0} . Since $(T_{N1})_S \approx L_{S0}/P_0$ while $(T_{N1})_{2 \text{ or } 3 \text{ loop}} \approx L_{10}/P_0$ in hf, it is seen that $|T_{N1}|_S < |T_{N1}|_{2,3}$ in $V_1 W_1$ in Fig. 4, vastly offset by $|T_{N1}|_{2,3} \ll |T_{N1}|_S$ over a much wider range — see Fig. 6 and note the different scales. This fast approximation of L_{10} is part of "Design Perspective", presented later.

In the above, L_{10} was assumed $\approx L_{S0}$ in lf, as if there is no saving in lf by letting L_{10} handle $T(P_1)$ instead of $T(P_1P_2P_3)$. It is next shown that the resulting saving is in fact quite small relative to that in hf. This is illustrated in Fig. 7a for $T(P)$ a vertical 20 db line, with allowed $\Delta|T|$ of 8 db, $P_0 = P_{\min}$. At $\arg L_0 = -130^\circ$ the bound on L_0 is -7.7 db with $|T'|_{\min} = -5.7$ db, $|T'|_{\max} = 2.3$ db. But it is easily seen that this L_0 is satisfactory for uncertainty (of a vertical line template) > 20 db, even semi-infinite. In fact, the template could even expand to include the entire region (shaded) between the loci of $|T'| = 2.3$ db and $|T'| = -5.7$ db. This property of "free uncertainty" is a vital feature of multiple-loop design,

which is highly transparent in the language of "frequency response". From examination of the $|T'|$ loci on the Nichols chart, it is seen that this property is not as nice for $\text{Arg } L_o \in [0, -90^\circ]$ but still very good. For example, if $\text{Arg } L_o = -50^\circ$ with the same $T(P)$ and allowed $\Delta|T|$ as before, $|L_o|_{\min} = 4.8 \text{ db}$ with $|T'|_{\min} = -3 \text{ db}$ in Fig. 7a. If 5.3 db is used for $|L_o|$ instead of 4.8 db, then it can handle semi-infinite gain uncertainty. In another example including uncertain poles and zeros giving $T(P) \sim 75^\circ$ wide, the maximum increase in L_{\min} needed (with $\text{Arg } L_o > -90^\circ$) was only 3 db, despite a difference of 40 db in the two templates.

The few db savings achievable in lf by using $T(P_1)$ instead of $T(P_1 P_2 P_3)$, may be important in some applications and would then be exploited. Since they are << hf savings achievable in this paper, they are ignored in all the designs in this paper, in order to simplify multiple-loop design. In all the examples, the outer loop L_{10} handles $T(P)$ for $\omega < \omega_{x1}$ defined in Fig. 3. In such cases $L_{10} \neq L_{S0}$ in lf is obviously justifiable. But even if $T(P_1)$ is used in lf design of L_{10} , the error is small (.. Design Perspective, by assuming $L_{10} \neq L_{S0}$ in lf.

2.3 inner Loop Design

L_{10} has been designed in hf as if P_{2e} of (7b) has little uncertainty (essentially a_1). Since $P_{2e} G_2 = L_2 / (1 + L_2)$, $L_2 = G_2 P_2 P_3$ (if $G_3 = 0$) with large $T(P_2 P_3)$, it would seem that $|L_{23}|$ must be $\gg 1$ over a large bandwidth. This is not necessarily so, due to the feature of "free uncertainty" discussed above.

There is only one region in which there is little "free uncertainty" for P_{2e} — where $L_{10}(j\omega)$ is underneath B_{h1} , $[\omega_{x1}, \omega_x]$ in Fig. 7b, necessitating

some α_1 overdesign. Suppose $T(P_1) = DE$, and $T(P_1 P_{2e}) \sim D E E_1 D_1$ for one design of L_{20} , which is satisfactory. In a different L_{20} design $T(P_1 P_{2e}) = D E E_2 \dots$, which violates γ_1 of (1b). Clearly, if $\alpha_1 = 0$ there would be very little "free uncertainty" and $|L_2|$ would have to be very large in this ω range. In practice a few db for α_1 suffice (Horowitz and Sidi 1973).

The actual tolerable $P_{2e}(j\omega)$ uncertainty, denoted by $U_{tol.}(P_{2e})$, is obtained in the above manner. From (7b), these are bounds on $\Delta \ln[L_2/(1+L_2)]$. Hence, the design of L_{20} to satisfy $U_{tol.}(P_{2e})$ despite $T(P_2 P_{3e})$ is similar to the design of L_{10} to satisfy (1a), despite $T(P_1)$. If L_3 is not used, $P_{3e} = P_3$ and $T(P_2 P_3)$ is used. If L_3 is used, $P_{3e} = P_3/(1+L_3)$ and it is assumed L_3 handles $T(P_3)$, just as it was assumed L_2 handles $T(P_{2e})$ in the design of L_1 . The resulting bounds $B_2(\omega)$ on $L_{20}(j\omega)$ are shown in Fig. 5a for the case L_3 is used, including a hand-calculated "practical optimum" L_{20} . Note the UHFB B_{h2} for L_{20} with its γ_2 , θ_{m2} analogous to B_{h1} etc. of L_{10} , and ω_{x2} of L_{20} cf. ω_{x1} of L_{10} . In view of the similarity of these hf parameters of L_{10} and L_{20} , it is not surprising that the hf shape of L_{20} is very similar to that of L_{10} . The next step is to design L_3 . $U_{tol.}(P_{3e})$ is obtained in the same manner as $U_{tol.}(P_{2e})$ above, giving bounds on $\Delta \ln L_3/(1+L_3)$, etc., leading to bounds $B_3(\omega)$ on $L_{30}(j\omega)$, shown in Fig. 5b, and finally the design of L_{30} . It is especially useful that very fast approximate $L_{20}^A(j\omega)$ may be derived from $L_{10}(j\omega)$, just as $L_{10}^A(j\omega)$ could be derived from $L_{S0}(j\omega)$, and in general L_{io}^A from $L_{i-1,0}^A$.

2.4 Design Perspective: Fast Derivation of $L_{10}^A(j\omega)$

The parameters needed are listed for any $L_{10}^A(j\omega)$.

θ_{mi} - the phase margin for L_{10} , related to γ_i , the maximum permitted value of $|L_i/(1+L_i)| = |\Gamma_i|$.

α_i - the overdesign or trade-off factor between L_{10} and $L_{i+1,0}$.

B_{hi} - the UHFB of L_{10} whose length $\ell(B_{hi})$ is determined by the hf uncertainty of P_i , its width by θ_{mi} .

ω_{xi} - at which L_{10} turns the bottom corner of B_{hi} and which decisively influences $L_{i+1,0}$.

ω_{mi} - at which $|L_{10}(j\omega)|$ has its maximum value ($i > i$); ω_{mi} is obtainable from $L_{i-1,0}$.

$M_i = |L_{10}(j\omega_{mi})|$, $i > i$.

$\Delta_i = \text{Min}(B_{hi}) - \alpha_i$, where $\text{Min}(B_{hi})$ is the minimum magnitude of B_{hi} .

Figs. 8a-c present "universal" hf (UHFC) L_{10} and M_i characteristics obtained from a study of numerical examples and theoretical considerations (Horowitz and Sidi 1972; 1973). These curves are used to derive L_{10}^A from $L_{i-1,0}^A$ for $i > i$. UHFC L_{10} in Fig. 8a (only for $\theta_{m1} = 50^\circ$), is used to obtain L_{10}^A from L_{So} . In all of these $e_i = 5$ is used. $L_{10}(\text{IF})$ in Fig. 8a is used to make the transition from If to hf.

Procedure for "Design Perspective"

- 1) Make a single-loop design L_{So} to handle the entire problem, as in Figs. 3,4 for Example 1. Let the hf portion of L_{So} be reasonably close to UHFC (L_{10}) in Fig. 8a.
- 2) Let ϕ_1 be the hf uncertainty of $P_2 P_3 \dots P_n$. Obtain L_{10} by shifting the UHFC portion of L_{So} upwards by $(\phi_1 - \alpha_1)$ db as in Figs. 3,4.

3) The value of ω_{m2} is at the arrow marked ω_m on UHFC (L_{10}) in Fig. 8a. The value of $M_2 = |L_{20}(j\omega_{m2})|$ is available from Fig. 8c, which together determine Q on L_{20}^A in Fig. 4. Draw a horizontal line in Fig. 4 at Δ_2 magnitude. If L_3 is not used, then $U(P_2 P_3)$ determines B_{h2} giving $\Delta_2 = -36$ db. If L_3 is used, $U(P_2)$ determines B_{h2} giving $\Delta_2 = -25$ db. Transparencies of Figs. 8a,b are assumed available. Place the transparency of $L_{10}(\text{IF})$ of Fig. 8a, on Fig. 4 so that the two Q points coincide. Find where $L_{10}(\text{IF})$ intersects the Δ_2 line, giving point C.

4) Pick the $L_{10}(\text{HF})$ curve in Fig. 8b according to the θ_{m2} value used for L_{20} . Lay the transparency of this $L_{10}(\text{HF})$ on Fig. 4, such that the two C points coincide. L_{20}^A consists of $L_{10}(\text{IF})$ of Fig. 8a in the intermediate ω range and of $L_{10}(\text{HF})$ of Fig. 8b in hf. Use the portion of $L_{10}(\text{HF})$ to the left of C to obtain a smooth curve for L_{20}^A .

5) Steps 3,4 are repeated in order to determine L_{30} . Use the arrow on the appropriate $L_{10}(\text{HF})$ of Fig. 8b, to locate ω_{m3} . Use Fig. 8c to obtain M_3 , giving a new Q in Fig. 4. Then lay $L_{10}(\text{IF})$ of Fig. 8a on Fig. 4, so that the Q's coincide, etc. A horizontal line of value Δ_3 is drawn, etc. The entire process is repeated until all the loops are exhausted.

The results in Fig. 4 and numerous others have shown excellent agreement between the L_{10}^A and the actual final detailed L_{10} designs. Of course, in designing L_{10} to satisfy its $B_i(\omega)$, one strives to achieve L_{10}^A knowing that it is a realistic practical optimum.

6) After each L_{10} is obtained, it is a good idea to sketch (as in Fig. 4) the effective P values to use for the sensor noise effect. From (7d-f), it is P_o for T_{N1} , $P_{20}' = P_{20}P_{30}$ for T_{N2} , P_{30} for T_{N3} . Sketches of L_{S0}/P_o , L_{10}/P_o , $L_{20}/P_{20}P_{30}$, L_{30}/P_{30} give the T_{N1} in hf.

If there is little N_1 sensor noise amplification ($|L_{S0}/P_0|$ not large over a large ω range), there may be no point in using more feedback loops. After L_{10}^A has been obtained, it is easy to see the saving in sensor N_1 noise effect by using L_2 . Sketch $P_{20}' = P_{20} \dots P_{n0}$ to see the hf N_2 sensor noise effect (L_{20}/P_{20}'). Similarly L_{10}/P_{10} , $P_{10} = P_{10} \dots P_{n0}$, gives the hf N_1 sensor noise effect. The fact that the design of L_{10} is insensitive to that of $L_{1+j,0}$ ($j > 1$), is central to this approach.

The designer has to decide which sensor noise points to use and the corresponding α_j trade-off values. "Design Perspective" enables him to very quickly evaluate different loop trade-offs. For example in Fig. 6, the T_{N2} (3-loop) effect < T_{N2} (2-loop) certainly if N_2 is white noise, but the improvement may not justify the cost of the additional sensor. If $(N_2)_{rms}$ is very large, he may try larger α_j , and quickly see the trade-off between T_{N1} and T_{N2} .

3. TWO-BRANCH CASCADE-PARALLEL PLANT

A special case of Fig. 2a, shown in Fig. 9, has been studied in detail (Horowitz and Wang 1977). Design Perspective, as simple as for the cascade plant, has since been developed. Also, the results are used in the more elaborate structure of Figs. 1b, 2 so Design Perspective for this case is presented with minimum essential background. In Fig. 9,

$$P \triangleq P_{11}(P_{12} \dots P_{1n}) + P_{21} \triangleq P_{11}P_a + P_{21} \quad (9a, b)$$

$$\frac{C}{R} = T = \frac{FGP}{\left(1 + \sum_2^n G_{11}P_{11}\right) + GP} \triangleq \frac{FGP}{(D_1) + GP} = \frac{FGP/D_1}{1 + (GP/D_1)} \triangleq F \frac{L_1}{1+L_1}$$

$$T_{N1} = \frac{-X}{N_1} = \frac{G}{D_1 + GP} = \frac{L_1/P}{1+L_1} \triangleq \frac{L_1}{P} = \frac{L_{10}}{P_0} \quad \text{in hf} \quad (10)$$

For minimum-phase P , a single-loop design can satisfy (1a,b) but the sensor noise effect can be disastrous. The best the inner loops can do for the outer loop L_1 , is to handle the uncertainty of P_a of (9a), denoted by $U(P_a)$. As in the cascade case, the great saving is in $\omega > \omega_{x_1}$, so attention is focused at hf where (5) applies. Let P' in which P_a is kept fixed be denoted by

$$P' = P_{11}P_{ao} + P_{21} \triangleq \lambda_{11}P_{110}P_{ao} + P_{21}, \quad L^1 = \frac{GP^1}{D_{10}} \quad (11a,b)$$

where as always, the sub-oh indicates a fixed value chosen as nominal. The nominal P_{110} for $i > 1$ appear in D_{10} .

In the notation of (5), $e_{21} = \sum_1^n e_{11}$ is assumed. It was found (Horowitz and Wang 1977) that if $b_{21}/a_{21} > b_{11}/a_{11}$, $T_{\min}(P')$ is obtained by letting $P_{ao} = a_a/s^{e_a}$ in (11a) (b_a for the opposite case). The universal hf B_{h1} for L_{10} then has length $\ell(B_{h1}) = (a_a b_{11} + b_{21})/(a_a a_{11} + a_{21})$, so the savings achievable by using G_{12} in Fig. 9 is $(b_a b_{11} + b_{21})/(a_a b_{11} + b_{21})$. The following example is used to describe the design procedure.

Design Example 2. $P_{1j} = k_{1j}/s$, $P_{21} = k_{21}/s^3$, $a_{12} = 20$, $a_{13} = 50$, $a_{11} = 1$, $a_{21} = 1000$, $b_{11} = 60$, $b_{12} = 800$, $b_{13} = 500$, $b_{21} = 200,000$. This simple form for the P_{1j} is taken because of the design concentration on hf, where each plant section assumes this form. There is no need to re-demonstrate lf design.

Time domain bounds on the acceptable step response are shown in Fig. 10a, and their translation into bounds on $|T(j\omega)|$ in Fig. 10b. Translation (recall (2)) is always possible, but good, economic translation is an engineering art. In practice, good results have been obtained with moderate effort - see Fig. 14 for design verification. Also, $\gamma_1 = 2.3 \text{ db} \rightarrow 24\%$ overshoot in a second-order model.

Design Perspective for Outer Loop L_{10} . A single-loop design L_{50} is first made - Fig. 12, with $\alpha(B_{HS}) = 81.7$ db cf. 42.3 db for $\alpha(B_{H1})$ in a multiple-loop design. Unlike the cascade case $\alpha_1 = 0$ can and was used, although $\alpha \neq 0$ may be used for trade-off between L_1 and the first inner loop L_{12} . Hence, L_{10}^A is obtained by shifting the UHFC portion of L_{50} upwards by $\phi_1 = 81.7 - 42.3 = 39.4$ db - see Fig. 12 where all the Design Perspective L_{ij}^A are dashed curves. Find ω_{m12} , at which $|L_{120}(j\omega)|$ is maximum, by use of the arrow on UHFC in Fig. 8a, as explained previously. However, Fig. 8c cannot be used to give M_{ij} for reasons given below.

First Inner Loop Design. The first inner loop via G_{12} need handle $T(P_{12})$ only, so replace P^1 , L_1^1 by

$$P^2 = P_{11}P_{12}P_{130}\dots P_{1n0} + P_{21} = \lambda_{11}\lambda_{12}P_{ao}P_{110} + P_{21} \quad (12)$$

$$\begin{aligned} L_1^2 &= \frac{GP^2}{D_1^2} = \frac{GP^2}{(1+G_{1n}P_{1n0}+\dots+G_{13}P_{1n0}\dots P_{130}) + G_{12}\lambda_{12}P_{ao}} \\ &\triangleq \frac{GP^2}{D_{20}(1+\lambda_{12}L_{120})}, \quad L_{120} = \frac{G_{12}P_{ao}}{D_{20}} \end{aligned} \quad (13a,b)$$

$$T_{N12} = \frac{-x}{N_{12}} = \frac{G_{12}/D_2 = L_{12}/P_a}{(1+L_{12})(1+L_1)} = \frac{L_{12}}{P_a} = \frac{L_{120}}{P_{ao}} \text{ at hf} \quad (14)$$

Note the difference between this and cascade design in Section 2. It is impossible here to treat each inner loop as a separate equivalent single-loop problem, which made cascade design conceptually so simple. Here, at every new inner loop stage, we must return to the outer loop and allow for more uncertainty in L_1 . Thus, in the outer loop design $P_a = P_{ao}$ is used with L_1^1 , P^1 , D_{10} notation. In the first inner loop design, $P_{12} \triangleq \lambda_{12}P_{120}$ replaces P_{120} (in P_a) with L_1^2 , P^2 , D_1^2 , D_{20} notation. In the next

stage $P_{12}P_{13}$ replaces $P_{120}P_{130}$ in P_a , giving $\lambda_{12}\lambda_{13}P_{ao}$, with L_1^3 , P^3 , D_1^3 , D_2^3 , D_{30} notation (see 15-17).

The first inner loop in (12,13) must be designed so that L_1^2 satisfies the same specifications as L_1^1 , although the latter dealt only with $U(P_{21}, P_{11})$, while the former must cope with P_{21} , P_{11} , P_{12} in (12,13). Despite the apparent great difference between this and cascade design philosophy, it was nevertheless found (Horowitz and Wang 1977) that the bounds $B_{12}(\omega)$ on L_{120} and the nature of the practical optimum design of the inner loops L_{120} , L_{130} , ... are very similar to those in cascade design, e.g. see Fig. 11b for $B_{12}(\omega)$, $L_{120}(j\omega)$. Design Perspective has now been extended to this structure. The peak values of L_{110} (at ω_{mi}) require different formulae than Fig. 8c, and are given in the Appendix. But Figs. 8a,b are useable with the Q_i , M_i , Δ_i , etc. exactly as before. The L_{110}^A in Fig. 12 were so obtained and agree very closely with the detailed design.

For the second inner loop, P^2 , L_1^2 , etc. in (12,13) are replaced in an obvious manner by

$$P^3 = \lambda_{11}\lambda_{12}\lambda_{13}P_{ao}P_{110} + P_{21} \quad (15)$$

$$L_1^3 = \frac{GP^3}{D_1^3} = \frac{GP^3}{D_{30}[1 + \lambda_{13}L_{130} + \lambda_{12}L_{120}(1 + L_{130})]} \quad (16a,c)$$

$$D_{30} = 1 + \sum_4^n G_{11}P_{110}, \quad L_{130} = \frac{G_{13}P_{110}\dots P_{140}P_{130}}{D_{30}}$$

$$T_{N13} = \frac{L_{13}/P_{1n}\dots P_{14}P_{13}}{(1 + L_{13})(1 + L_{12})(1 + L_1)} = \frac{L_{130}}{P_{1no}\dots P_{130}} \text{ in hf} \quad (17)$$

Tremendous improvement in sensor noise effects are obtained by multiple-loop design - see Fig. 13. This is due to the large hf uncertainties deliberately assigned in Ex. 2 to emphasize this property. The step and

disturbance response for a large number of plant parameter values are shown in Figs. 14a,b. It is seen that the problem tolerances are well satisfied with the extremes right at the boundaries. This is highly satisfying, as it indicates hardly any overdesign. The very slight excursions in Fig. 14a are typical of a good economical translation of time domain into ω -domain bounds - i.e. one with very little waste in bandwidth.

4. THE GENERAL TRIANGULAR MULTIPLE-LOOP SYSTEM

Quantitative design for the general triangular feedback system of Fig. 1b, including Design Perspective, is next presented. The following notation is convenient.

$$\begin{aligned} P_n &= P_{nc} \quad , \quad P_{n-1} = P_n P_{n-1,b} + P_{n-1,c} \quad , \\ P_{n-2} &= P_{n-1} P_{n-2,b} + P_{n-2,c} \quad , \quad P_{n-3} = P_{n-2} P_{n-3,b} + P_{n-3,c} \\ \dots \quad P_3 &= P_4 P_{3b} + P_{3c} \quad , \quad P_2 = P_3 P_{2b} + P_{2c} \quad , \\ P &= P_2 P_{1b} + P_{1c} \quad . \end{aligned} \tag{18}$$

$$\frac{C}{R} = T = \frac{FP_1 G_1}{\left(1 + \sum_{i=2}^n P_i G_i\right) + PG_1} \triangleq \frac{FP_1 G_1}{D = D_1 + PG_1} = F \frac{L_1}{1 + L_1} \tag{19a-c}$$

$$L_1 = \frac{PG_1}{D_1} \quad , \quad T_{N1} = \frac{-X}{M_1} = \frac{G_1}{D_1} = \frac{L_1/P}{1+L_1} = \frac{L_{10}}{P_0} \quad \text{in hf} \quad .$$

Hence to ease T_{N1} , as before let L_1 handle $T(P)$ for $\omega < \omega_{x1}$, at which L_{10} turns the corner of its B_{h1} , but with $\ell(B_{h1})$ given by $T(P^1)$ defined by (cf. (11))

$$P^1 = P_{20} P_{1b} + P_{1c} \quad , \quad \text{with } L_1^1 \triangleq G_1 P^1 / D_{10} \quad . \tag{20}$$

Thus in hf at which (5) applies, L_{10} ignores $U(P_2)$, and L_{10} is designed precisely as in Section 3, including Design Perspective. The following design example is used.

Design Example 3. In Fig. 1b, $n=4$ with

$$\begin{aligned} P_{4c} &= \frac{[1,40]10^3}{s}, \quad P_{3b} = \frac{[1,18]100}{s}, \quad P_{3c} = \frac{[1,60]10^5}{s^2} \\ P_{2b} &= \frac{[1,18]10}{s}, \quad P_{2c} = \frac{[2,120]10^6}{s^3} \\ P_{1b} &= \frac{[1,60]}{s}, \quad P_{1c} = \frac{[4,800]:0^6}{s^4}. \end{aligned} \quad (21)$$

The numbers were deliberately chosen so that the outer loop and first inner loop designs are identical to those of Ex. 2. The tolerances (1a,b, Figs. 10a,b) are also the same. In the notation of (22),

$$\begin{aligned} P_4 &= P_{4c} = [1,40]10^3/s, \quad P_3 = P_4 P_{3b} + P_{3c} = [2,780]10^5/s^2, \\ P_3^0 &= P_{40} P_{3b} + P_{3c} = [2,78]10^5/s^2, \quad P_2 = P_3 P_{2b} + P_{2c} = [4,14160]10^6/s^3, \\ P_2^0 &= P_{30} P_{2b} + P_{2c} = [4,156]10^6/s^3, \quad P = P_2 P_{1b} + P_{1c} = [8,850400]10^6/s^4, \\ P_1 &= P_{20} P_{1b} + P_{1c} = [8,1040]10^6/s^4. \end{aligned} \quad (22)$$

In case A first treated, only θ_{m1} on L_1 is specified. In case B, $\theta_{mi} = 18^\circ$ ($i > 1$) must be also satisfied $\forall P_{ij} \in P_{ij}$.

First Inner Loop. $U(P_2)$ previously neglected is now considered, but only of

$$P_2^1 \triangleq P_{30} P_{2b} + P_{2c} \triangleq \lambda_2^1 (P_{30} P_{2bo} + P_{2co}) = \lambda_2^1 P_{20}, \quad (23)$$

giving the effective plant and loop (cf. 12-14)

$$P^2 = \lambda_2^1 P_{20} P_{1b} + P_{1c}, \quad L_1^2 = \frac{P^2 G_1}{D_1^2} = \frac{P_1^2 G_1}{D_{20}(1 + \lambda_2^1 L_{20})} \quad (24a,b)$$

$$D_{20} = 1 + \sum_3^n P_{10} G_1 , \quad L_{20} = \frac{P_{20} G_2}{D_{20}} \quad (24c-e)$$

$$T_{N20} = \frac{-X}{N_2} = \frac{G_2}{D_{20}(1+L_{10})(1+L_{20})} \doteq \frac{L_{20}}{P_{20}} \text{ in hf.}$$

Bounds $B_2(\omega)$ are found on L_{20} so that L_1^2 satisfies B_{h1} even though $U(P_{2b}, P_{2c})$ previously neglected, are now included. By comparing (23,24) with (12-14), it is clear that the exact design and Design Perspective are identical with Section 2. Here $\lambda(B_{h2}) = (\lambda_2^1)_{\max} = [2(18) + 120]/(2+2) = 39$, and $\theta_{m2} = 18^\circ$ is used. The resulting bounds $B_2(\omega)$ and L_{20} are shown in Figs. 15a,16a.

Second Inner Loop. $U(P_{3b}, P_{3c})$ are next included, giving the effective plant and loop functions, etc.

$$P^3 = \lambda_2^2 P_{20} P_{1b} + P_{1c} , \quad \lambda_2^2 = (\lambda_3^2 P_{30} P_{2b} + P_{2c})/P_{20} ,$$

$$\lambda_3^2 = \frac{P_{40} P_{3b} + P_{3c}}{P_{30}} , \quad L^3 = \frac{P^3 G_1}{D_{30}[1 + \lambda_3^2 L_{30} + \lambda_2^2 L_{20}(1+L_{30})]} ,$$

$$L_{30} = \frac{P_{30} G_3}{D_{30}} , \quad D_{30} = 1 + \sum_4^n P_{10} G_1 , \quad T_{N30} \doteq \frac{L_{30}}{P_{30}} \text{ at hf. (25a-g)}$$

Here $(\lambda_2^2)_{\max} = [(39)(2)(18) + 120]/2 = 381$. By comparing (25) with (15-17), it is seen that the exact and perspective designs here are precisely the same as in Section 3. It is also obvious how the third and higher inner loops may be formulated so that their designs are exactly the same as in Section 3. For later purposes, note that the effective first inner loop is now (cf. 24b)

$$L_2^3 = G_2 \frac{(\lambda_3^2 P_{30} P_{2b} + P_{2c})}{D_{30}(1 + \lambda_3^2 L_{30})} \quad (26)$$

The designs are shown in Figs. 15b,16a. Note the excellent agreement between Design Perspective and the detailed designs. The tremendous improvement in sensor noise effects are seen in Fig. 16b.

Case B. In this case θ_{mi} , $\forall i$ (not just $i=1$ as in Case A) must be maintained $\forall P_{ij} \in P_{ij}$. The designs of L_{10} , L_{20} are as in Case A, but the demand on L_{30} to maintain θ_{m2} is usually more stringent than that due to θ_{m1} . In general, the dominant requirement on L_{10} is $\theta_{m,i-1}$ for $i > 2$, seen as follows.

The obligation on the second inner loop L_{30} begins at ω_{x2} , at which L_{10} is very small and its angle close to its final value (e.g. here -94 db at $\omega_{x2} = 1000$). The only real danger it offers is that $1+L_1^3 \approx 0$ at some parameter combination, leading to a vertical bound of length $(\lambda_3^2)_{\max}$, on the Nichols chart, at -180° . However, the limitation on L_{30} to satisfy B_{h2} with its θ_{m2} also begins at ω_{x2} but $|L_{20}(j\omega_{x2})| \gg |L_{10}(j\omega_{x2})|$ generally (-32 db here). When $U(P_{3b}, P_{3c})$ are considered, the effective first inner loop is given by L_2^3 in (26), which is identical in form to (13a) of Section 3. Thus, the obligation on L_{30} to maintain θ_{m2} is precisely of the same nature as the obligation on the first inner loop to maintain θ_{m1} , in the cascade-parallel problem of Section 3, and with the same technique of Design Perspective.

The above is true in general, i.e. θ_{mi} dominates the design of $L_{i+1,0}$ and the resulting constraint on the latter is identical to that on the first inner loop to maintain θ_{m1} in Section 3. Thus, when $T(P_{4b}, P_{4c})$ are considered, L_{30} of (25) is replaced by

$$L_3^4 = \frac{\lambda_4^3 P_{40} P_{3b} + P_{3c}}{D_{40}(1 + \lambda_4^3 L_{40})} \quad (27)$$

identical in form to (26), and with obvious expressions for λ_4^3 , D_{40} , L_{40} .

Application of Case B to Ex. 3. The outer and first inner loop designs are the same as in Case A, inasmuch as $\theta_{mi} = 18^\circ$ was deliberately used in the designs of all the inner loops L_{io} , as seen in Fig. 16. The first change is in L_{30} for which θ_{m2} of L_2 now dominates, etc. The resulting designs and T_{Ni} effects are shown in Figs. 17a-d. As expected, the "feedback cost" for the L_{io} (Case B) and T_{Ni} are greater in Case B, than in Case A for $i \geq 3$. Note the good agreement with Design Perspective for Case B based on $\theta_{mi} = 18^\circ$, in Fig. 17c.

5. THE ELEMENTARY PARALLEL-CASCADE STRUCTURE

Quantitative synthesis is next developed for the structure in Fig. 2, consisting of m parallel branches, the i -th having n_i cascade sections, $i = 1, 2, \dots, m$. An elementary member of this class is shown in Fig. 18. Its solution is highly useful for the general case, so it is presented first. Several design philosophies are developed, enabling the designer to divide the feedback burden among the loops and see the trade-offs. The first step in all cases is the design of the outer-loop L_1 . At one extreme, ($\alpha_1 = 0$) it need handle only $U(P_{11}, P_{21})$ of Fig. 18, but α_1 may be used for trade-off. As noted previously, the major gain is at hf so L_1 is assumed to handle the entire $T(P)$, $P = P_{12}P_{11} + P_{22}P_{21}$ for $\omega < \omega_{x1}$. The value of ω_{x1} is based on L_1 hf uncertainty of $(k_{120}k_{11} + k_{220}k_{21})$ where as in (5) $P_{ij} \rightarrow k_{ij}/s^{e_{ij}}$ at hf, $k_{ij} \in [a_{ij}, b_{ij}]$ and k_{120} , k_{220} are fixed nominal values taken at a_{ij} , $i = 1, 2$. This part is precisely the same as before, including Design Perspective.

The different approaches are for the design of the inner loop via G_{12} , G_{22} . It is very useful to note that for $\omega > \omega_{x1}$ the greatest problem of violating the γ_1 constraint due to the $U(P_{12}, F_{22})$ ignored in the L_{10} design, is at the top of the template - at point E in Fig. 7b, at which $k_{11} = b_{11}$, $k_{21} = b_{21}$. Thus, at hf $L_1 = \frac{g_1(k_{11}k_{12} + k_{21}k_{22})}{1 + P_{12}G_{12} + P_{22}G_{22}}$, where $e_{11} + e_{12} = e_{21} + e_{22} = e$ is assumed and $G_1 \triangleq g_1 s^e$. $|L_1(k_{11}, k_{21})| \leq |L_1(b_{11}, b_{21})|$ while $\text{Arg } L_1(k_{11}, k_{21}) = \text{Arg } L_1(b_{11}, b_{21})$, so if G_{12}, G_{22} are chosen such that $L_1(b_{11}, b_{21})$ does not violate γ_1 , $\forall P_{12} \in P_{12}$, $P_{22} \in P_{22}$, the design works for all k_{11}, k_{21} values. Henceforth, L_i^i , $i > 1$ used in inner loop synthesis is always at $k_{ii} = k_{i1x} = b_{ii} s^{e_{ii}}$ ($G_{i2} \triangleq g_{i2} s^{e_{i2}}$).

$$L_1^2 = \frac{g_1(b_{11}k_{12} + b_{21}k_{22})}{1 + k_{12}g_{12} + k_{22}g_{22}} . \quad (28a)$$

In the first design approach choose $g_{12} = b_{11}g_2$, $g_{22} = b_{21}g_2$, and then

$$L_1^2 = \frac{g_1(b_{11}k_{12} + b_{21}k_{22})}{1 + (b_{11}k_{12} + b_{21}k_{22})g_2} \triangleq \frac{g_1 k_e}{1 + g_2 k_e} . \quad (28b)$$

This corresponds precisely to a two-section cascade problem (Fig. 1a), with k_e of (28b) analogous to P_{2e} of (7a), and P_1 of (7a) set at a fixed P_{1x} ($k_1 = b_1$) and can therefore be ignored. The design technique and Design Perspective of Section 2, therefore apply here. This approach is convenient when the uncertainties and orders of magnitude of P_{12} , P_{22} and of N_{12} , N_{22} are similar. However, if they significantly differ, the following second approach is more flexible. Let

$$b_{21}g_{12} - b_{11}g_{22} = x(j\omega)b_{21} . \quad (29)$$

Suppose T_{N22} is the big problem, so g_{22} design economy is sought. Design

g_{22} first to handle $U(k_{22})$ only (setting $k_{12} = a_{12}$), by using (29) to eliminate g_{12} in (28a), giving

$$L_1^2 = \frac{g_1 b_{21} L_2^2}{g_{22}(1+L_2^2)}, \quad L_2^2 = \frac{g_{22}}{b_{21}} \frac{k_{22e}}{(1+x a_{12})}, \quad k_{22e} = b_{11} a_{12} + b_{21} k_{22}. \quad (30a-c)$$

Thus, $x(j\omega)$ is assumed to handle $U(k_{12})$ leaving $T(k_{22e})$ to g_{22} . From (30a), (34b) just as for (28b), the design of g_{22} , so that L_1^2 does not violate γ_1 despite $T(k_{22e})$, is precisely that of the first inner loop in a cascade structure (Section 2) with its Design Perspective. The factor a_2 is used as trade-off between g_{22} and x (i.e. g_{12}). This gives bounds $B_2(\omega)$ which L_{20}^2 must satisfy over $T(k_{22e})$.

The final step is to consider $U(k_{12})$ with a_{12} in (30b,c) replaced by k_{12} . The resulting new L_2 is

$$L_2^3 = \frac{g_{22}}{b_{21}} \frac{(b_{11} k_{12} + b_{21} k_{22})}{1 + k_{12} x(j\omega)}, \quad L_x = k_{12} x \quad (31a,b)$$

which is precisely of the same form as L_1^2 in (24a,b). Thus, the design of $L_{x0} = a_{12} x$ so that L_2^3 satisfies the $B_2(\omega)$ (derived with $U(k_{12})$ ignored), is the same as the design of the first inner loop in Section 4, so that L_1^2 satisfies $B_1(\omega)$ derived by ignoring $U(P_{2b}, P_{2c})$.

Design Example 4. Fig. 18 with $P_{12} = [1, 90]/s^2$, $P_{11} = [1, 10]/s$, $P_{22} = [.1, 2/s^2]$, $P_{21} = [1, 10]/s$. The time domain bounds are in Fig. 19a, and their derived "equivalent" ω -domain bounds in Fig. 19b; $\gamma_1 = 2.3$ db.

For $\omega < \omega_{x1}$, L_1 handles the entire P uncertainty - $[90(10) + 2(10)]/[1 + (.1)] = 836$; but for $\omega > \omega_{x1}$, only $[10 + (.1)10]/[1 + (.1)] = 10$. The detailed designs of the loops for $x=0$ and $x \neq 0$, the latter for different α_{22} values (for trade-off between

L_{22} and L_x), are shown in Fig. 20a, together with the excellent approximations obtained very rapidly by Design Perspective. The sensor noise responses are compared in Fig. 20b, based on the equations (at hf)

$$T_{N22} \doteq \frac{L_{22}}{P_{12} \frac{b_{11}}{b_{21}} + P_{22}}, \quad T_{N12} \doteq \frac{b_{11}}{b_{21}} T_{N22} + \frac{L_x}{P_{12}}. \quad (32a,b)$$

It is clear from Fig. 20a,b how x and a_{22} provide means of design trade-off. Of course, if T_{N12} is more serious than T_{N22} , then the $G_{12}P_{12}$ loop may be designed first. The above notation can be retained by simply changing the numbering.

6. THE GENERAL PARALLEL-CASCADE STRUCTURE

The design theory of all the previous structures are used in the final structure of Fig. 2. The design (including Perspective) of the outer loop L_1 is precisely as in all the preceding — to handle the entire $T(P)$ for $\omega < \omega_{x1}$ and only the P_{1i} for $\omega \geq \omega_{x1}$. It is very helpful to use a specific example.

Design Example 5. Fig. 2 with $P_{ij} = k_{ij}/s$ for $i = 3,4$, $j = 1-3$, and $ij = 11,22$. $P_{12} = k_{12}A/s(s+A)$, $P_{21} = k_{21}(s+z)/2s(s^2 + Bs + C)$.

Uncertainties (all independent): $k_{11}, k_{21} \in [4,40]$; $k_{12}, k_{22} \in [25,750]$, $k_{31}, k_{41} \in [4,20]$; $k_{32}, k_{42} \in [5,40]$; $k_{33}, k_{43} \in [5,75]$; $z, A \in [1,2]$; $B \in [0,1]$, $C \in [.04,1]$.

Specifications: (1a) same as for Ex. 4, Figs. 20a,b; $\gamma_1 = 2.3$ db.

Design. For $\omega < \omega_{x1}$, L_1 handles $T(P)$ but for $\omega > \omega_{x1}$, it handles only $U(P_{11})$, with notation

$$L^1 = \frac{P^1 G_1}{1 + H_{30} + H_{20}} , \quad H_3 = P_{33} G_{33} + P_{43} G_{43} ,$$

$$H_2 = P_{43} P_{42} G_{42} + P_{33} P_{32} G_{32} + P_{22} G_{22} + P_{12} G_{12} , \quad (33a-d)$$

$$P^1 = P_{430} P_{420} P_{41} + P_{330} P_{320} P_{31} + P_{220} P_{21} + P_{120} P_{11} .$$

The next stage is the design of G_{i2} to handle $U(P_{i2})$, $i = 1, \dots, 4$ letting P_{ij} (for $j > 2$) = P_{ijo} and $P_{i1} = P_{i1x}$, the sub-x denoting maximum values, i.e. at $k_{ij} = b_{ij}$. If the first approach of Section 5 is used, take $G_{i2} = P_{i1x} G_2$, giving

$$L_1^2 = \frac{L_2^2 G_1 / G_2}{1 + L_2^2} , \quad L_2^2 = \frac{G_2 P^2}{1 + H_{30}} ,$$

$$P^2 = P^1 \text{ (at } P_{i1} = P_{i1x} , P_{ij} = P_{ijo} \text{ for } j > 2 \text{)} . \quad (34a-c)$$

As in (28b), this is analogous to the first inner loop problem in cascade design resulting in bounds $B_2(\omega)$ on L_{20}^2 , whose design determines all the G_{i2} . Other options for the design of the G_{i2} are considered later. Next, consider G_{33}, G_{43} in H_3 of (33b). The two methods of Section 5 are available. In the first, $G_{i3} = P_{i2x} P_{i1x} G_3$ for $i = 3, 4$ and all $P_{ij} = P_{ijx}$ except for $1j = 33, 43$ giving

$$L_1^3 = \frac{L_2^3 G_1 / G_2}{1 + L_2^3} , \quad L_2^3 = \frac{G_2 (P_{34e} + P_{bx})}{1 + G_3 P_{34e}}$$

$$P_{34e} = P_{43} P_{42x} P_{41x} + P_{33} P_{32x} P_{31x} = \lambda_3 P_{34eo} , \quad (35a-e)$$

$$P_{bx} = P_{22x} P_{21x} + P_{12x} P_{11x} , \quad L_3 = G_3 P_{34e} .$$

$L_{30} = G_3 P_{34eo}$ must be designed so that L_2^3 satisfies $B_2(\omega)$ previously obtained on L_{20}^2 in which $U(P_{i3}, P_{33})$ was ignored. Consider Fig. 1b with its $G_1 = G_2$ here, its $G_2 = G_3$ here, $P_{1b} = 1$, $P_{1c} = P_{bx}$, $P_{2c} = P_{34e}$

and all others zero. The design problem for G_2 (there) so that $U(P_{2c})$ ignored does not spoil the outer loop design, is exactly that of G_3 here. Bode plots of the L_{10} including Design Perspective are shown in Fig. 21a. L_{20}^* is L_{20} for the case the $G_{i3}=0$. The extra cost is, of course, in bandwidth and in the sensor noise effect, as seen in Fig. 21b.

Suppose the second approach in Section 5 is used for L_{33} , G_{43} with G_{33} to be economized. Let

$$G_{43}P_{32x}P_{31x} - G_{33}P_{42x}P_{41x} = yP_{32x}P_{31x} \quad (36)$$

$P_{43} = P_{430}$ and $P_{ij} = P_{ijx}$ except $ij = 33, 43$ giving the new

$$L_1^3 = \frac{L_2^3 G_1 / G_2}{1 + L_2^3}, \quad L_2^3 = \frac{G_2 (P_{3e}^3 + P_{bx})}{(1 + L_{40})(1 + L_3^3)}, \quad (37a-e)$$

$$L_3^3 = \frac{G_{33} P_{3e}^3}{1 + L_{40}}, \quad P_{3e}^3 = P_{34e} \text{ (at } P_{43} = P_{430}) \quad , \quad L_{40} = yP_{430}$$

The difference between this and (35) is that L_3^3 need handle only $U(P_{3e}) < U(P_{34e})$, but otherwise the design philosophy is the same, giving bounds $B_3(\omega)$ on L_{30}^3 . The final step is to design $y(j\omega)$ to handle $U(P_{43})$. In (37), replace P_{430} by P_{43} and L_{40} must be designed so that $L_3^4 = G_{33} P_{3e}^4 / (1 + L_4)$ with $P_{3e}^4 = P_{3e}^3$ (with P_{430} replaced by P_{43}) satisfies $B_3(\omega)$ despite $U(P_{43})$, previously ignored. This is again analogous to the first inner loop problem of Sections 3,4. Of course a may be used to trade-off between G_{33} and G_{43} , as in Section 5, Figs. 21,22.

Other Design Options. Approach 1 was used in the design of the G_{12} , but combinations of 1 and 2 are possible. For example, if G_{22} is to be economized while the other 3 are to be of the same order of magnitude, let

$$G_{12}P_{21x} - G_{22}P_{11x} = v(j\omega)P_{21x}, \quad G_{12}P_{11x} = G_{12}P_{21x} \text{ for } i=3,4. \quad (38a,b)$$

In the design of G_{22} , i.e. in P^2 below, only $U(P_{22})$ is considered as the P_{11} are all set at P_{11x} , and the balance of the P_{1j} are set at P_{1j0} . This gives (in place of 34a-c where $U(\text{all } P_{ij})$ were considered),

$$L_1^2 = \frac{G_1 P_{21x} L_2^2 / G_{22}}{1 + L_2^2}, \quad L_2^2 = \frac{G_{22} P^2}{P_{21x}(1 + H_{30} + vP_{2b}^2)}, \quad (39a-c)$$

$$P_{2b}^2 = (P_{430} P_{420} P_{41x} + P_{330} P_{320} P_{31x} + P_{120} P_{11x}) / P_{11x}.$$

The design of L_{20}^2 is obviously of the same form as in (34a-c), giving the bounds $B_2(\omega)$ on L_{20}^2 , etc. The next step is to design $v(j\omega)$ to handle $U(P_{ij})$, $i = 1, 3, 4$. The P_{2j0} for $i = 1, 3, 4$ are replaced by P_{2i} , P_{22} by P_{22x} , giving

$$L_2^3 = \frac{G_{22} P^3}{P_{21x}(1 + H_{30})(1 + L_3^3)}, \quad L_3^3 = \frac{vP_{2b}^3}{1 + H_{30}}, \quad (40a-d)$$

$$P^3 = P_{2b}^3 + P_{21x} P_{22x}, \quad P_{2b}^3 = \lambda_3 P_{2b}^2 = P_{11x} P_{12} + P_{31x} P_{32} P_{330} + P_{41x} P_{42} P_{430}$$

The similarity between (35) and (40) is obvious, so the design philosophy for L_{30}^3 is similar to that for L_{30} of (35), even though the latter deals with the G_{i3} . The next step is the design of the G_{i3} , whose options have already been discussed.

As there are four G_{ij} , there are several more options besides the above two. The most extreme is to apply the second approach of Section 5 to each, say in the order $i = 2, 1, 3, 4$ by letting

$$P_{21x} G_{12} - P_{11x} G_{22} = y_1 P_{21x}, \quad P_{11x} G_{32} - P_{31x} G_{12} = y_3 P_{11x}, \\ P_{31x} G_{42} - P_{41x} G_{32} = y_4 P_{31x}. \quad (41a-c)$$

Just as in (39), only $U(P_{22})$ is handled by L_2^2 , as P^2 here is the same as in (39). But in the next step, only $U(P_{12})$ is considered, so L_2^3 , P^3

of (40a) are here replaced by

$$L_2^3 = \frac{G_{22}P^3 = G_{22}(P_{1e}^3 + P_{21x}P_{22x})}{P_{21x}(1+H_{30}+E_2^3)(1+L_3^3)},$$

$$E_2^3 = y_4P_{420}P_{430} + y_3P_m^3, \quad P_m^3 = P_{31x}P_{320}P_{330} + P_{41x}P_{420}P_{430} \quad (42a-d)$$

$$L_3^3 = \frac{y_1P_{1e}^3}{P_{11x}(1+H_{30}+E_2^3)} = \frac{y_1(P_{11x}P_{12} + P_{31x}P_{320}P_{330} + P_{41x}P_{420}P_{430})}{P_{11x}(1+H_{30}+E_2^3)}$$

The similarity of (42a), (35b) is obvious, even though the elements involved are quite different. Hence the same design philosophy is applicable, giving bounds $B_3(\omega)$ on L_3^3 and its design.

Next, y_3 is designed to handle $U(P_{32})$, so P_{12} is replaced by P_{12x} , P_{320} by P_{32} , and L_3^3 in (42) is replaced by

$$L_3^4 = \frac{y_1P_{1e}^4 = y_1(P_m^4 + P_{11x}P_{12x})}{P_{11x}M_{30}\left(1 + \frac{y_3P_m^4}{M_{30}}\right)}, \quad P_m^4 = P_{31x}P_{32}P_{330} + P_{41x}P_{420}P_{430}$$

$$M_{30} = 1 + H_{30} + y_4P_{420}P_{30}, \quad L_4^4 = \frac{y_3P_m^4}{D_{30}} \quad (43a-d)$$

L_4^4 must be designed so that L_3^4 satisfies $B_3(\omega)$ previously obtained on L_3^3 . By comparing (43a) with (35b), it is seen that the design philosophy for L_3^3 there applies to L_4^4 here, giving $B_4(\omega)$ on L_4^4 , etc. The next step is to design y_4 to handle $U(P_{42})$, so P_{420} is replaced by P_{42} , P_{32} by P_{32x} , giving

$$L_4^5 = \frac{y_3(P_{41x}P_{42}P_{430} + P_{31x}P_{32x}P_{330})}{(1+H_{30})(1+L_5^5)}, \quad L_5^5 = \frac{y_4P_{42}P_{30}}{(1+H_{30})}. \quad (44a,b)$$

L_5^5 must be designed so that L_4^5 satisfies $B_4(\omega)$ and the design philosophy is obviously again that for (35).

Design Simulation. Only the simplest design of Eqs. (33,35) resulting in the L_{10} of Fig. 21a was implemented. The simulation results are shown in Figs. 22a,b.

7. CONCLUSIONS

Frequency response and Quantitative design provide a deep comprehension of the trade-offs between design complexity, multiple-loop use and the resulting savings in loop bandwidths and sensor noise effects. Design Perspective gives very quick but accurate estimates of the loop transmission and sensor noise effects. The designer is thus able to decide, without the need for a detailed design, which sensors and loops to use and their trade-off values (the α_{ij}). The improvement in sensor noise effects can be enormous in plants with large uncertainty.

APPENDIX

Transfer Functions for the Numerical Examples. The orders of outer loop L_{10} functions are considerably larger than those of the inner loop $L_{10}, i > 1$. Part of the reason is the larger uncertainty and need to satisfy $B_1(w) \forall w$ including the lf range. The other is that the L_{10} were obtained by means of a computer program. If the time constants τ_i , i.e. in the form $(1+\tau_i s)$, are given, the data is preceded by $\tau_i = \dots$. If the zeros or poles are given, the notation $z_i = \dots$, or $p_i = \dots$, is used. Complex pair data is given as (ζ_i, ω_n) for the factor $[1 + (2\zeta s/\omega_n) + s^2/\omega_n^2]$. The zero w gain factor is given by K , the ∞w gain factor by KI . The numerator data is always first terminating in a semicolon,

Example 1.

L_{10} : $K = 5, \tau_i = 1.087, 1.05, .0576, .0384, .0074, .0028, (.7, 2200);$
 $K = 1, \tau_i = \infty, 1.954, 1.89, .164, .0265, .026, .005, 2 \times .0004,$
 $(.35, 2600), 2 \times (.35, 22000).$

L_{20} : $K = .5, z_i = 1080, 8640, 13800; p_i = 900, 19200, (.2, 1920), 2 \times (.3, 16000).$

L_{30} : $K = .645, z = 45000; (.3, 11250), (.15, 45000), (1, 180000).$

Example 2.

L_{10} : $KI = (1.6)10^{10}, z_i = 1.96, 15.8, 39.5, (.707, 3.27), (.83, 4.71);$
 $p_i = 0, 2.16, (.84, 2.8), (.56, 5.0), (.65, 19.3), (.41, 392), (.41, 398).$

L_{120} : $K = .14, z_i = 800, 2000; p = 600, (.2, 340), 2 \times (.25, 2500).$

L_{130} : $K = .63, z = 6000; (.3, 1750), 2 \times (.3, 15000).$

$F : KI = (1.59)10^5, z = 5.05; (.66, 2.79), (.45, 321).$

Example 3.

Case A.

$$L_{20}: K = .168, z_i = 180, 1440, 2286; p_i = 150, 3200, (.2, 320), 2 \times (.3, 2680).$$

$$L_{30}: K = .068, z_i = 7000, 14400, (.4, 2250); p = 23000, (.2, 2300), (.2, 2300), (.3, 2250), 2 \times (.3, 14000).$$

$$L_{40}: K = .068, z_i = 36540, 75200, (.4, 11740); p = 120000, (.2, 11745), (.2, 12000), 2 \times (.3, 73000).$$

Case B.

$$L_{30}: K = .168, z_i = 1260, 10000, 16000; p_i = 1050, 22400, (.2, 2240), 2 \times (.3, 18760).$$

$$L_{40}: K = .168, z_i = 8820, 70000, 112000; p_i = 7350, 156800, (.2, 15680), 2 \times (.3, 130900).$$

Example 4.

$$L_{10}: KI = (.171)10^7, z = 8, (.84, 1.93); p_i = 0, 5.6, (.72, 1.78), 2 \times (.45, 40.5).$$

$$F : KI = (.186)10^5, \text{ Numerator } \sum_0^4 a_i s^i: 947.3, 764, 217.4, 29.17, 1; \\ \text{Denominator } \sum_0^7 b_i s^i: (.176)10^8, (.247)10^8, (.161)10^8, (.628)10^7, \\ (.101)10^7, 81820, 778, 1.$$

$$L_{220} (\alpha_{22} = 5): K = .645, z = 100; (.3, 25), (.15, 100), (.1, 400).$$

$$L_{220} (\alpha_{22} = 15): K = .6, z = 100; (.3, 27), 2 \times (.4, 250).$$

$$L_{220} (\alpha_{22} = 30): K = .6, z_i = 210, 400; p = 420, (.3, 27), 2 \times (.4, 800).$$

$$L_{x0} (\alpha_{22} = 5): K = .07, z_i = 450, 800; p = 1600, (.2, 100), 2 \times (.35, 900).$$

Example 5.

F : K = 1 , z = 8 ; p = 2,2,3 .

L_{SO}: K = 2.2 , z_i = .5 , 30 , 100 , 4200 ; p_i = 0 , 0 , 20 , 45 , 1000 , 2×(.25,2800) .

L₁₀: K = 2.2 , z_i = .5 , 30 , 100 ; p_i = 0 , 0 , 20 , 45 , 2×(.35,115) .

L₂₀^{*}: K = .59 , z = 700 ; (.2,90) , 2×(.35,2000) .

L₂₀: K = .59 , z = 500 ; (.2,90) , 2×(.35,1250) .

L₃₀: K = .084 ; (.4,1000) , 2×(.1,3000) .

Design Perspective: Estimates of Peak Values |L_{1j0}(ω_{m1})| for

Noncascade Designs. (Fig. 9)

First inner loop L₁₂ . M₁₂(db) = 10 log₁₀ $\left(\frac{\mu^2 - v^2}{v^2 \lambda_{12x}^2 - \mu^2} \right) + 1.5$

where $(a_1)_{db} = 20 \log_{10} v$, $\mu = \frac{\lambda_{12x} a_{11} b_{21} + b_{21}}{a_{11} b_{21}}$

$\lambda_{12x} = \max \lambda_{12} = b_{12}/a_{12}$,

e.g. in Ex. 2, Fig. 12, $\lambda_{12x} = 40$, $v = 1$, $\mu = 10$, gives $M_{12} \approx -10$ db .

REFERENCES

Bode, H.W., 1945, Network Analysis and Feedback Amplifier Design (New York: Van Nostrand).

Horowitz, I., 1963, Synthesis of Feedback Systems (New York: Academic Press); 1973, Int. J. Control., 18, 97; 1975, I.E.E.E. Trans. Autom. Control, 20, 454; 1976, Proc. I.E.E.E., 64, 123.

Horowitz, I., and Shaked, U., 1975, I.E.E.E. Trans. Autom. Control, 20, 84.

Horowitz, I., and Sidi, M., 1972, Int. J. Control., 16, 287; 1973, Automatica, 9, 589; 1978, Int. J. Control., 27, 361.

Horowitz, I., and Wang, T.S., 1977, Int. J. Control., to appear.

Krishnan, K., and Cruickshank, A., 1977, Int. J. Control., 25, 609.

Wang, B.C., and Horowitz, I., 1978, Synthesis of Multiple-Loop Feedback Systems with Plant Modification, Dept. of Electrical Engg., University of Colorado, Boulder, Co., to appear in Int. J. Control.

Wang, T.S., 1978, Ph.D. Thesis, Dept. of Applied Math., Weizmann Institute of Science, Rehovot, Israel.

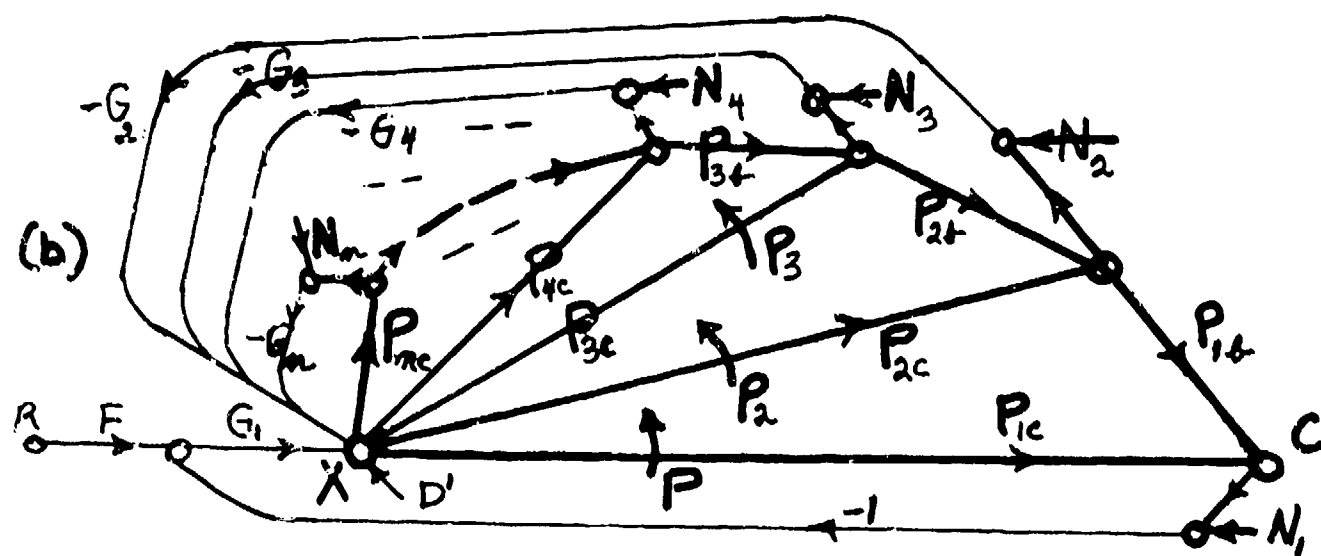
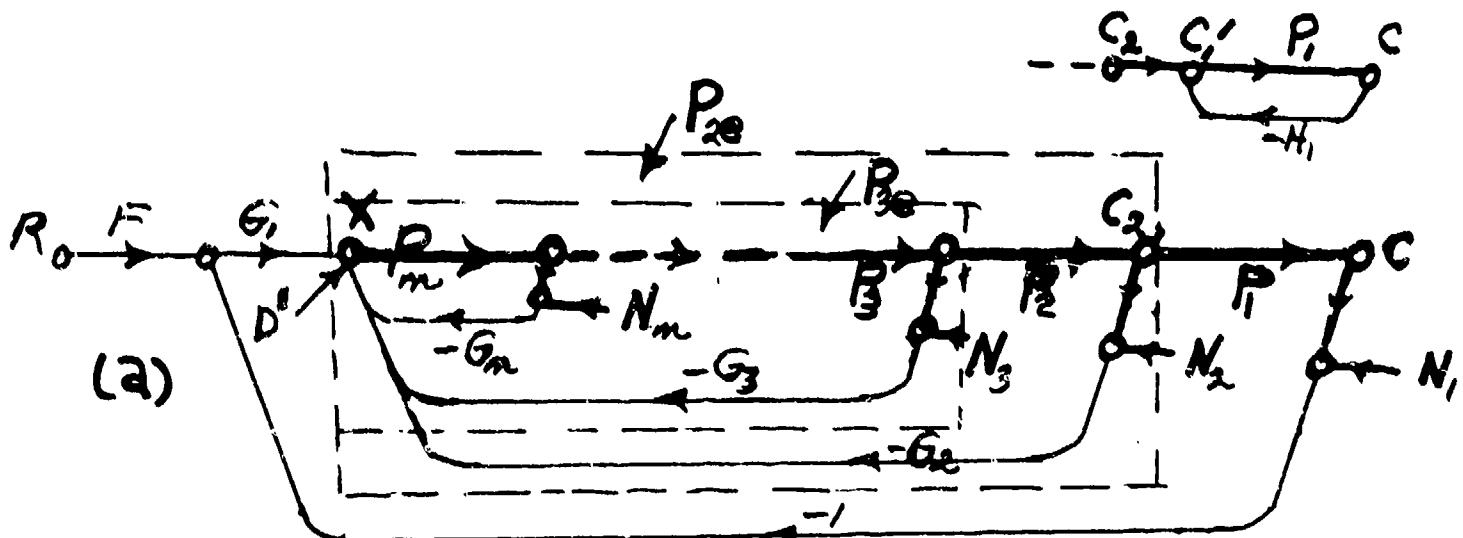


Figure 1. The general cascade and triangular multiple-loop feedback structures. Darker lines indicate constrained plant and sensor noise.

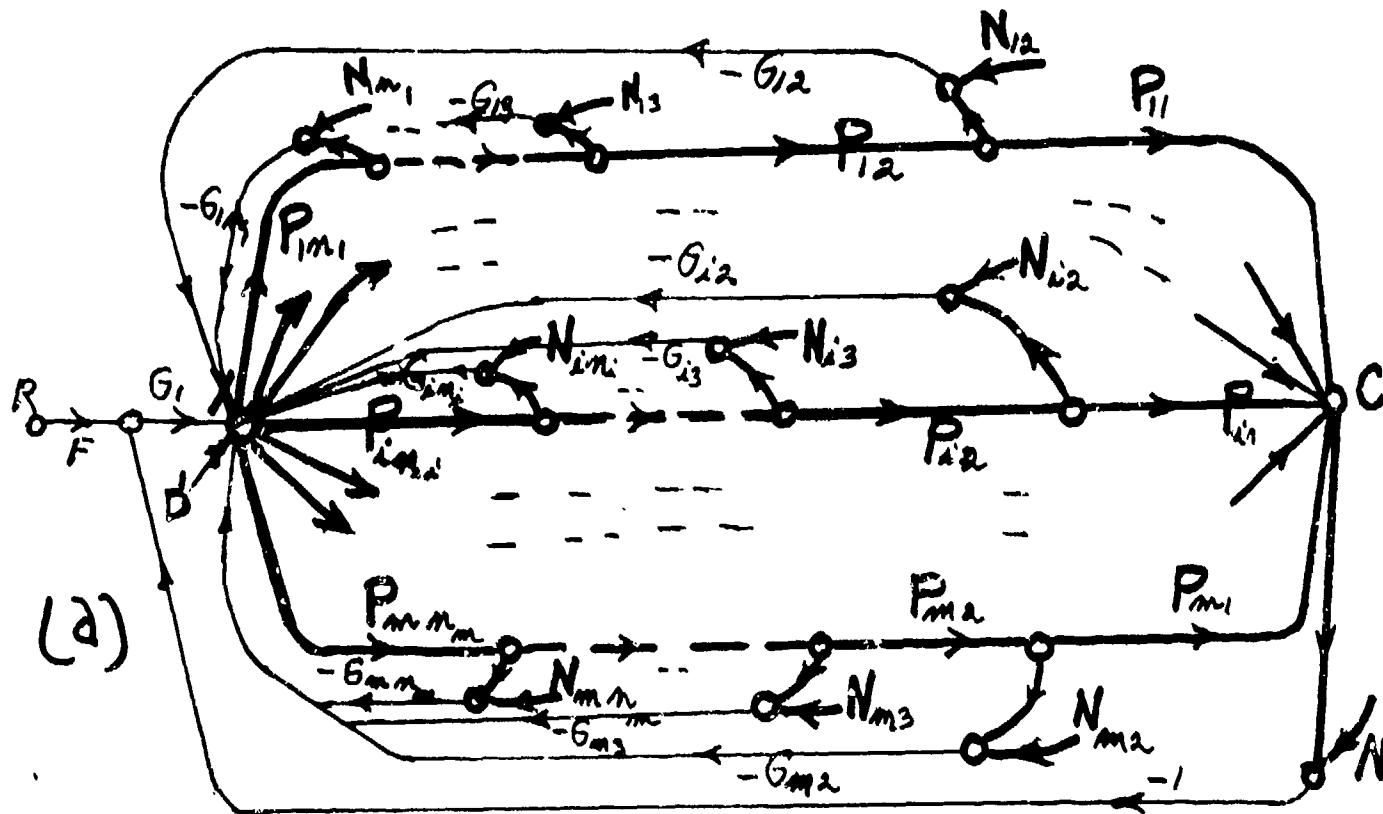


Figure 2a. The parallel-cascade structure.

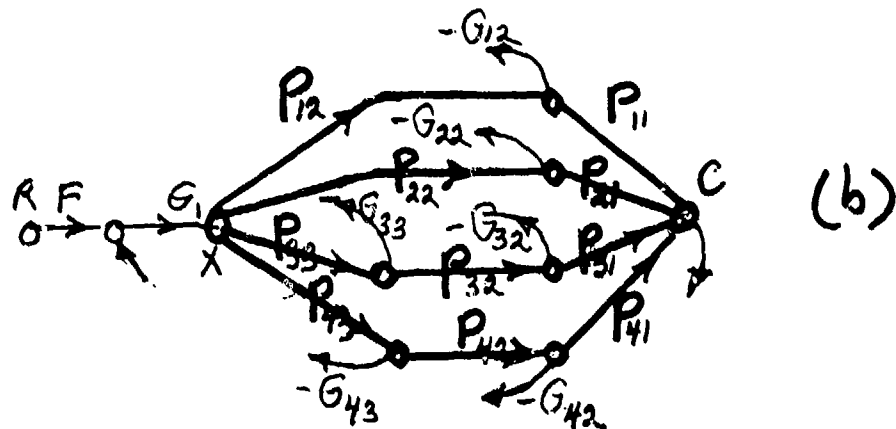


Figure 2b. Structure for Example 5.

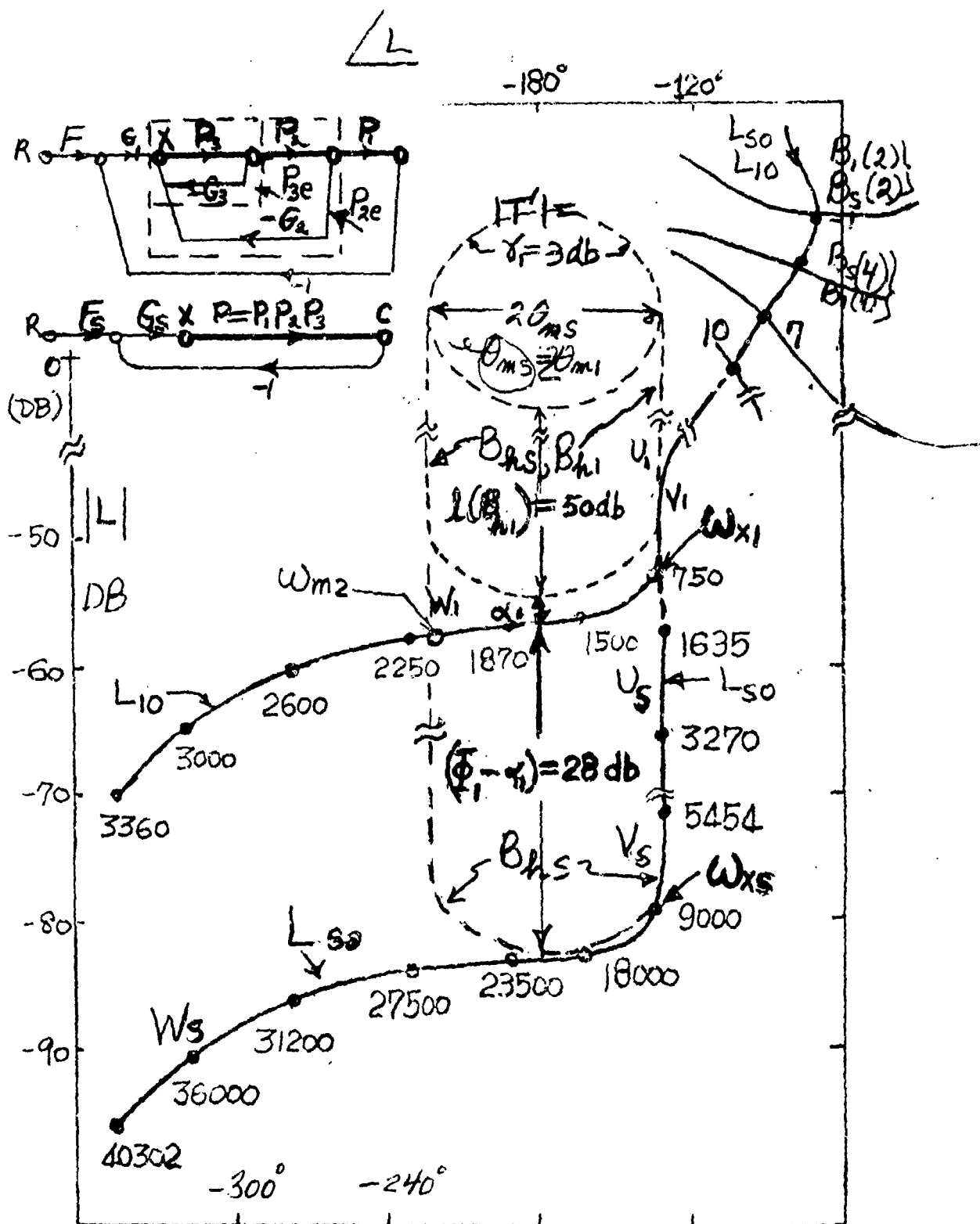


Figure 3. Example 1. Bounds $B_S(\omega)$, $B_1(\omega)$ on L_{50} , L_{10} and designs on Nichols chart.

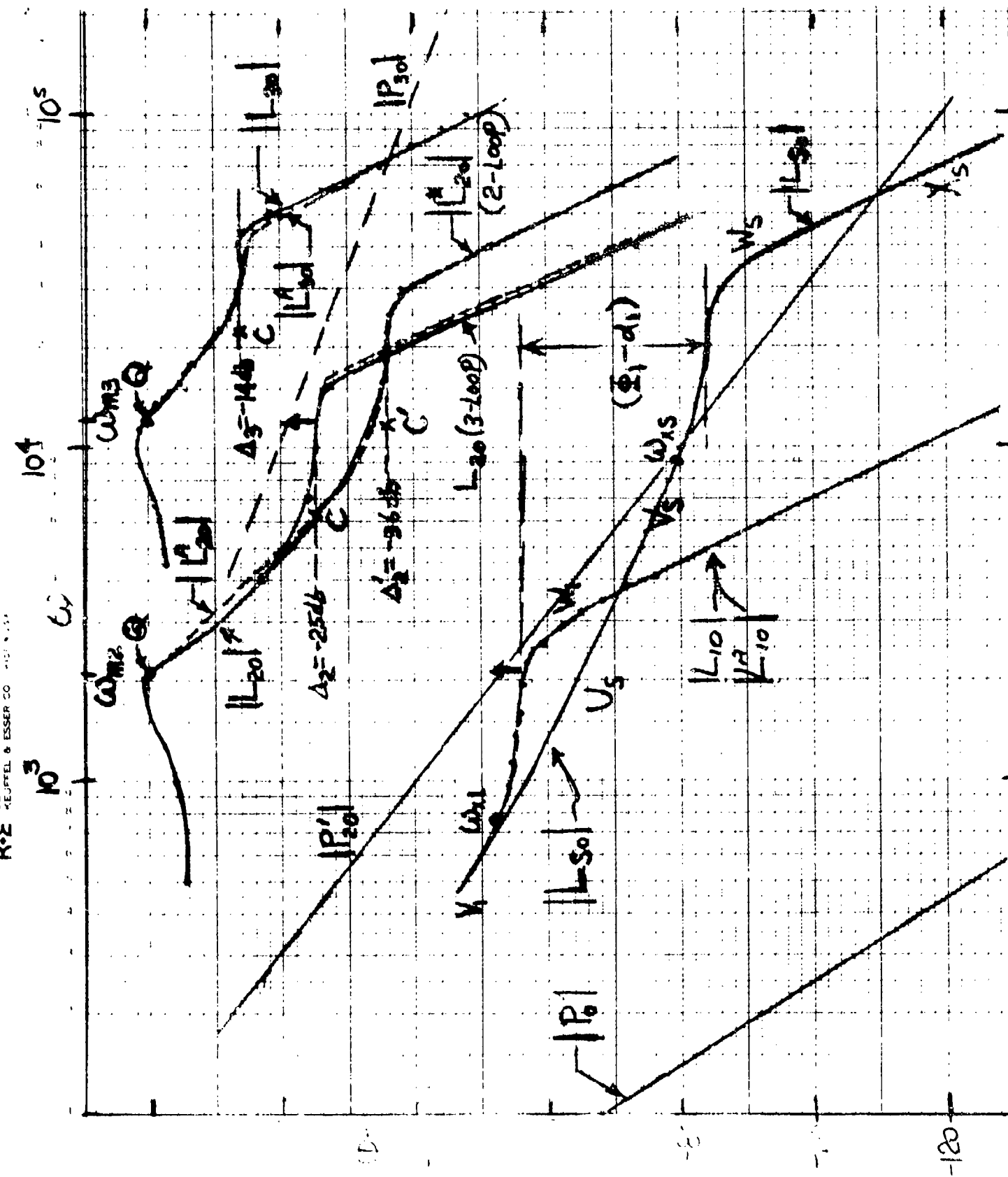


Figure 4. Example 1. Comparison of Design Perspective (dashed) and exact designs.

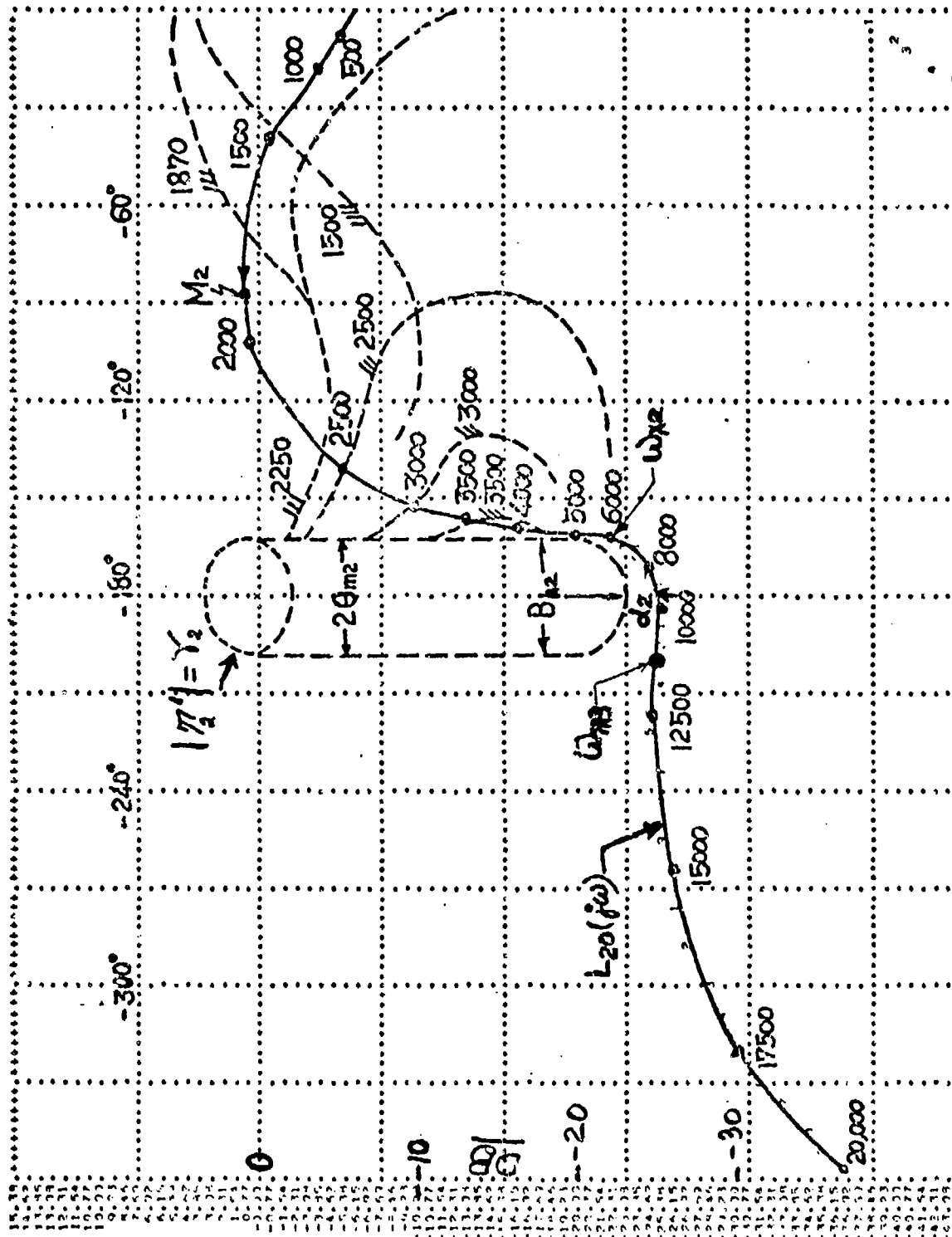


Figure 5a. Example 1. Bounds $B_2(\omega)$ on L_{20} and exact design on Nichols chart.

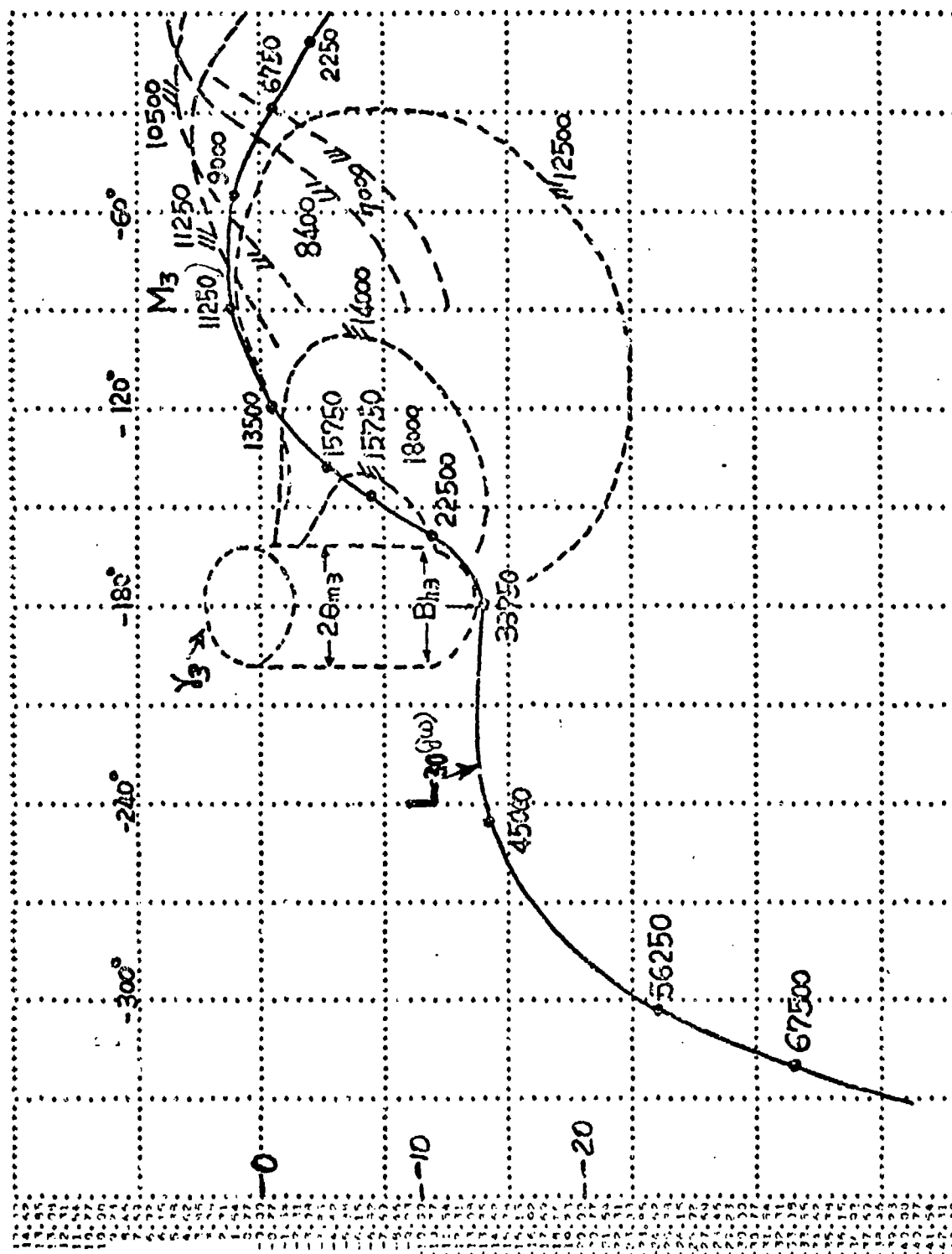
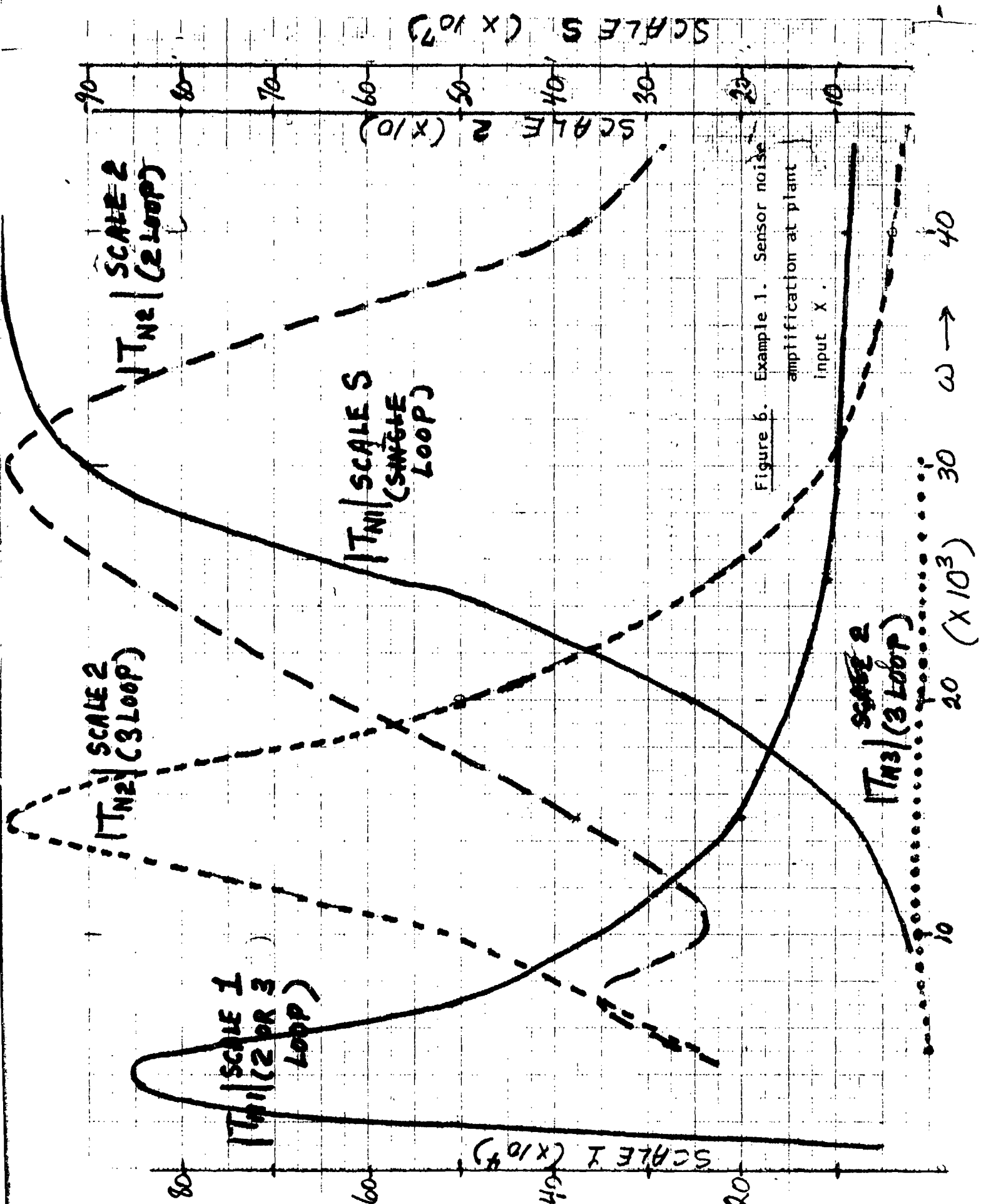
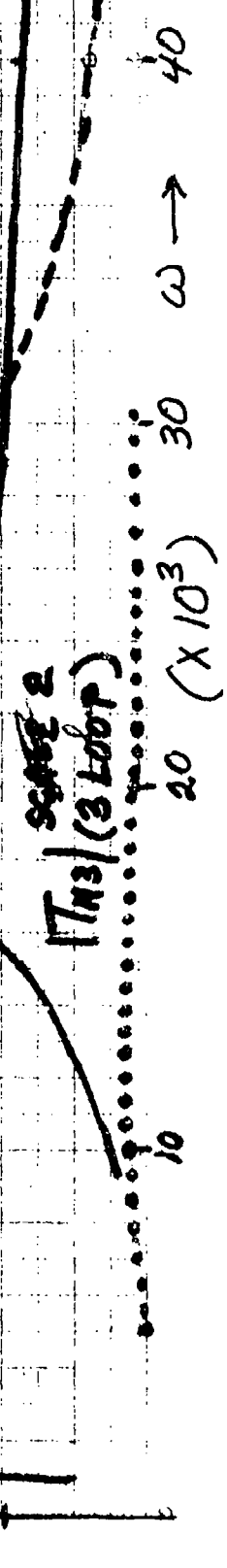


Figure 5b. Example 1. Bounds $B_3(\omega)$ on L_{30} and exact design on Nichols chart.

Figure 6. Example 1. Sensor noise

amplification at plant

input X



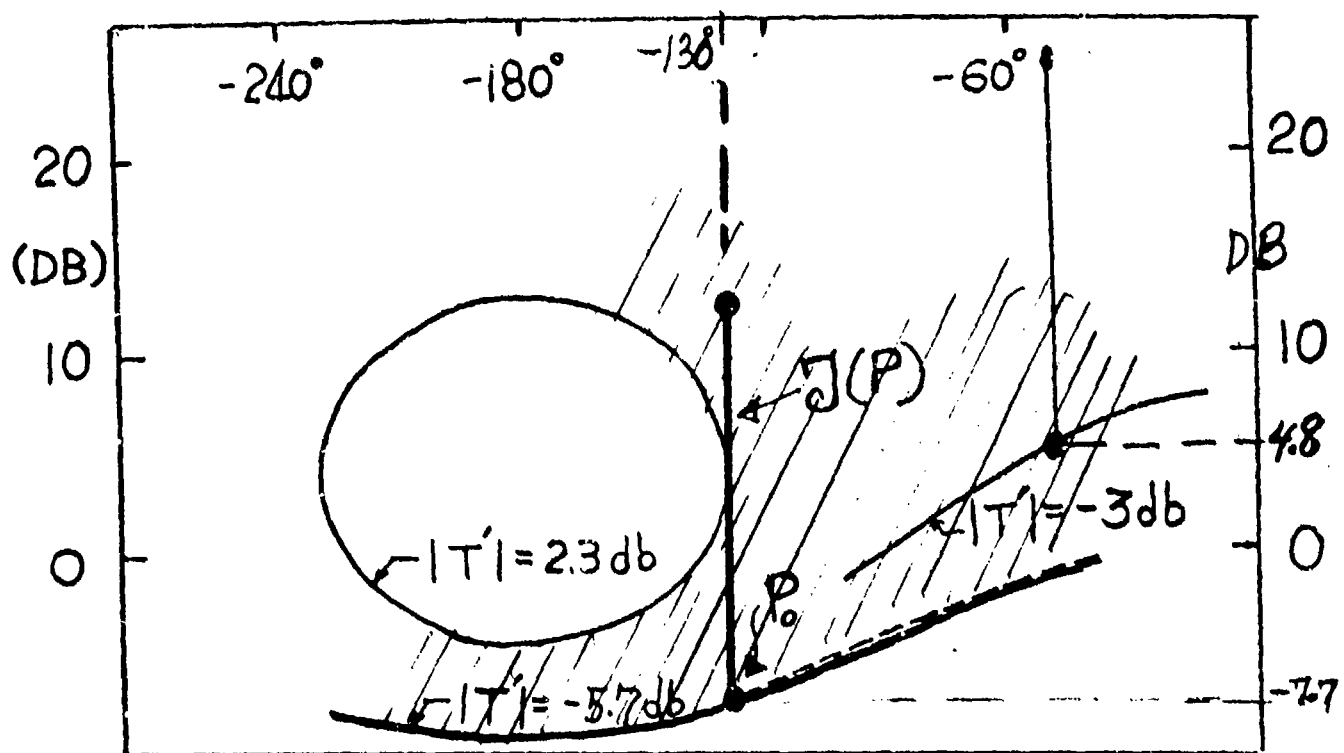


Figure 7a. The minor saving at low frequencies due to multiple-loop design.

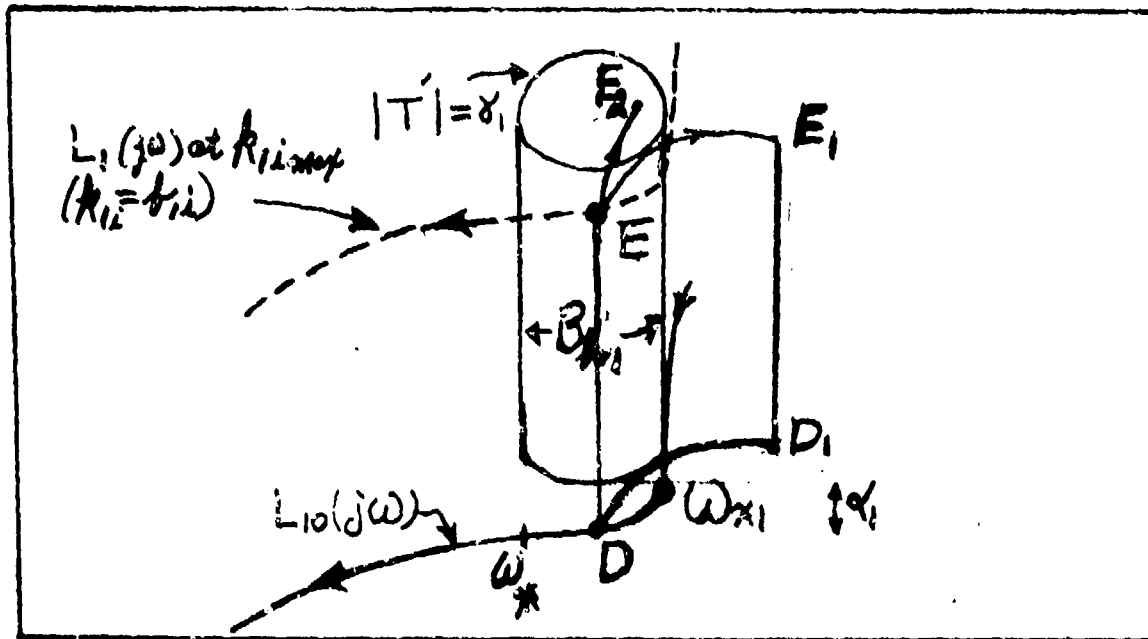


Figure 7b. Need for overdesign of outer loop in (ω_{x_1}, ω_x) — cascade structure.

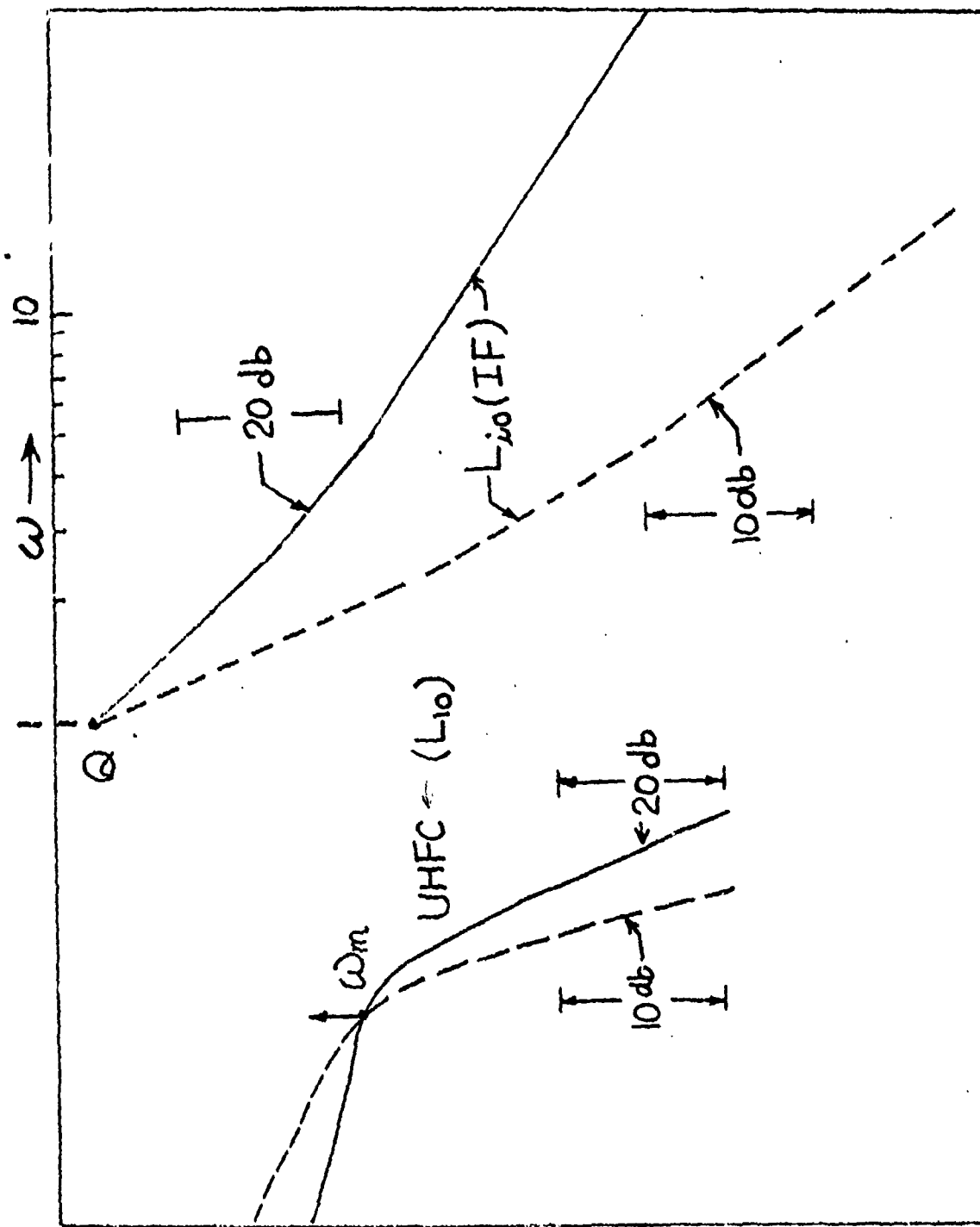


Figure 8a. Design Perspective: Universal outer loop high frequency (UHFC) and intermediate frequency (IF) characteristics.

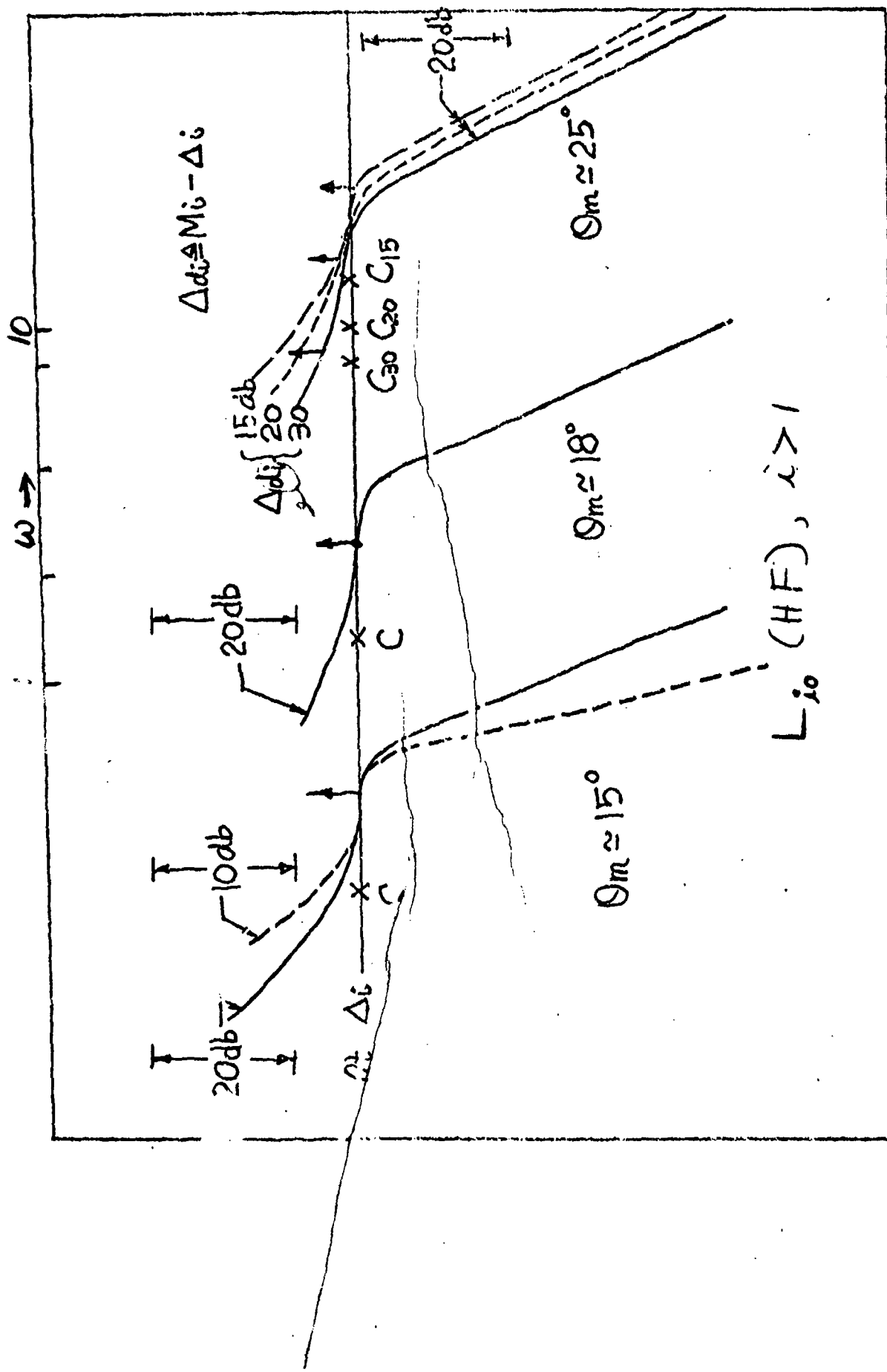


Figure 8b. UHFC for inner loop.

M_i peak value (db)

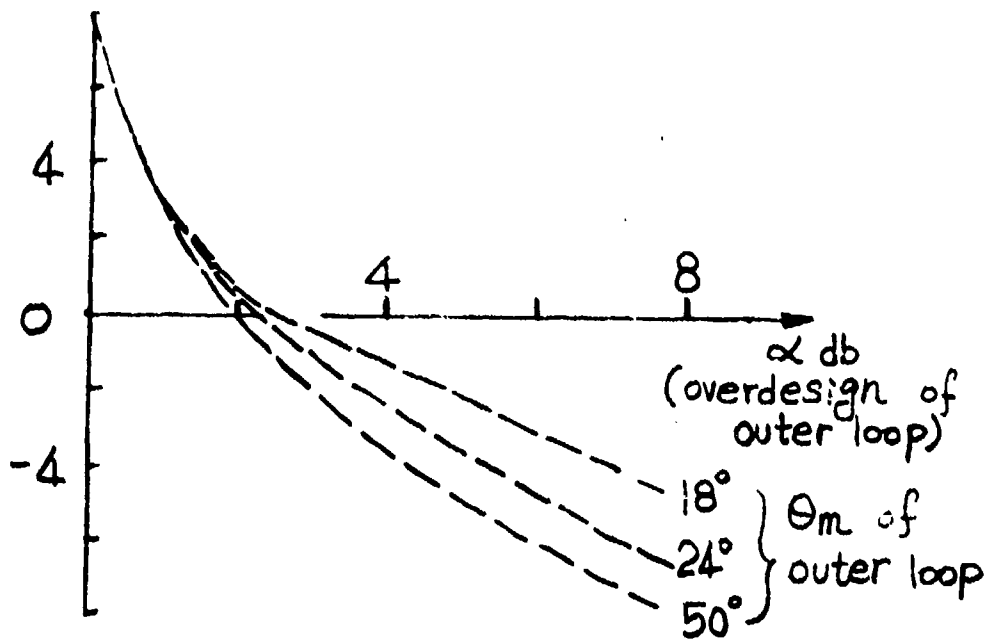


Figure 8c. Peak values M_i of $|L_{i_0}(j\omega)|$ (at ω_{mi}) - Cascade structure.

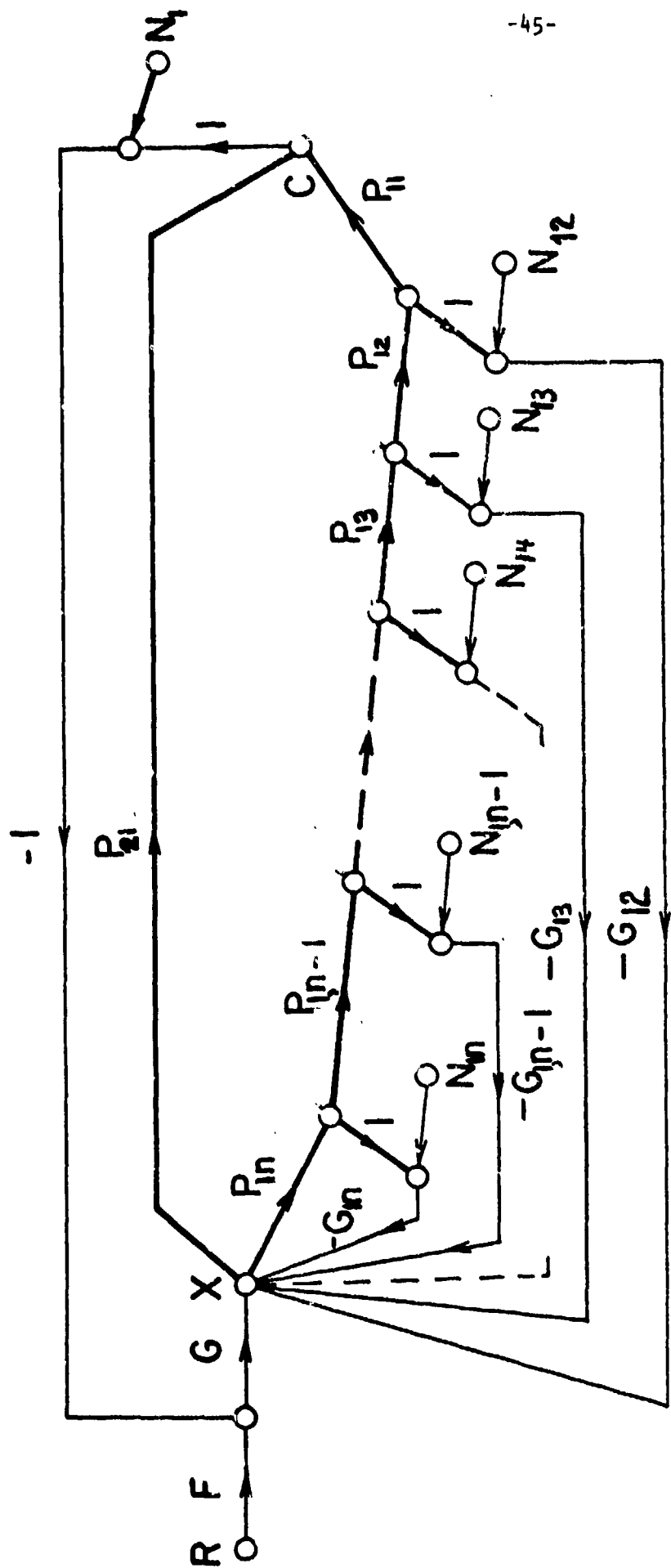


Figure 9. Example 2. Special case of Figure 1b. ($P_a = P_{11}P_{12}\dots P_{1n}$)

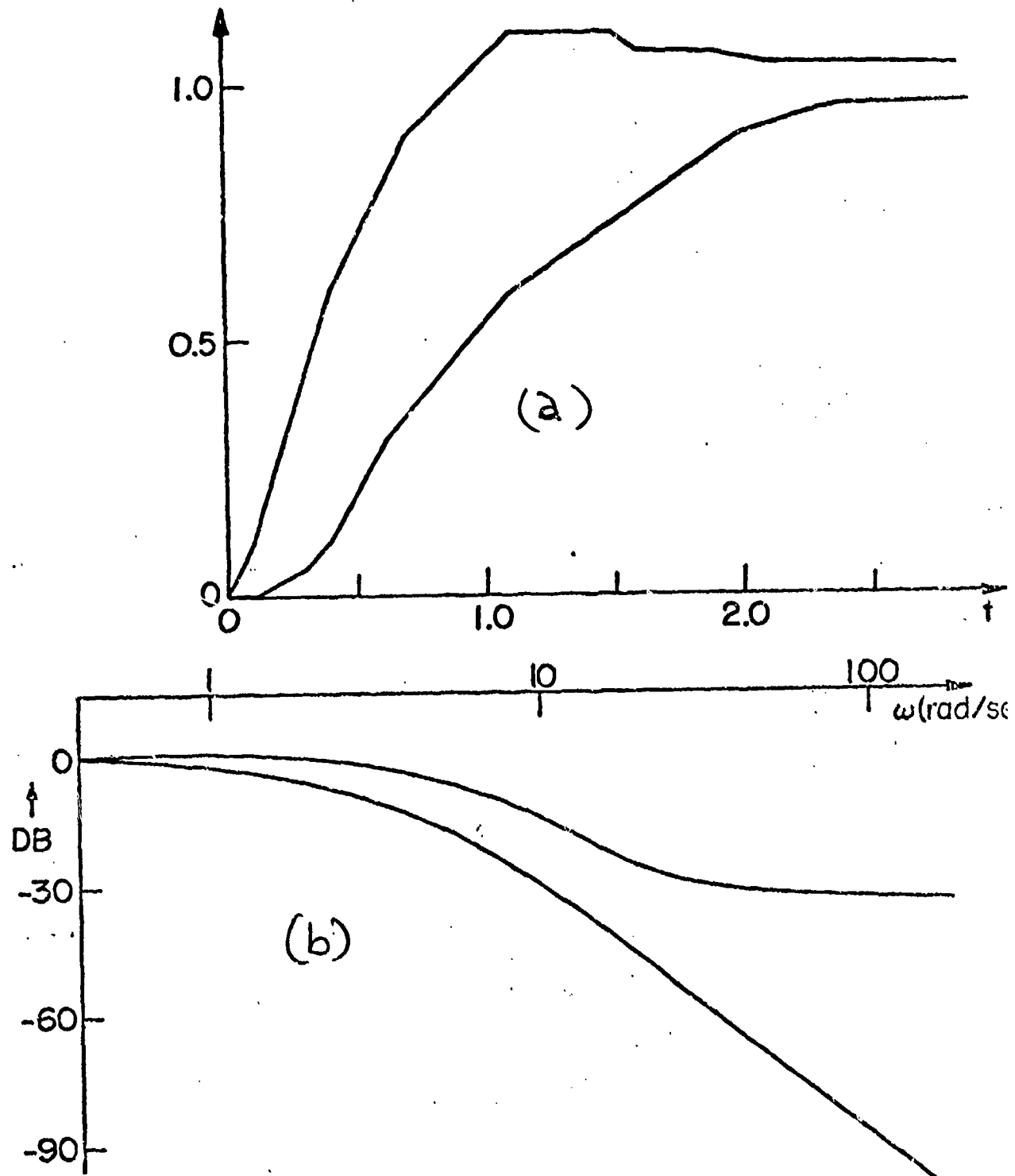


Figure 10a. Example 2. Specified time-domain tolerances on step response.

Figure 10b. Derived "equivalent" ω -domain tolerances.

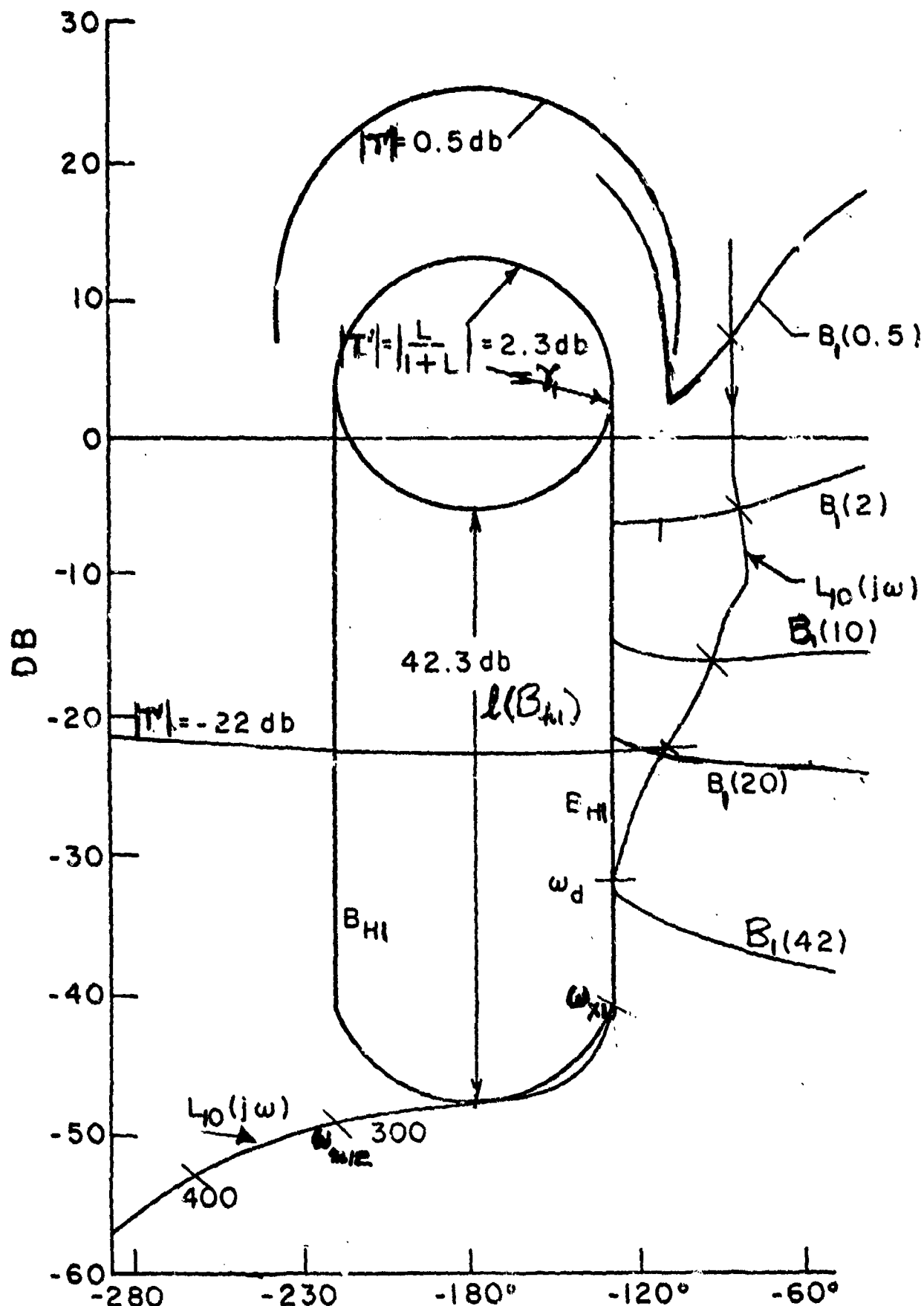


Figure 11a. Example 2. Bounds $B_1(\omega)$ on L_{10} on Nichols chart.

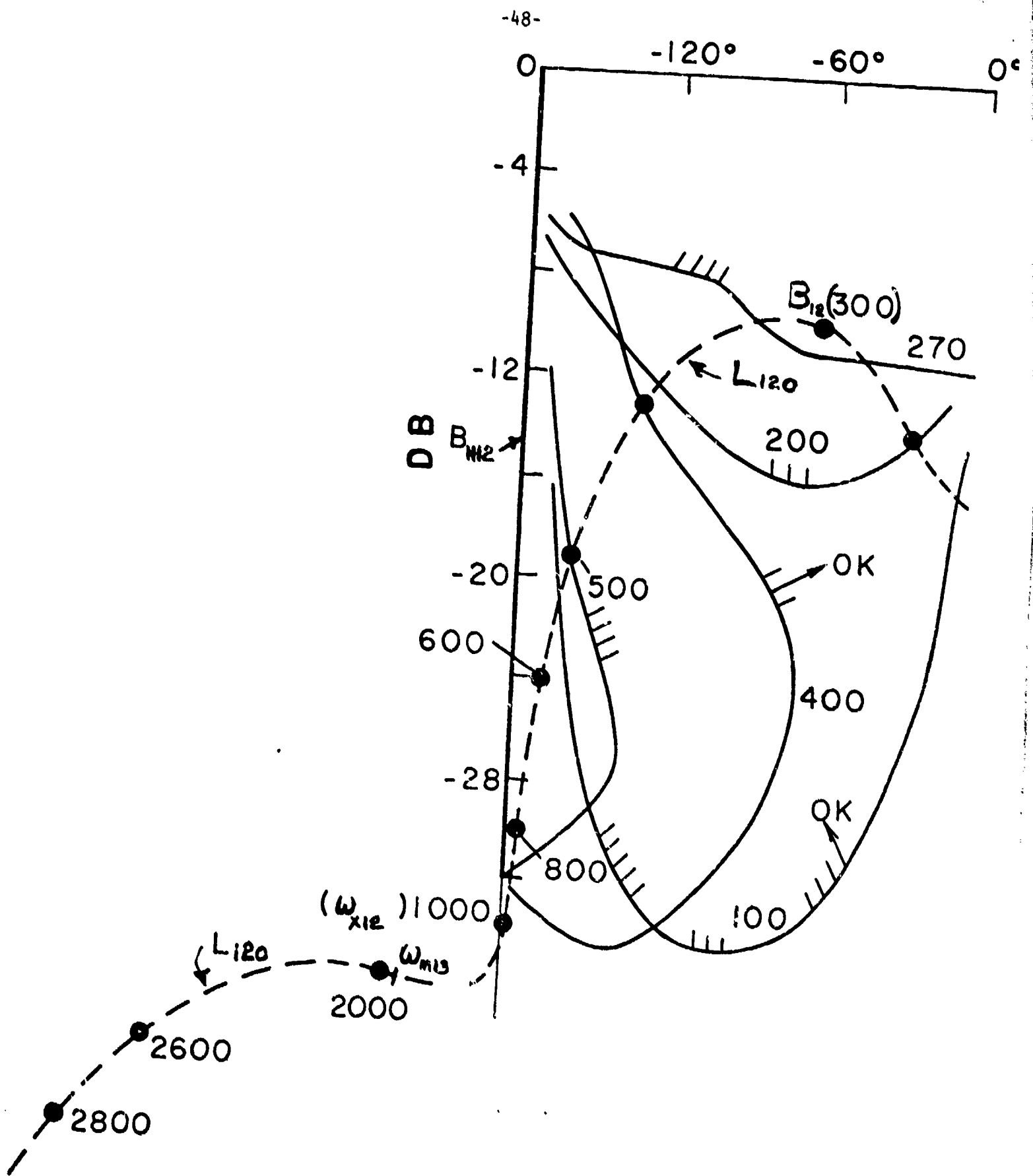


Figure 11b. Example 2. Bounds $B_{12}(\omega)$ on L_{120}

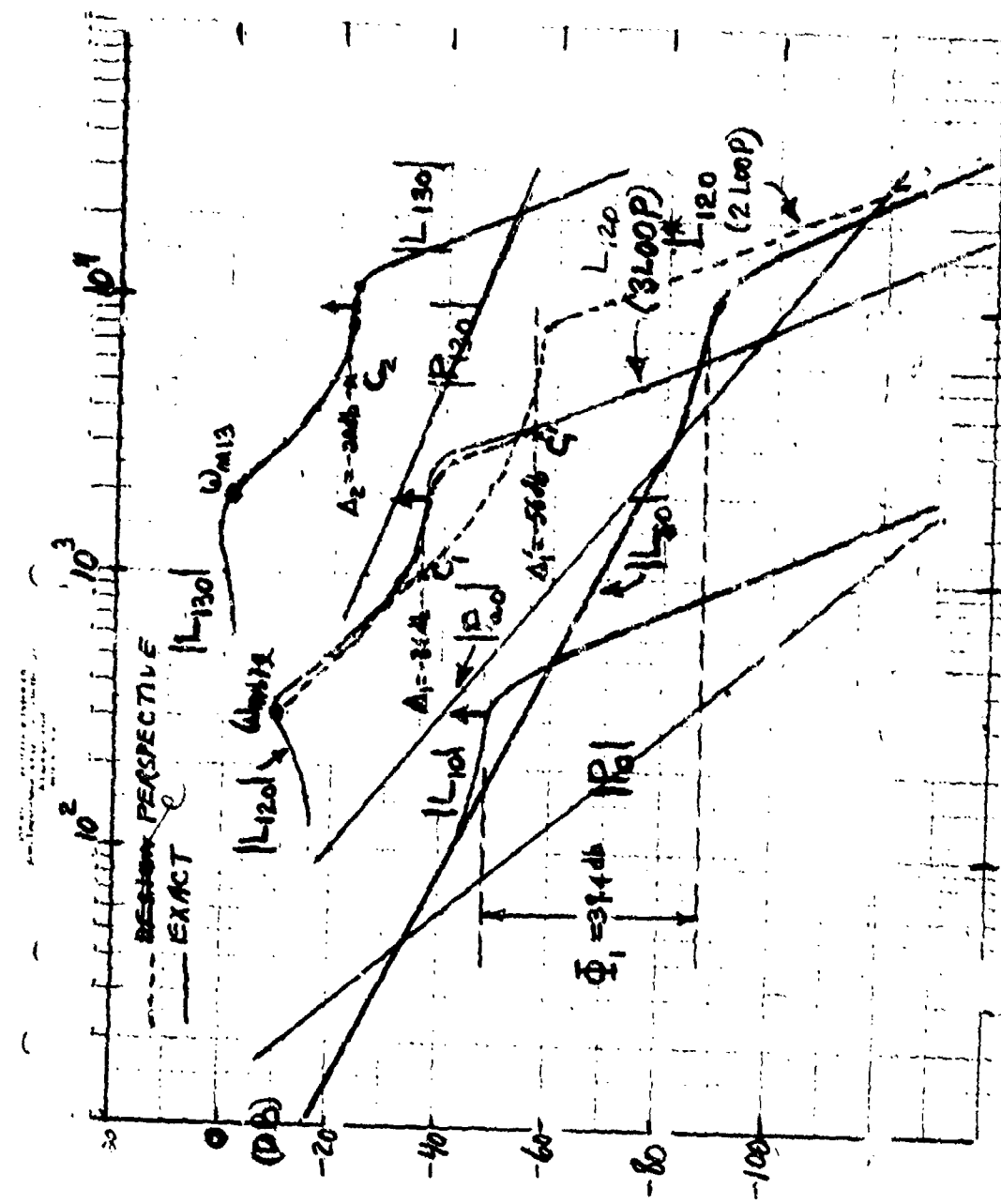
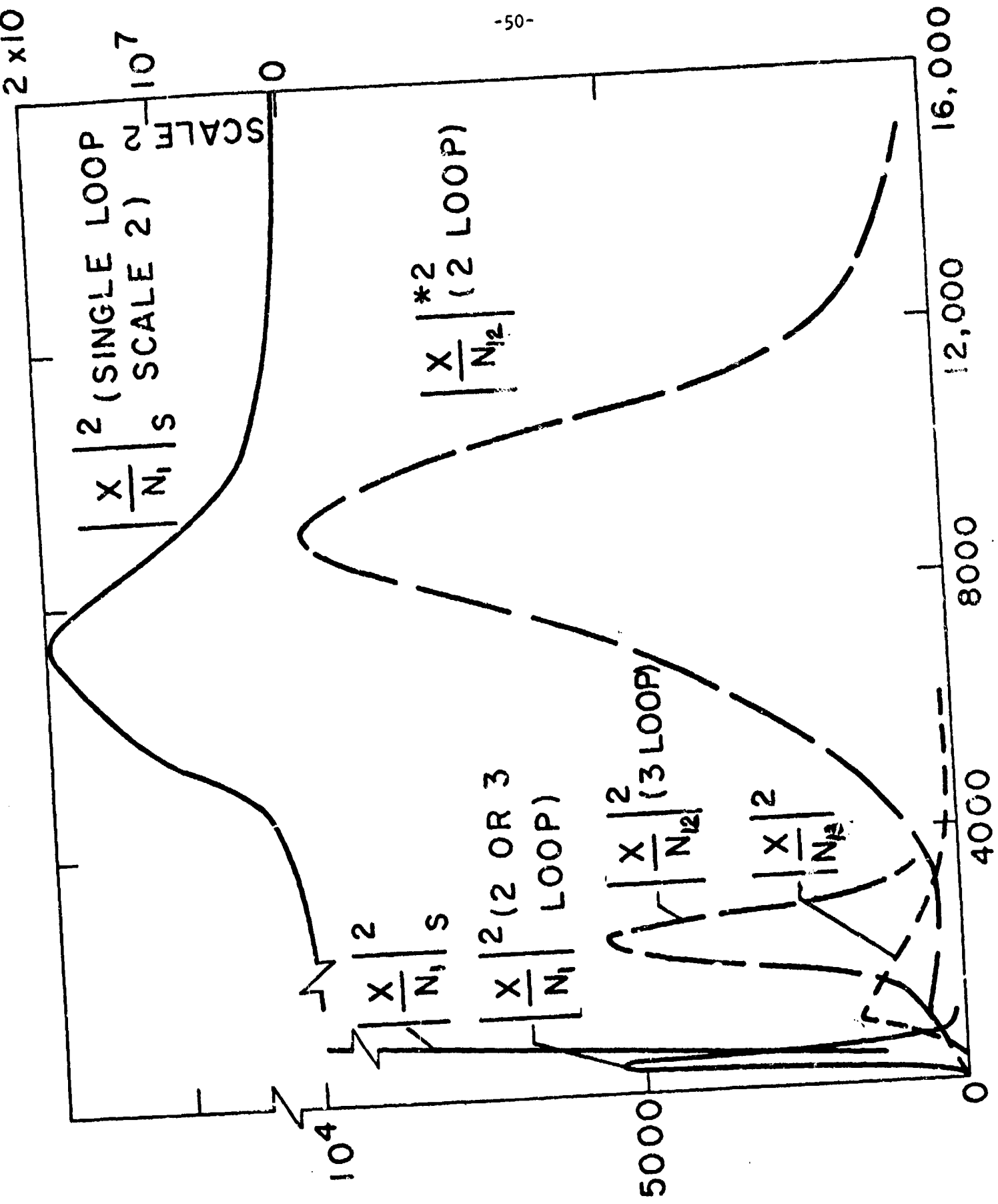


Figure 12. Example 2. Design perspective (dashed) and exact design.



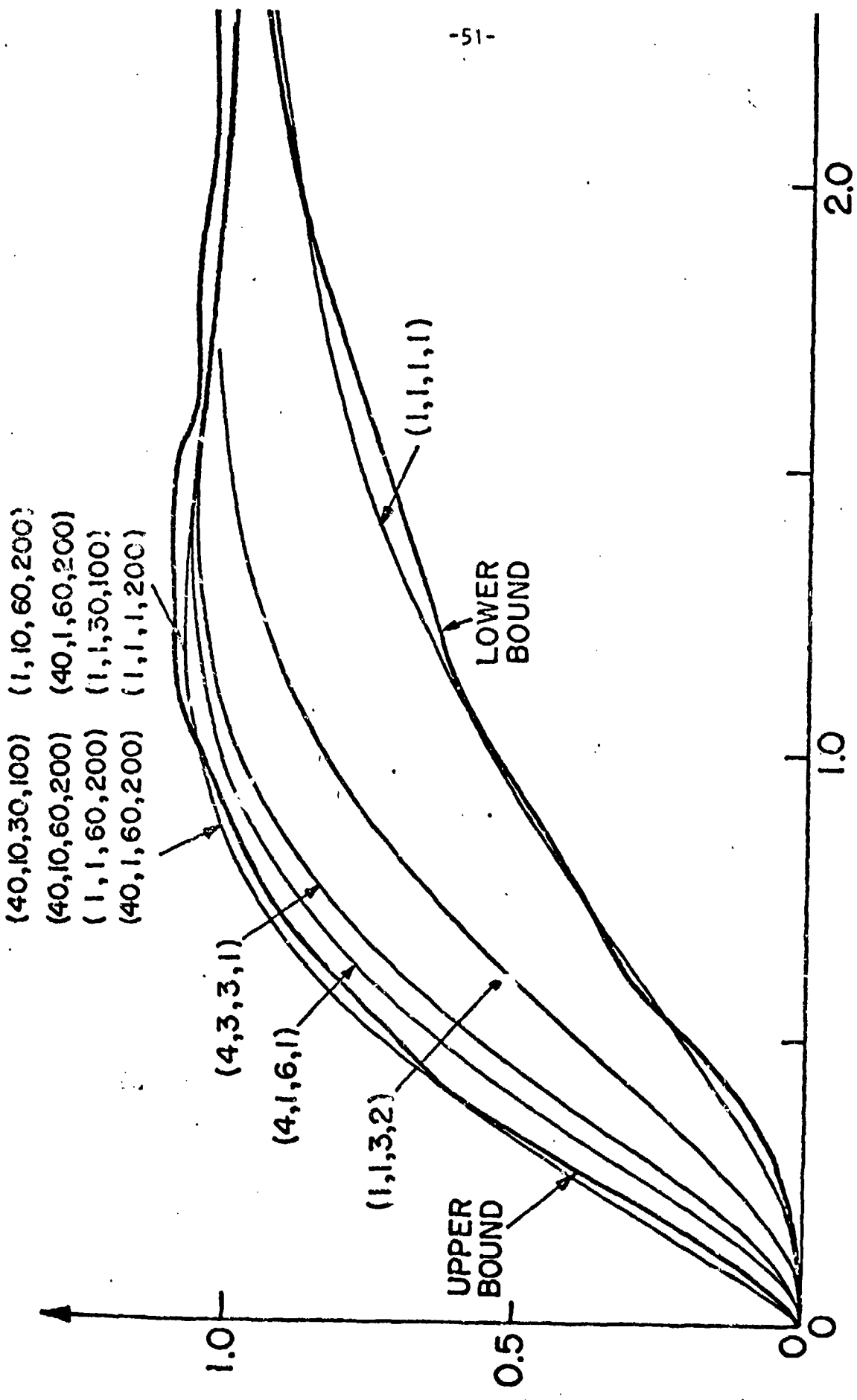


Figure 14a. Example 2. Design simulation results for various parameter combinations. Step response.

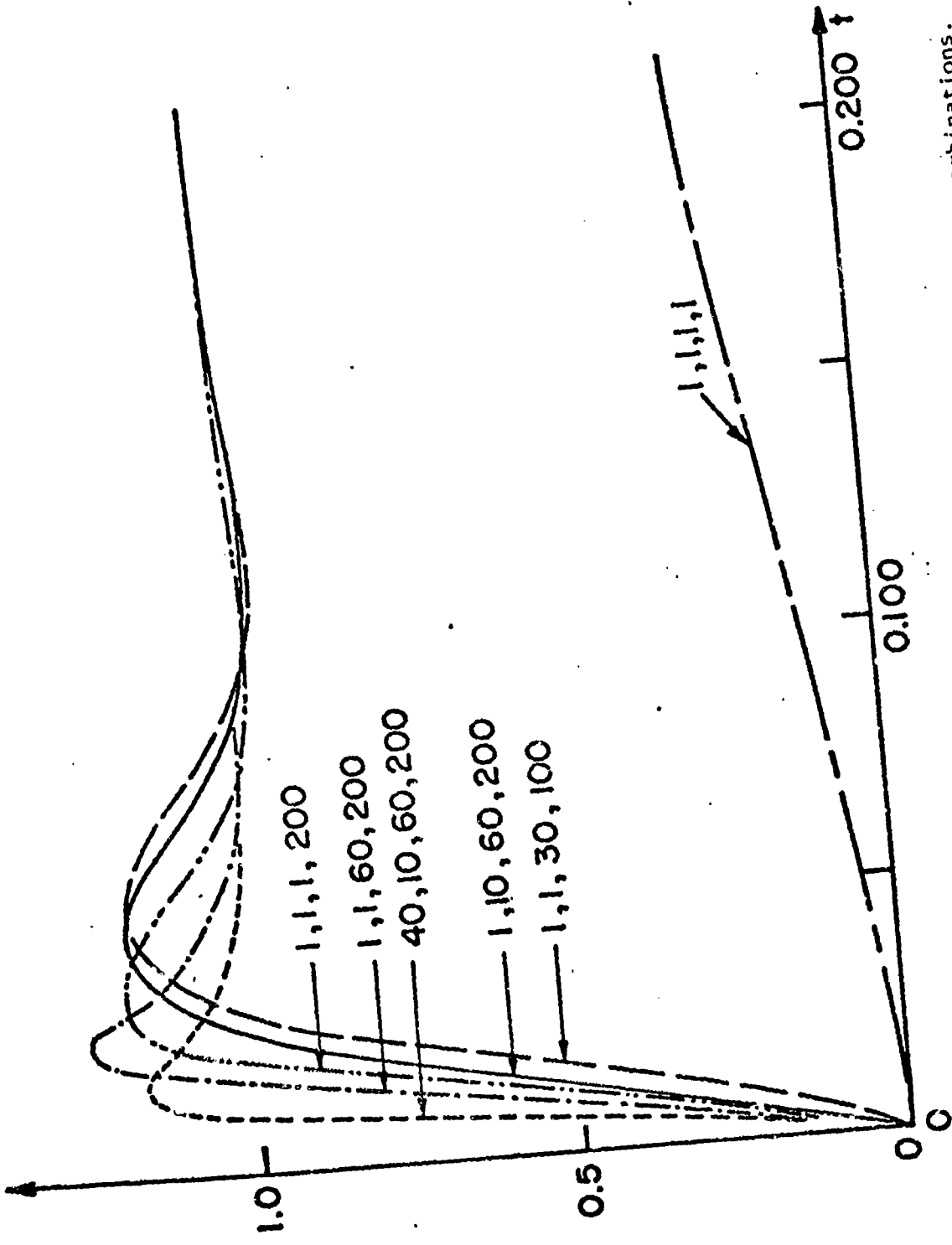


Figure 14b. Example 2. Design simulation results for various parameter combinations.
Figure 14b. Disturbance response.

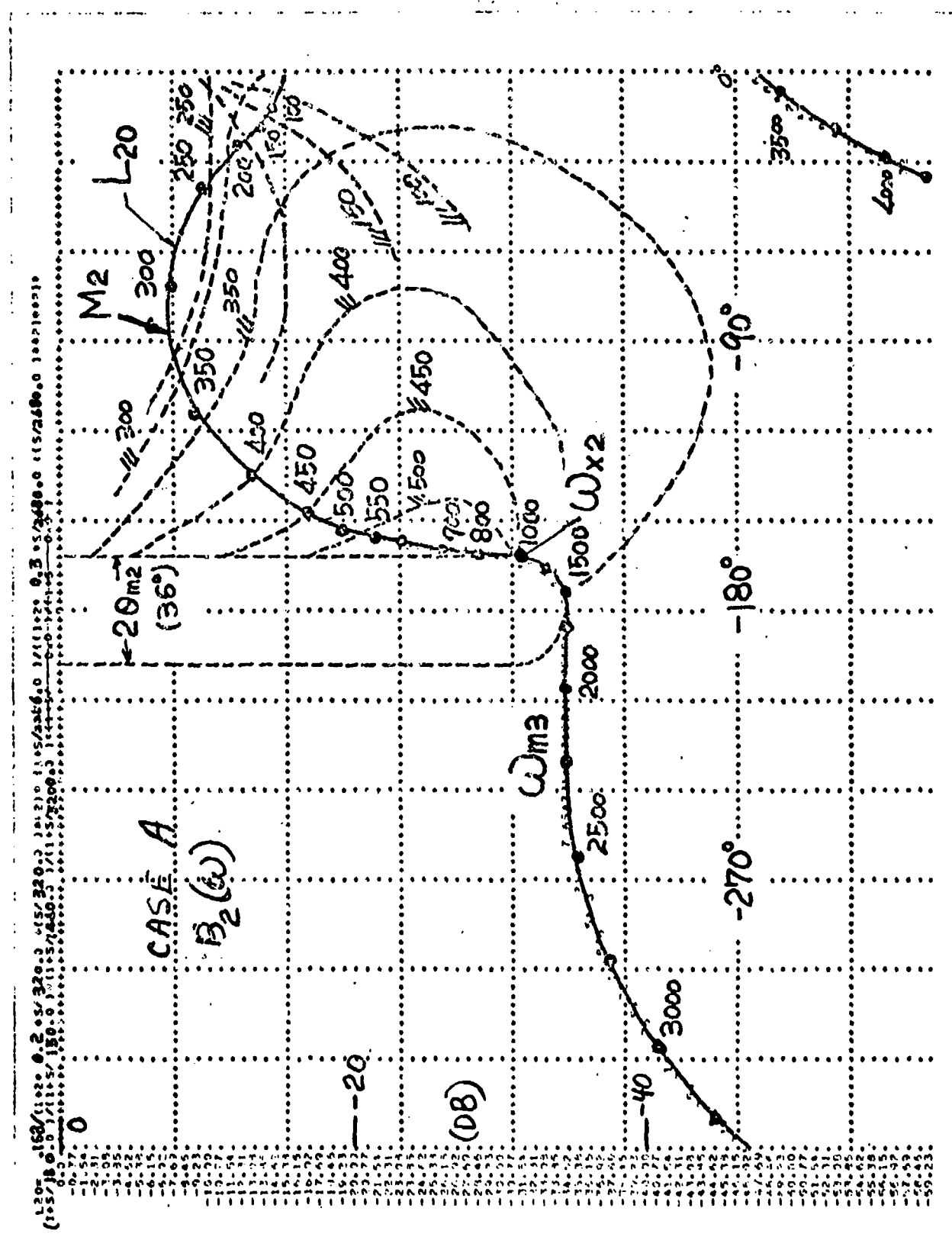


Figure 15a. Example 3. Case A. Bounds $\beta_2(\omega)$ on Nichols chart.

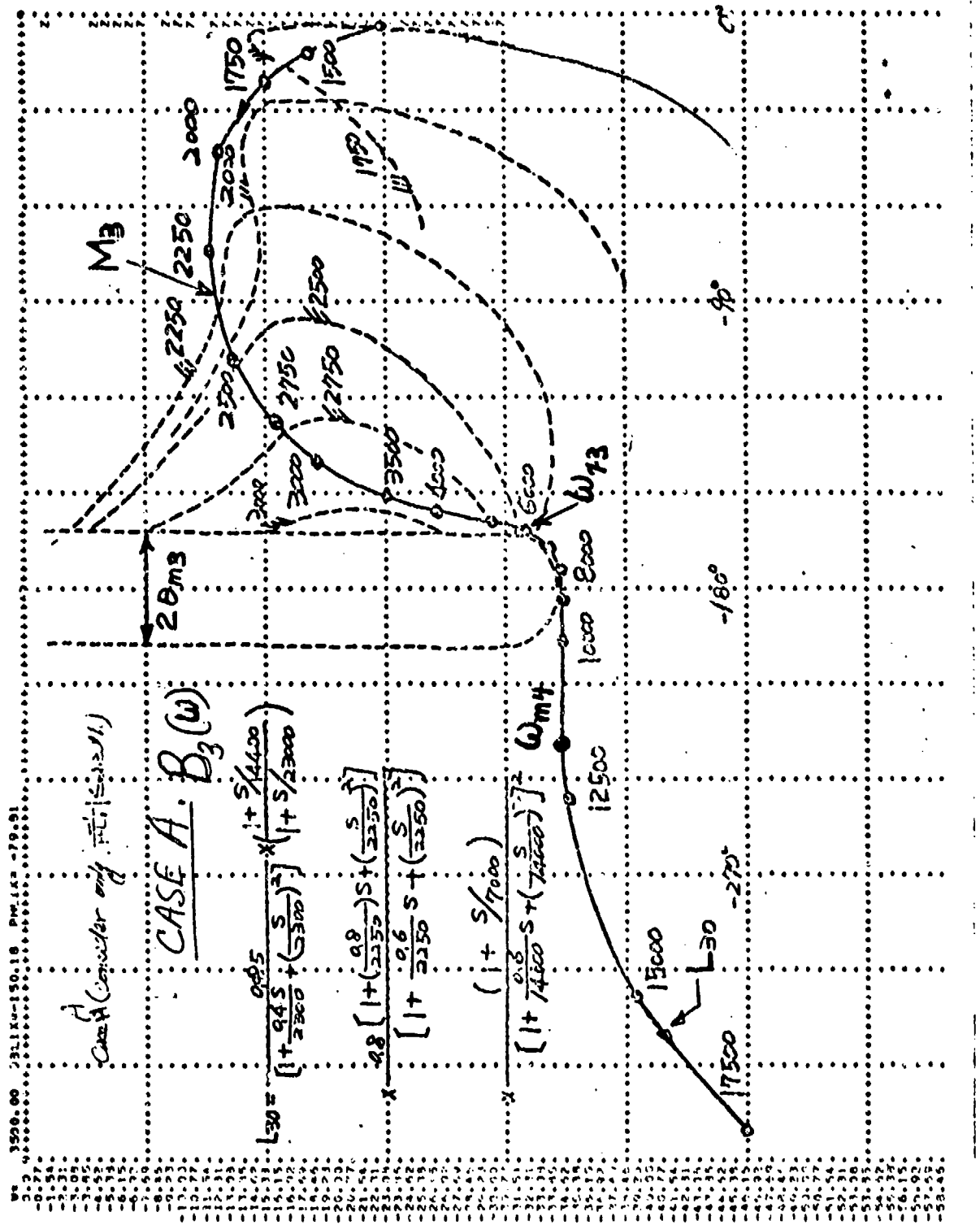


Figure 15b. Example 3. Case A. Bounds $B_3(\omega)$ on Nichols chart.

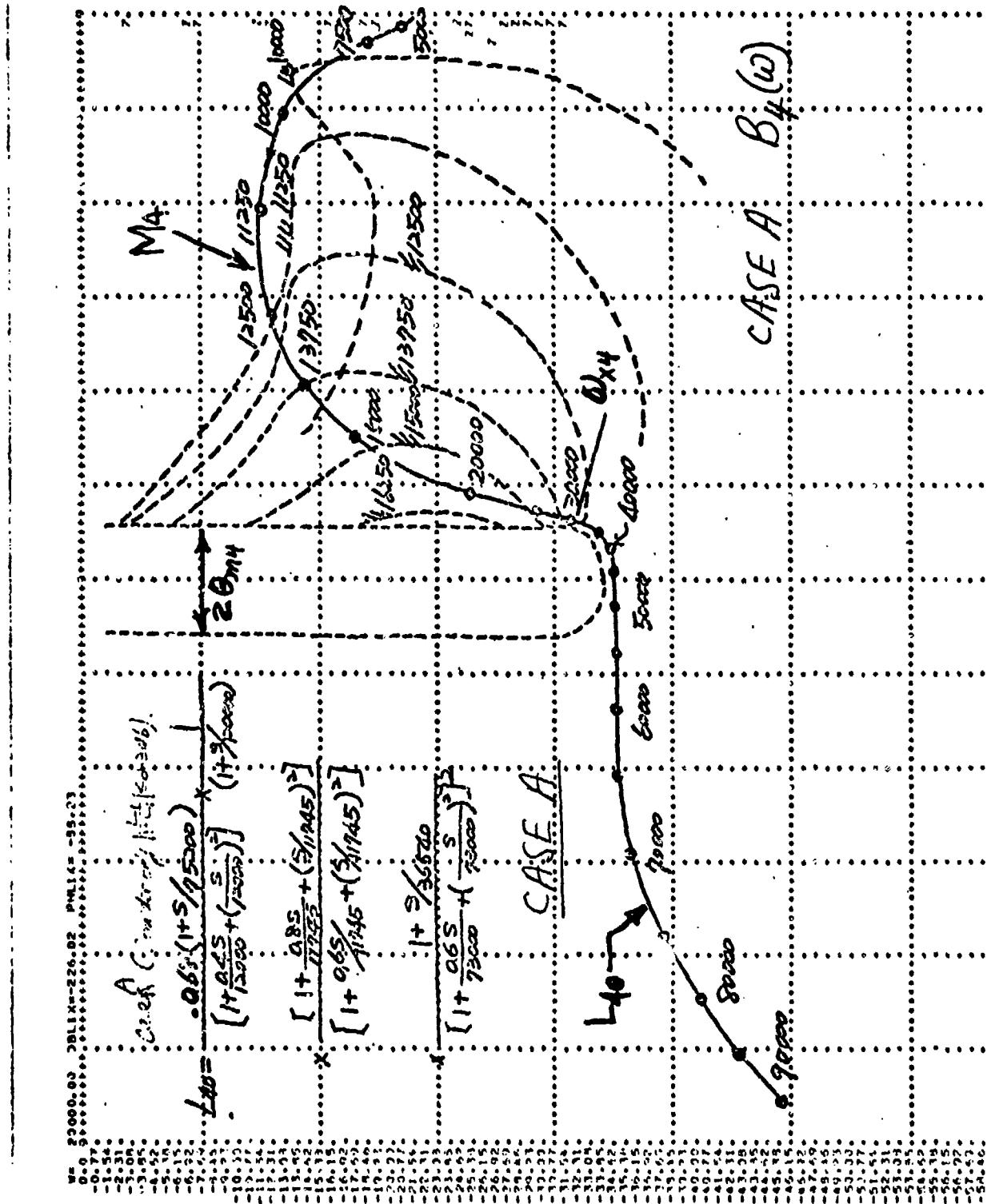
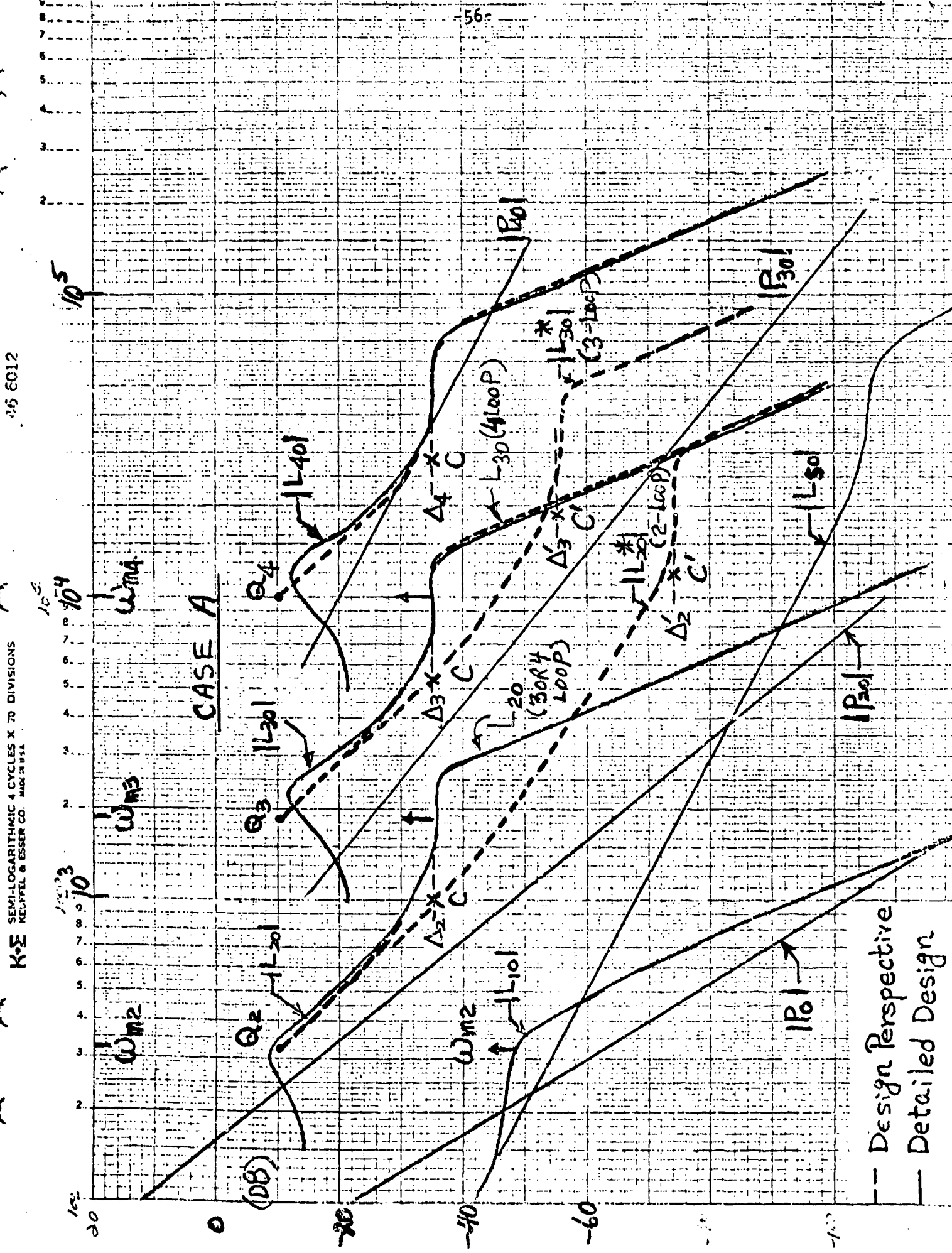
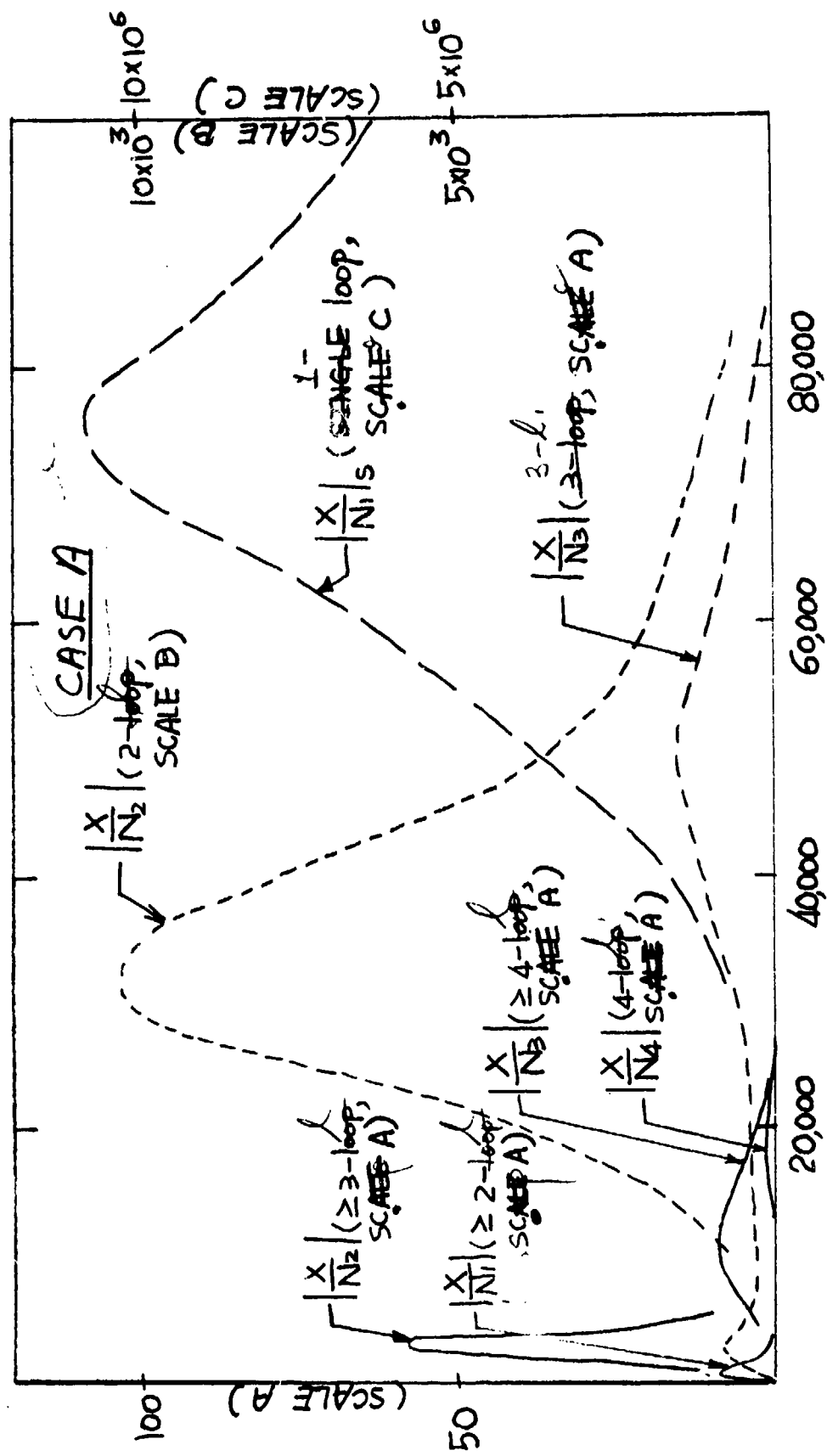


Figure 15c. Example 3. Case A. Bounds $B_4(\omega)$ on Nichols chart.





Example 16b. Example 3. Case A. Sensor noise amplification at plant input X .

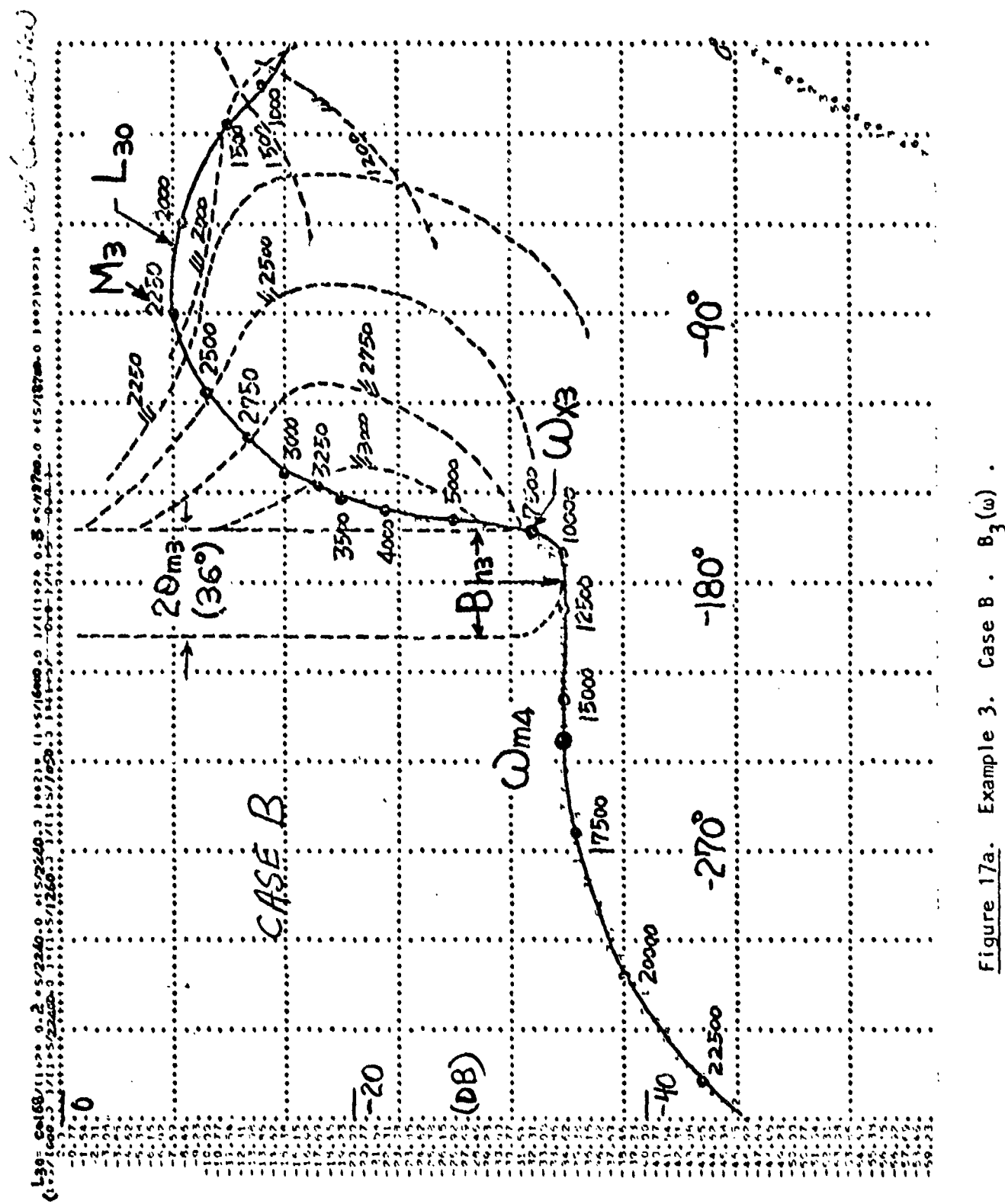


Figure 17a. Example 3. Case B . $B_3(\omega)$.

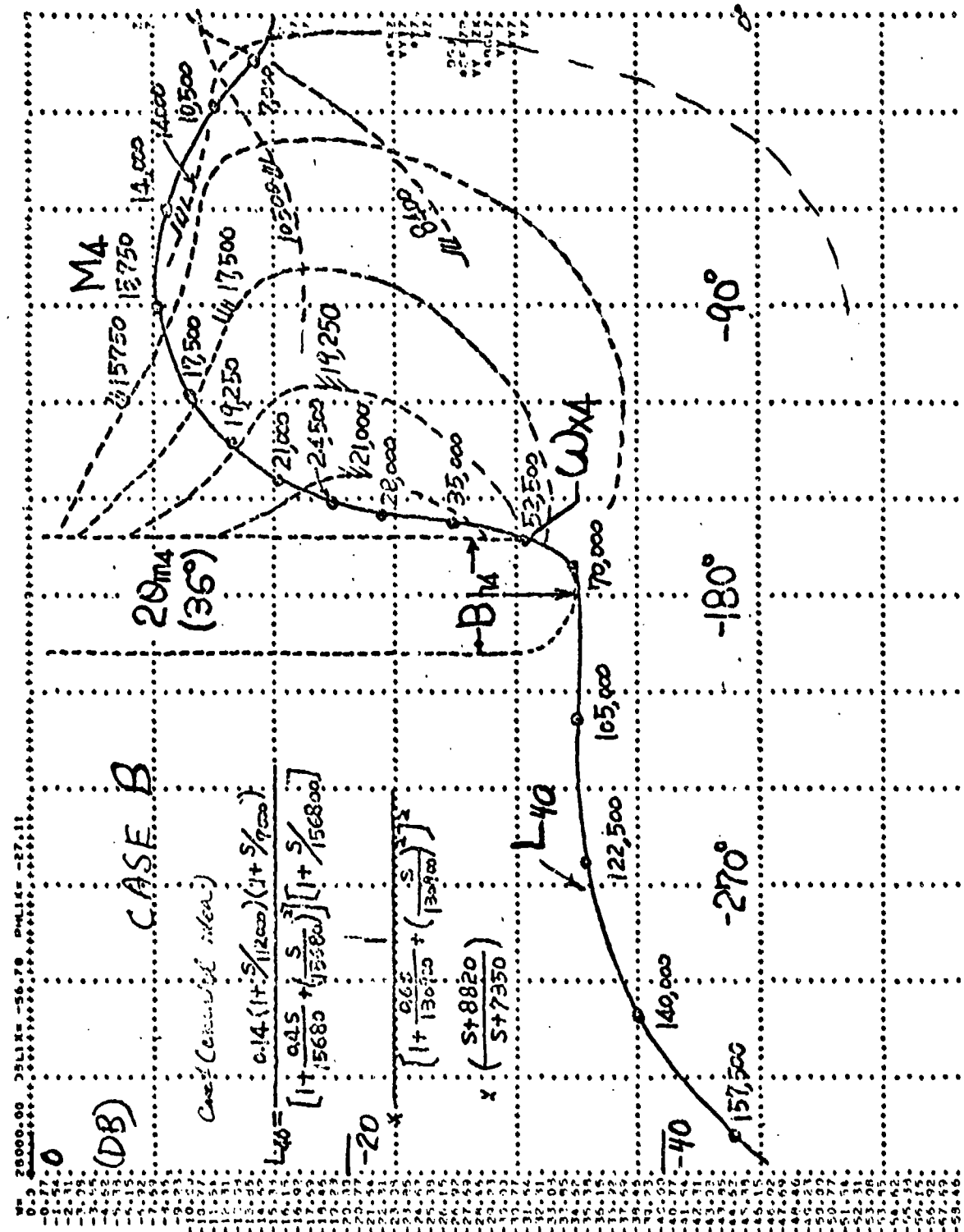


Figure 17b. Example 3. Case 3. $B_4(w)$.

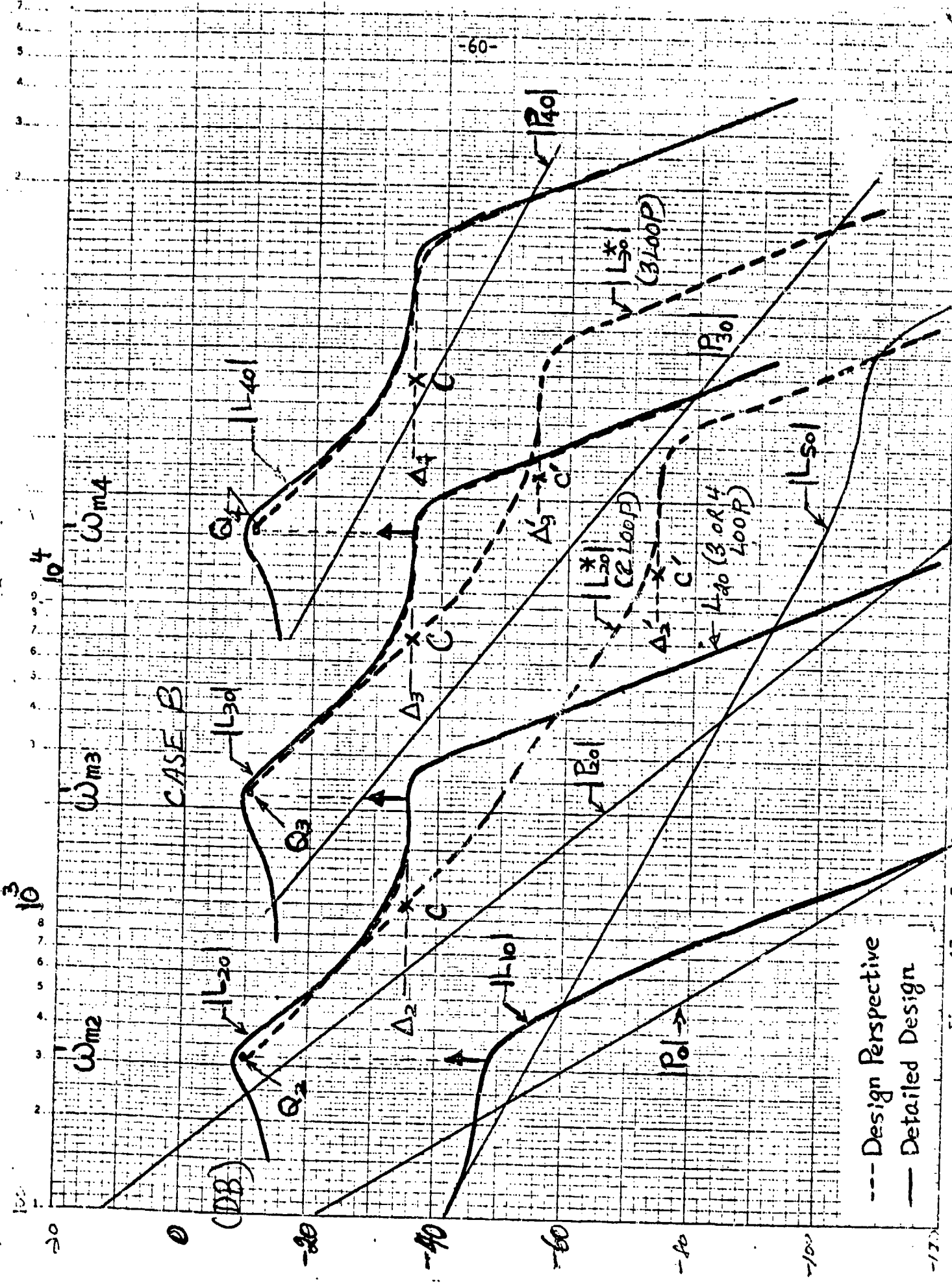


Figure 17c. Example 3. Case B. Design Perspective (dashed) and exact design.

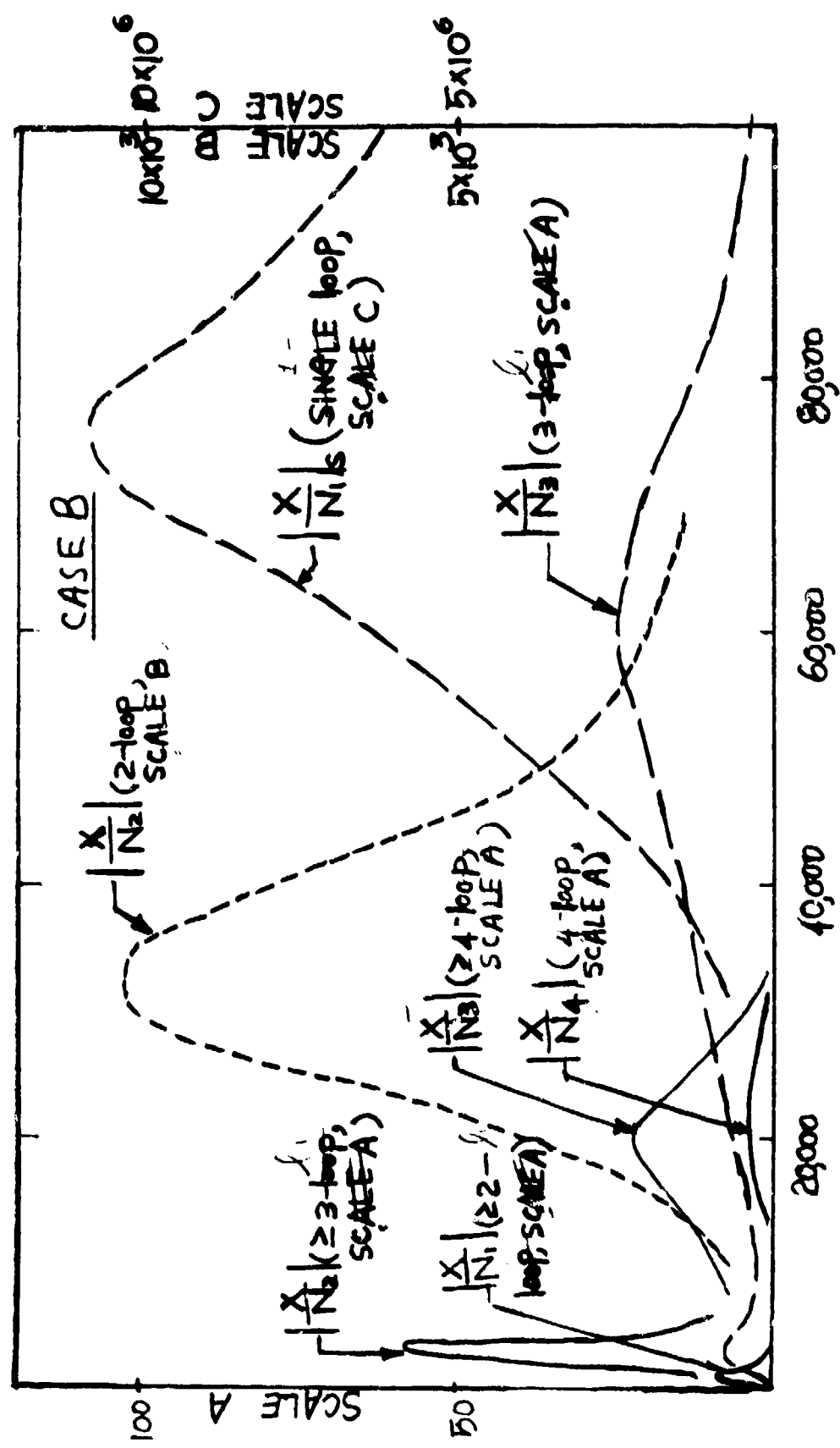


Figure 17d. Example 3. Case B. Sensor noise amplification at plant input X .

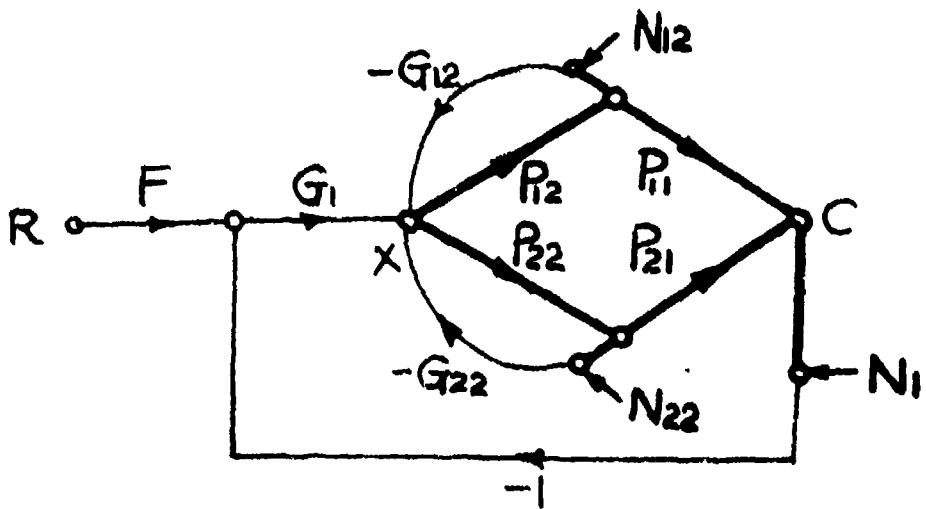


Figure 18. The elementary parallel-cascade structure.

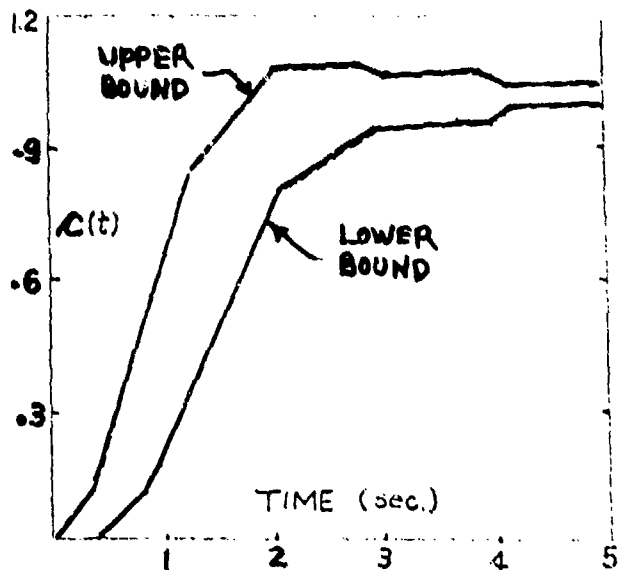


Figure 19a. Specified time domain bounds on step response.

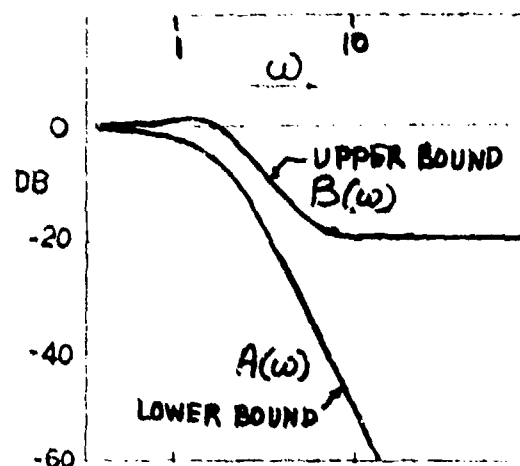


Figure 19b. "Equivalent" frequency-domain bounds.

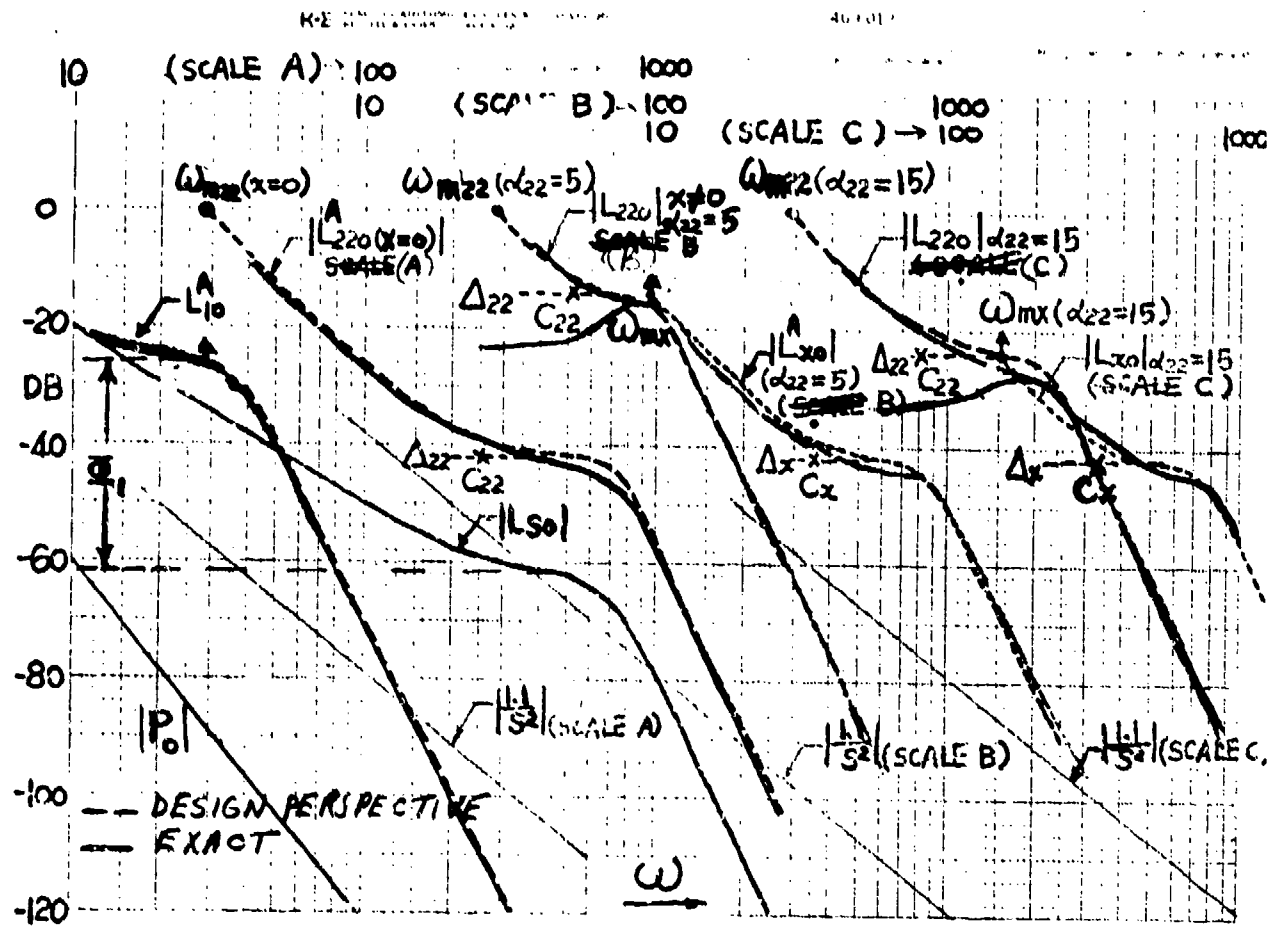


Figure 20a. Example 4. Design Perspective (dashed) and exact design.

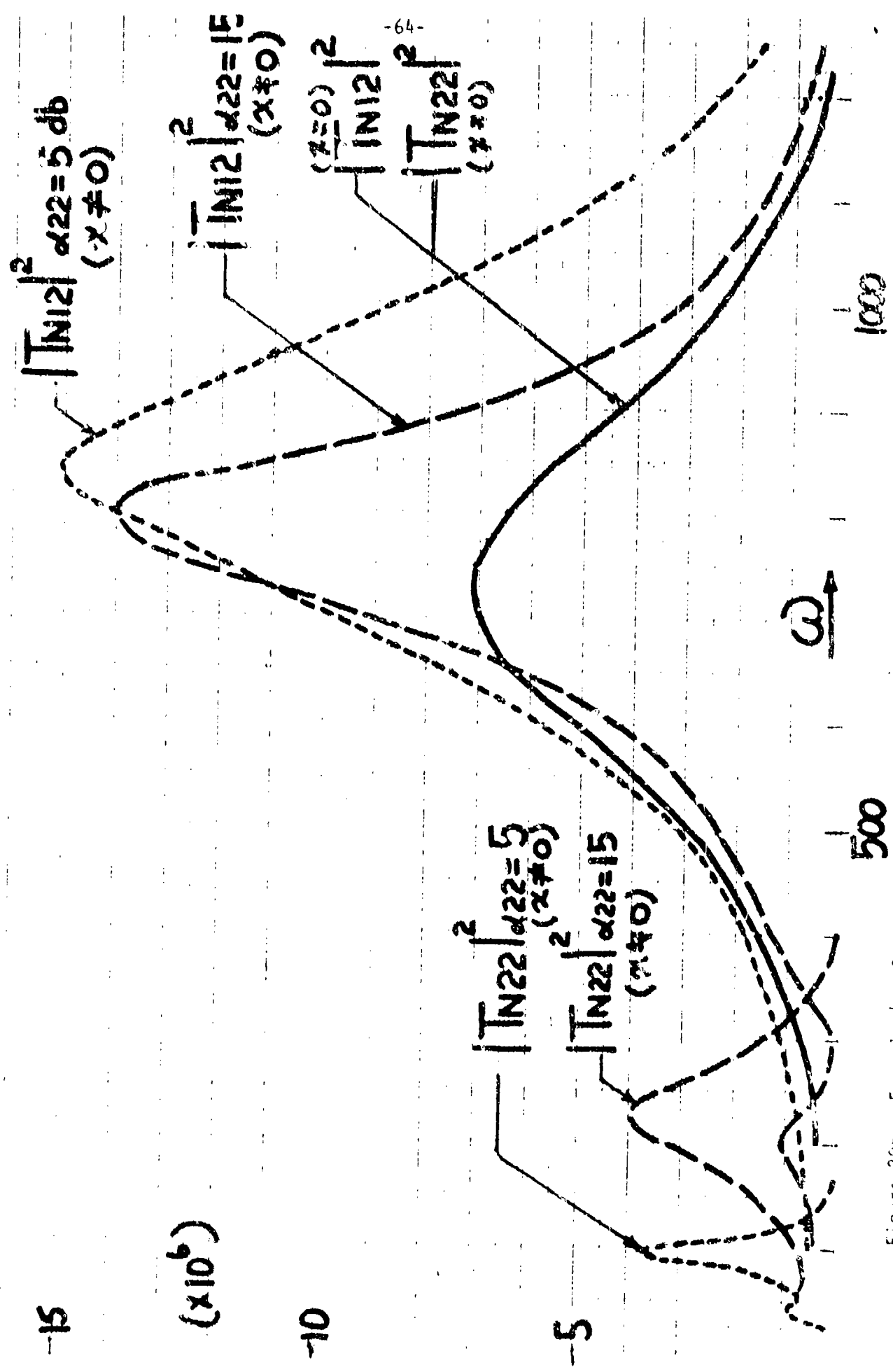


FIGURE 212 - Frequency Response Amplitude in db vs. Frequency ω

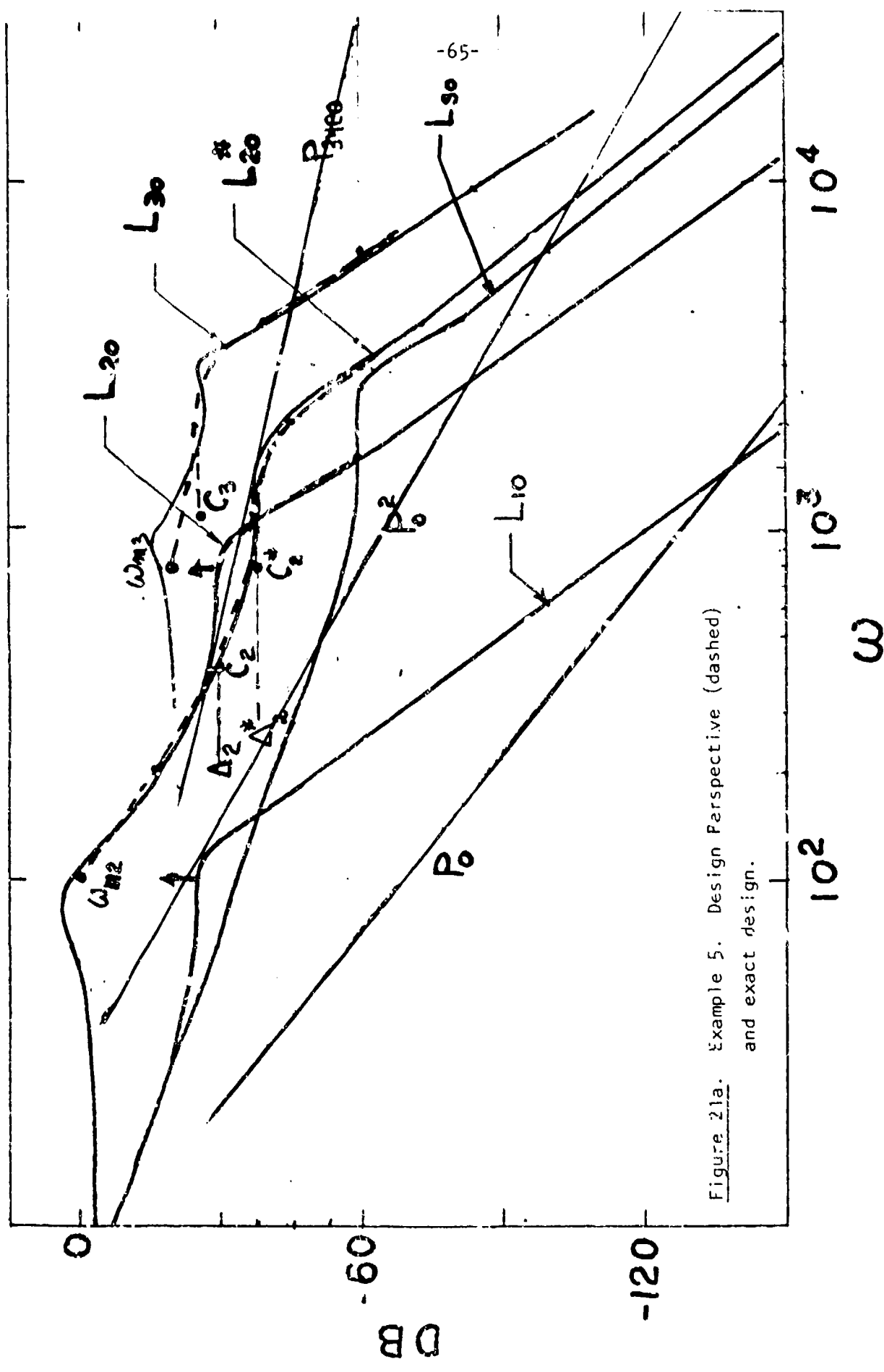


Figure 21a. Example 5. Design Perspective (dashed)
and exact design.

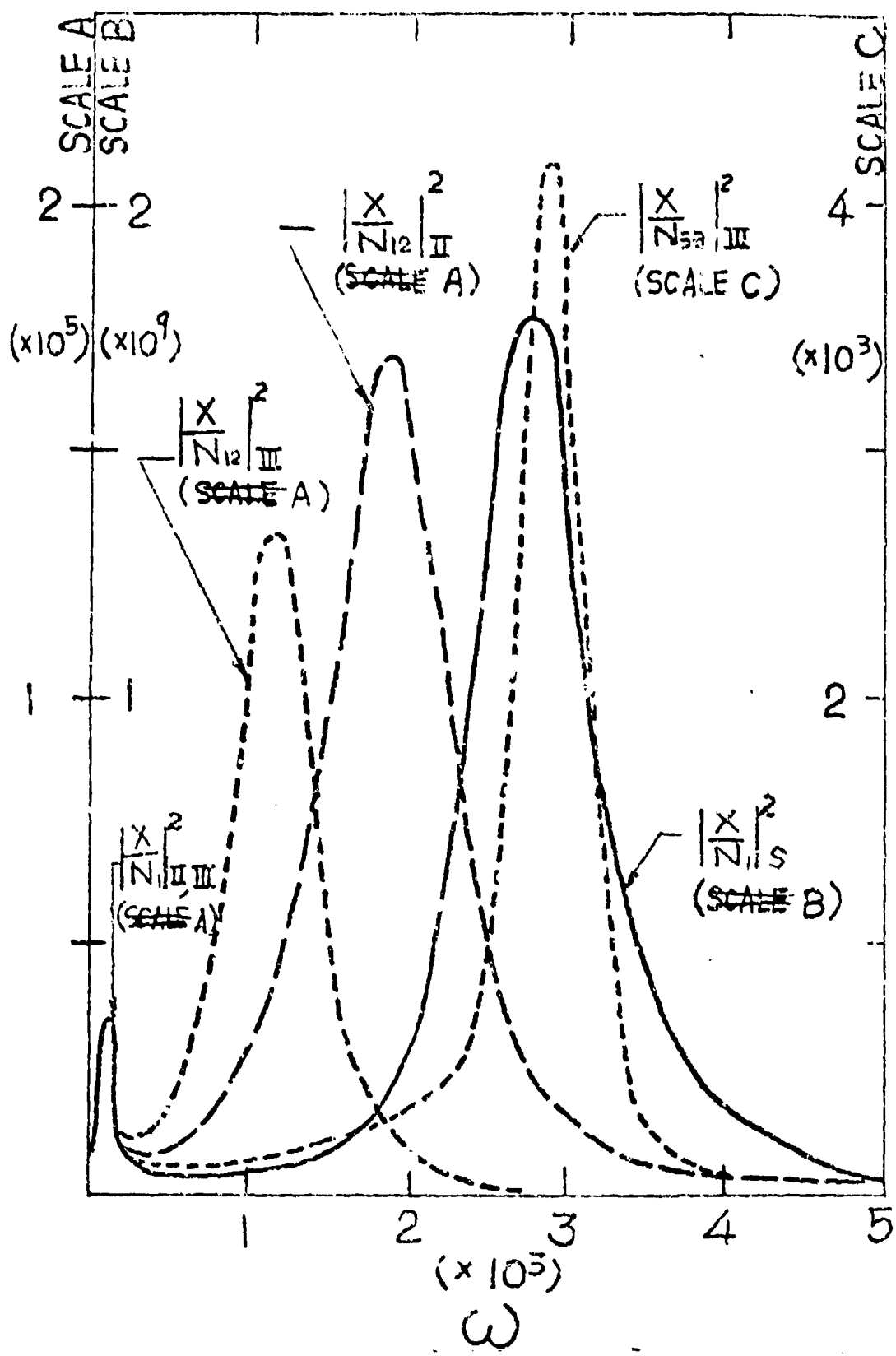


Figure 21b. Example 5. Sensor noise amplification at plant input X .

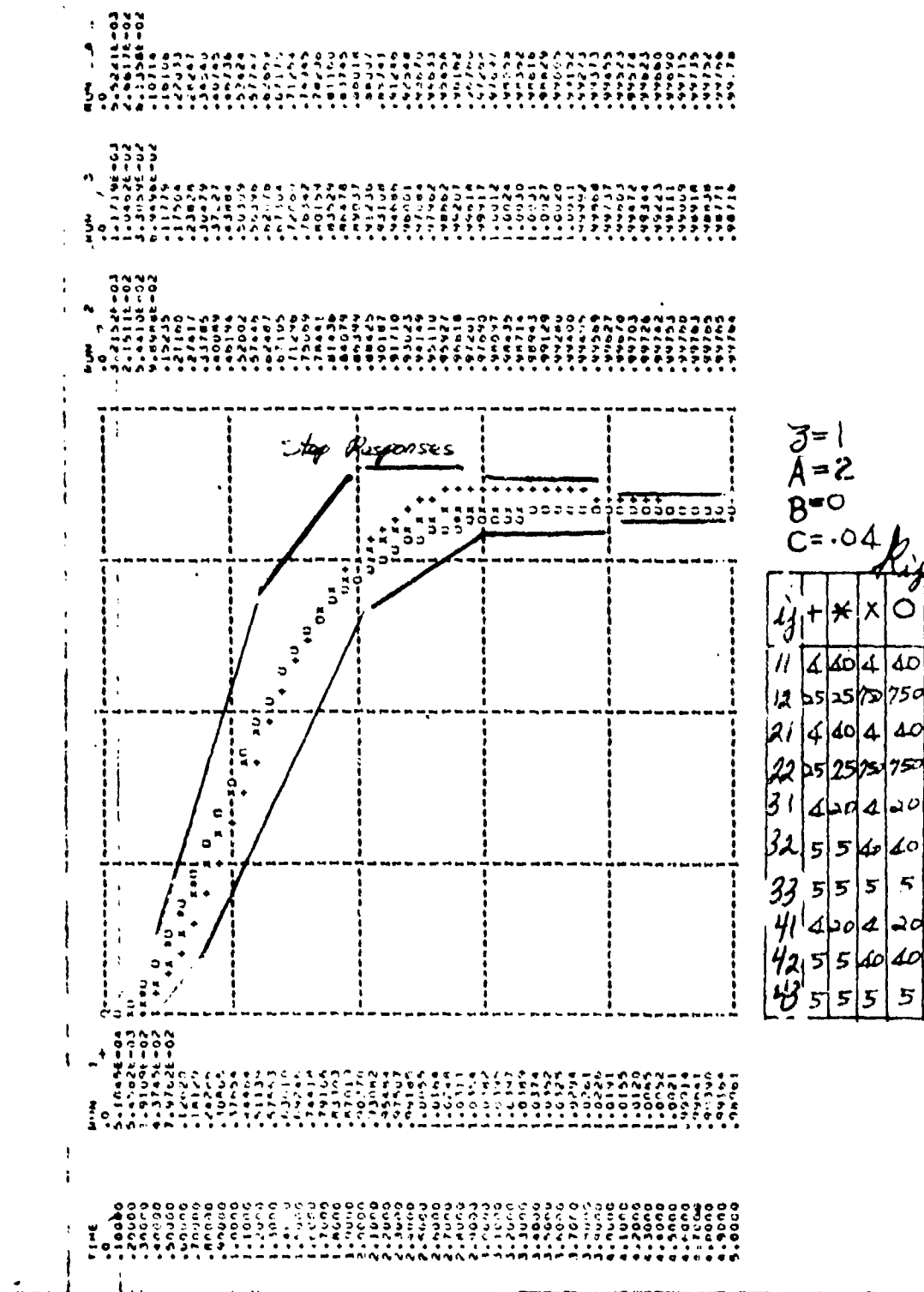


Figure 2.2a Simulation results — step response.

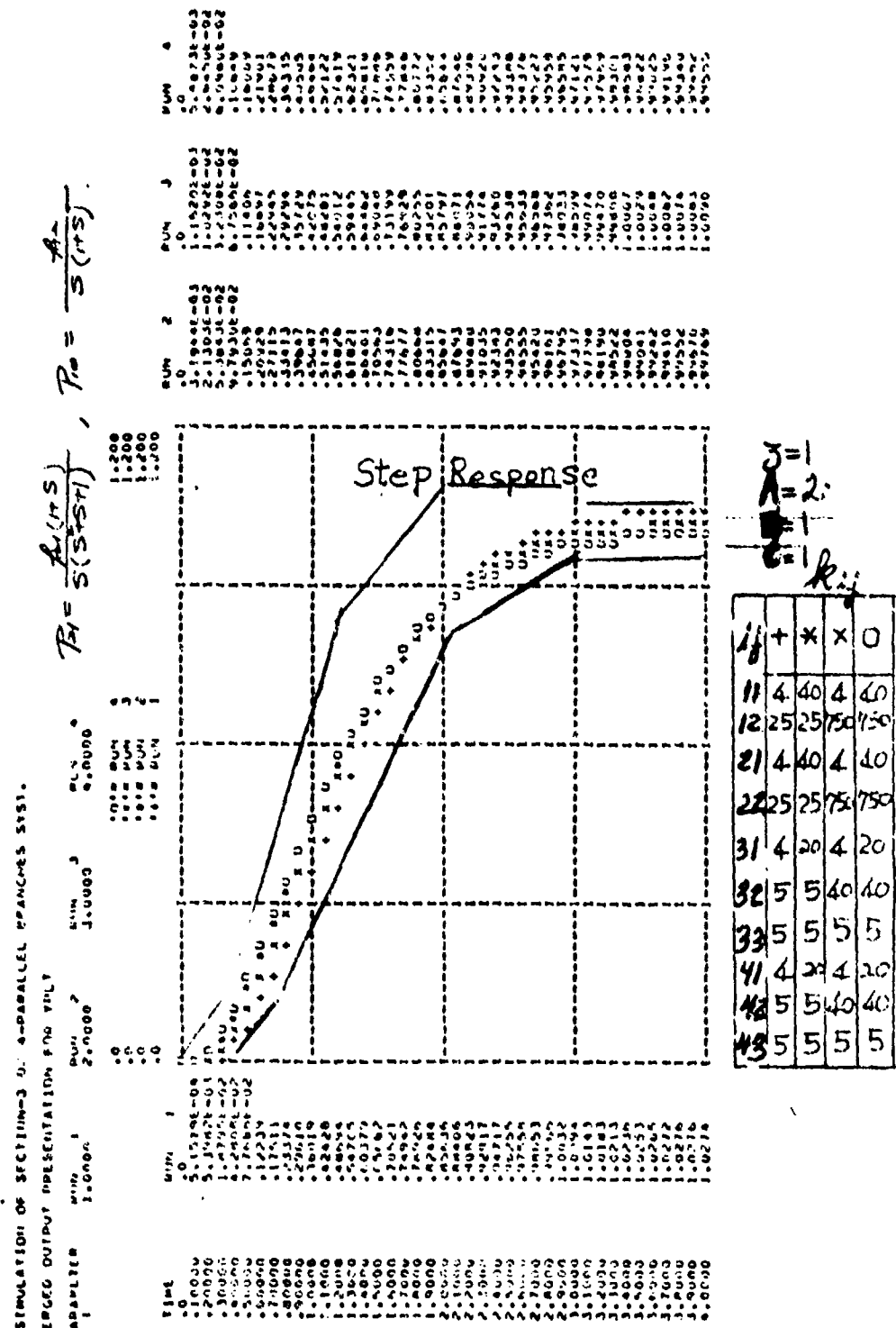


Figure 222 Simulation results - step response.

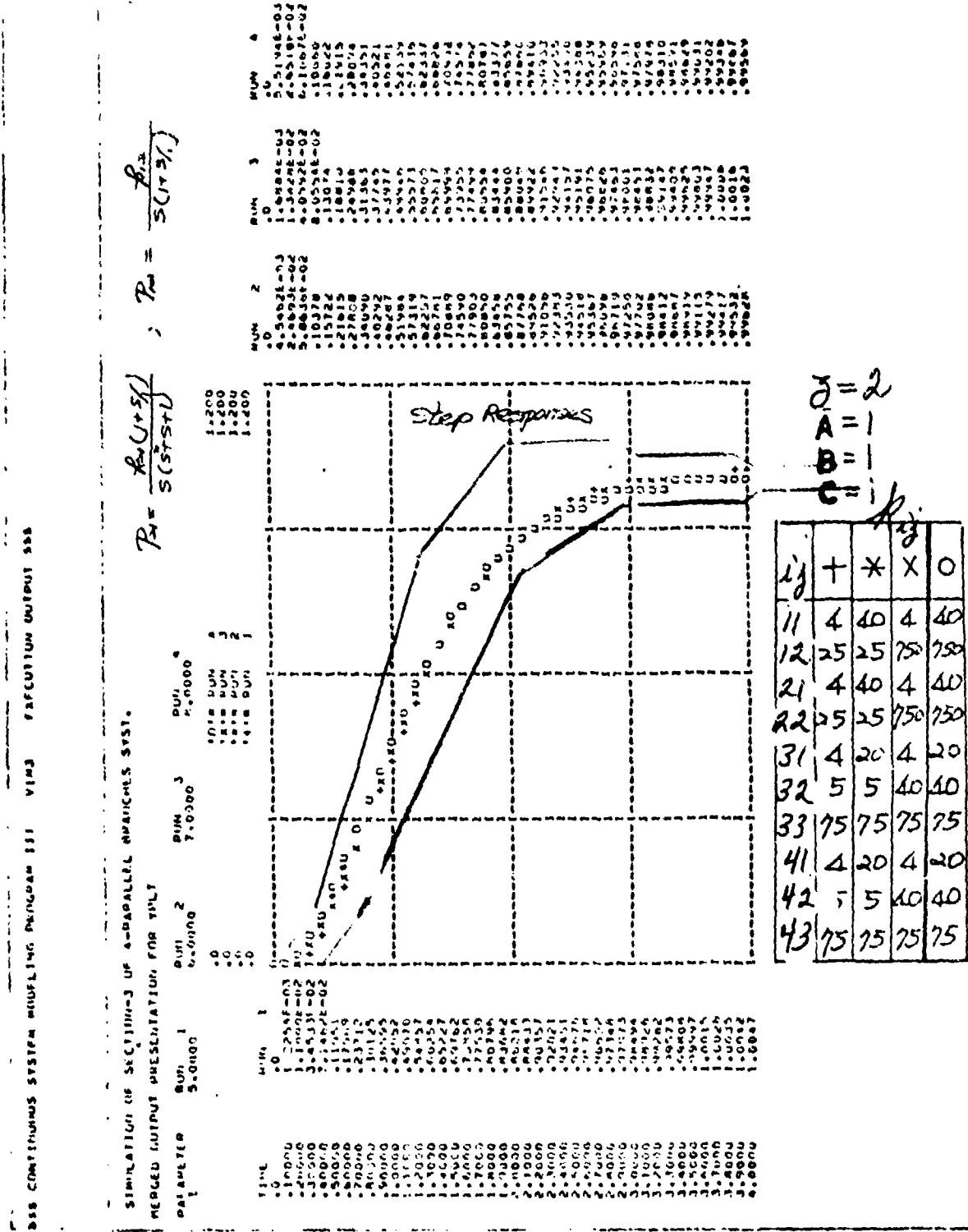


Figure 22 Simulation results — step response.

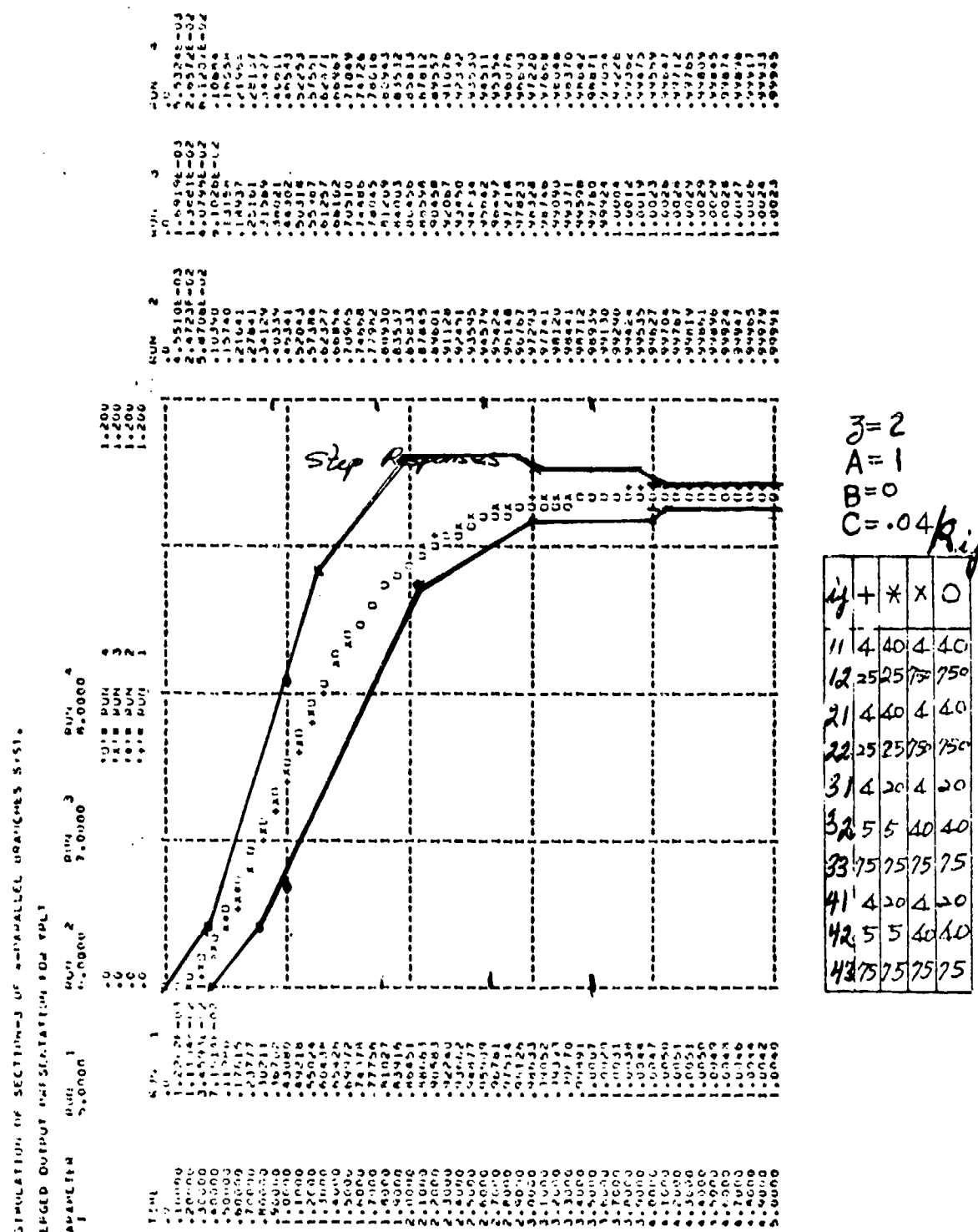


Figure 22d Simulation results — step response.

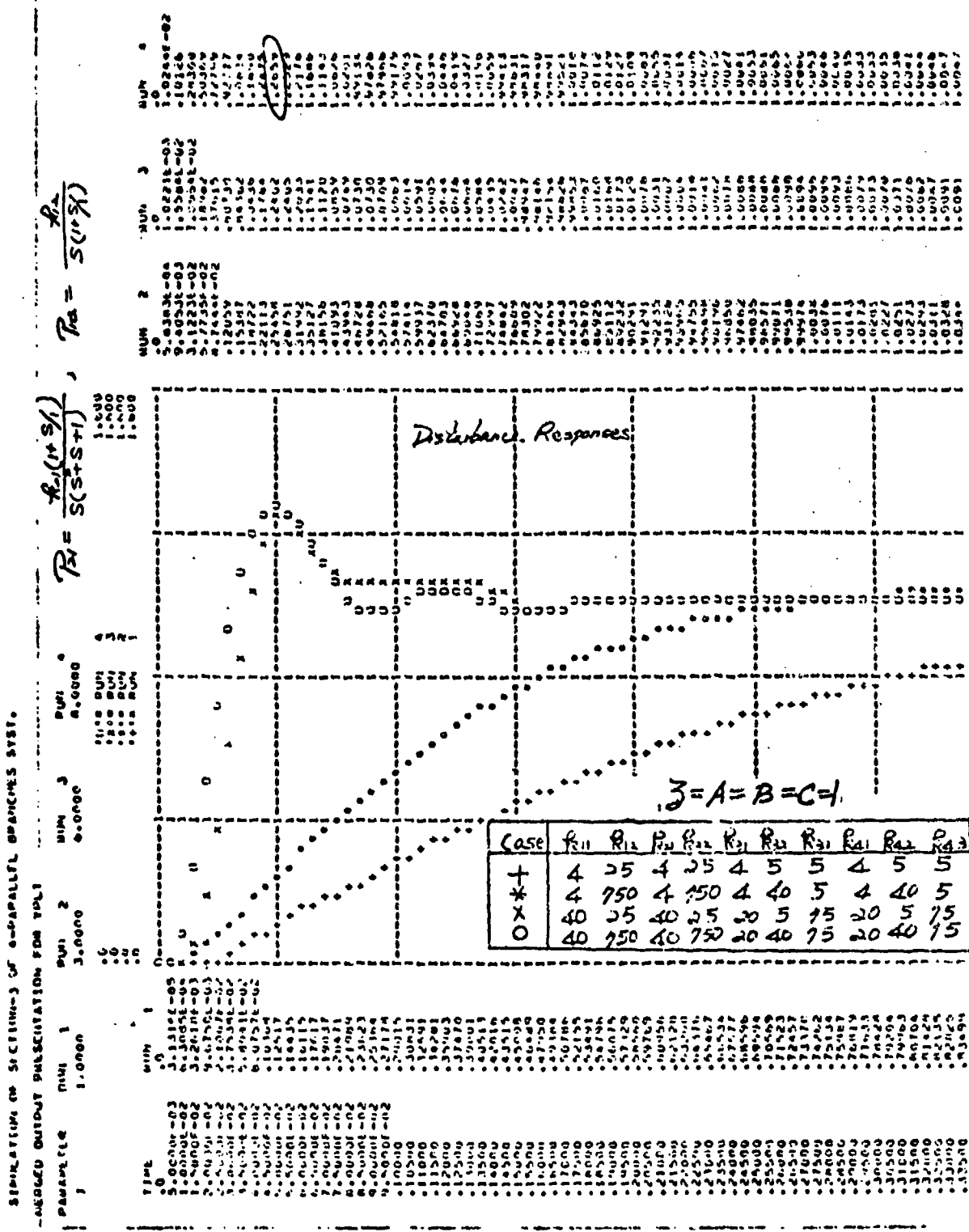


Figure 22b Simulation results — disturbance response.

(PAGES 71-73 WILL BE PUT INTO ONE FIGURE)

SIMULATION OF SECTION-3 ON A-PARALLEL NETWORKS SYSTEM.

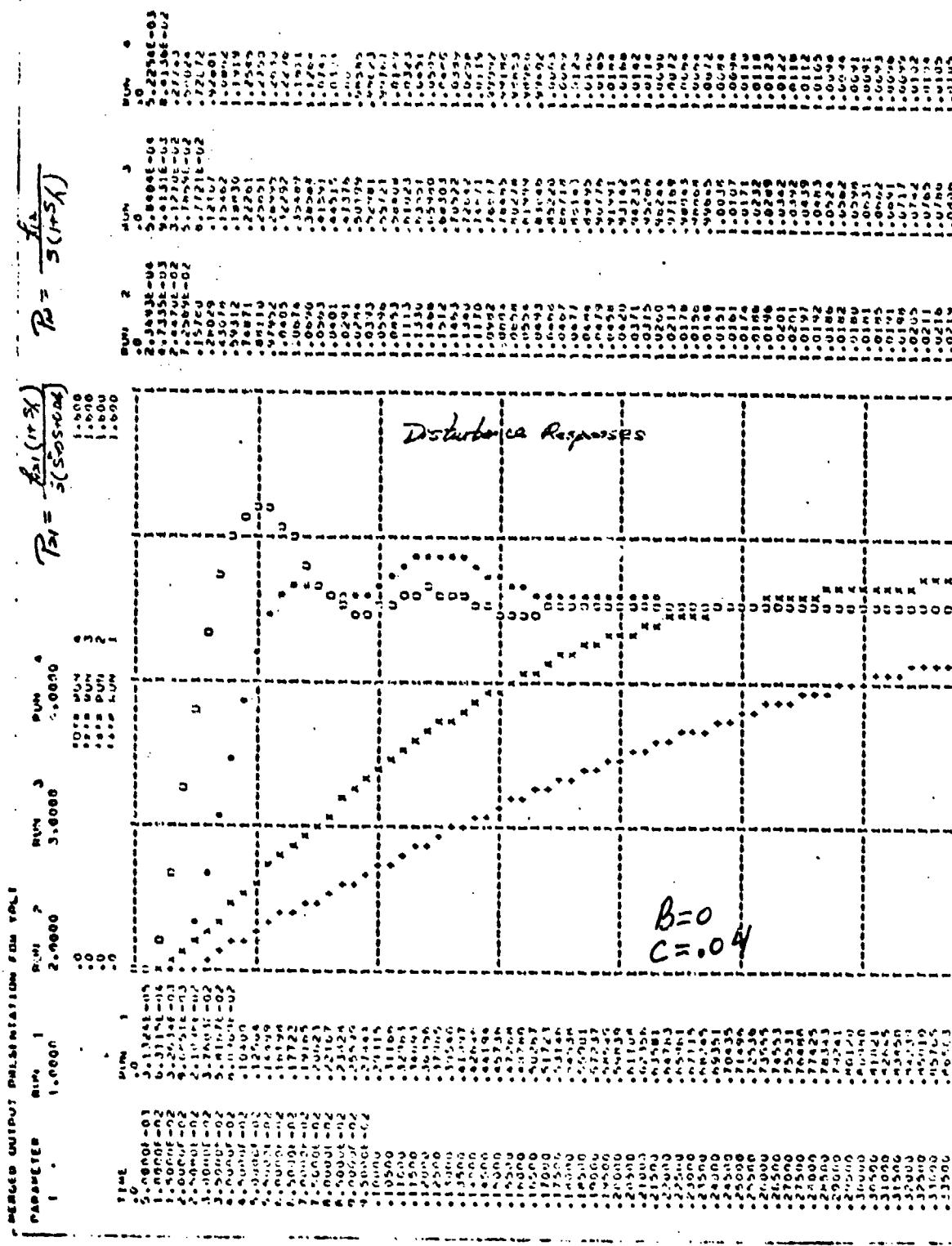


Figure 22 b Simulation results — disturbance response
(same parameter set as Figure).

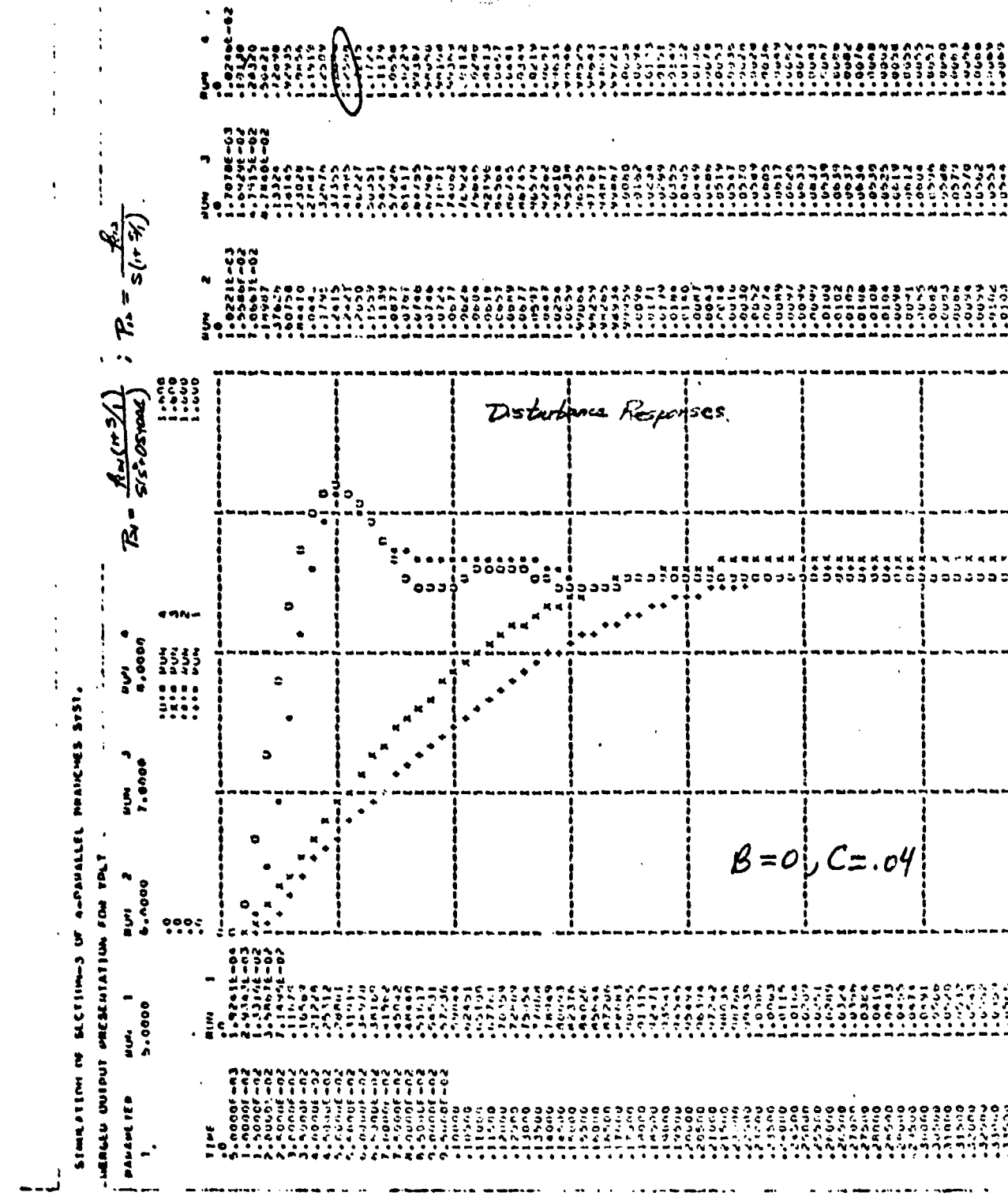


Figure 22b Simulation results - disturbance response
(same parameter set as Figure 1).